2011

Commercial Program Development for a Ground Loop Geothermal System: Energy Loads, GUI, Turbulent Flow, Heat Pump Model and Grid Study

Paul A. Gross II
Wright State University

Commercial Program Development for a Ground Loop Geothermal System: Energy Loads, GUI, Turbulent Flow, Heat Pump Model and Grid Study

A thesis submitted in partial fulfillment
of the requirements for the degree of
Master of Science in Engineering

By

Paul Allen Gross
B.S.M.E., Wright State University, 2010

2011
Wright State University

WRIGHT STATE UNIVERSITY

SCHOOL OF GRADUATE STUDIES

December 7, 2011

I HEREBY RECOMMEND THAT THE THESIS PREPARED UNDER MY SUPERVISION BY Paul Allen Gross ENTITLED **Commercial Program Development for a Ground Loop Geothermal System: Energy Loads, GUI, Turbulent Flow, Heat Pump Model, and Grid Study** BE ACCEPTED IN PARTIAL FULFILLMENT OF THE REQUIREMENTS FOR THE DEGREE OF Master of Science in Engineering.

_____

James Menart, Ph.D
Thesis Director

_____

George P.G. Huang, Ph.D.,
Chair
Department of Mechanical and Materials Engineering

_____

Andrew T. Hsu, Ph.D.,
Dean
School of Graduate Studies

Committee on Final Examination

_____
James Menart, Ph.D

_____
Hong Huang, Ph.D

_____
Chung-Jen Tam, Ph.D

ABSTRACT

Gross, Paul Allen. M.S.Egr., Department of Mechanical and Materials Engineering, Wright State University, 2011.

Commercial Program Development for a Ground Loop Geothermal System: Energy Loads, GUI, Turbulent Flow, Heat Pump Model, and Grid Study

The use of the earth's thermal energy to heat and cool building space is nothing new; however, the heat transfer approximations used in modeling geothermal systems, leave uncertainty and lead to over sizing. The present work is part of a Wright State effort to improve the computer modeling tools used to simulate ground loop geothermal heating and cooling systems. The modern computer processor has equipped us with the computation speed to use a finite volume technique to solve the unsteady heat equation with hourly time steps for multi-year analyses in multiple spatial dimensions. Thus we feel there is more need to use approximate heat transfer solution techniques to model geothermal heating and cooling systems.

As part of a DOE funded project Wright State has been developing a ground loop geothermal computer modeling tool that uses a detailed heat transfer model based on the governing differential energy equation. This tool is meant to be more physically detailed and accurate than current commercial ground loop geothermal computer codes. The Wright State code allows the geothermal designer to optimize the system using a number of outputs including temperature field outputs, existing fluid temperature plots, heat exchange plots, and even a histogram of the COP data. Careful attention to the algorithm speed allows for multi-year simulations with minimal computation cost. Once the thermal and heat transfer computations are complete, a payback period calculator can compare any conventional heating and cooling system to the designed geothermal system and payback periods are displayed.

The work being presented as part of this thesis deals with five issues that were required to make the Wright State geothermal computer code a reality. The five aspects of this modeling tool addressed by this thesis work are: energy load calculations, GUI (graphical user interface) development, turbulence model development, heat pump model development, and two-dimensional numerical grid development. The energy load, or heating and cooling load, calculations are handled using the sophisticated DOE program called EnergyPlus. This thesis work developed a technique for coupling EnergyPlus to the Wright State geothermal code and devising a way for novice users to obtain energy loads quickly and easily, while still allowing expert users to utilize the full strength of EnergyPlus. The GUI for the Wright State computer program was developed with the novice and expert users in mind. The GUI offers ease of use while maintaining the ability for the expert users to setup unique designs for simulation. A unique way of modeling the effects of turbulent flow in the ground tube has allowed the Wright State code to maintain low computation times, while having small errors for a wide range of Reynolds numbers. To make the Wright State ground loop computer model more complete, a heat pump was developed as part of this work. The heat pump model uses the performance characteristics of commercial heat pumps to determine the performance of the geothermal system. The energy transport in the fluid is determined and used to select one of eighteen water-to-air heat pumps that calculate hourly COP's for all system conditions. The calculated heat pump efficiencies are used in an energy balance with hourly building loads to calculate the next iteration's bulk temperature entering the ground loop. Additional details are provided in this thesis on each of these five, important, computer modeling issues.

TABLE OF CONTENTS

LIST OF FIGURES

NOMENCLATURE

$\%af$	Percentage of antifreeze concentration
A	Area of surface
cv	Control volume
C	Thermal capacitance of a layer
C_p	Heat capacity of the fluid
COP_C	Coefficient of performance for cooling
COP_H	Coefficient of performance for heating
CC	Cooling capacity
CP	Cooling compressor power
eff_{ng}	Natural gas furnace efficiency
eff_{oil}	Fuel oil furnace efficiency
eff_{pr}	Propane gas furnace efficiency
EWT	Entering Water Temperature
FV	Future value dollars
h	Convective heat transfer coefficient
h_n	Natural Convective heat transfer coefficient
h_r	Radiation heat transfer coefficient
h_{glass}	Convective heat transfer coefficient on a smooth glass surface
h_f	Enthalpy of the fluid
h_g	Enthalpy of the vapor
HC	Heating capacity
HP	Heating compressor power
i	Interest rate
$I_\circ$	Total available irraditaion
I_b	Intensity of direct beam radiation
I_s	Intensity of sky diffuse radiation
I_g	Intensity of ground reflected diffuse radiation
k_t	Turbulent thermal conductivity of the fluid
k_{eff}	Effective thermal conductivity of the fluid
k	Thermal conductivity of the fluid
k_{soil}	Thermal conductivity of the soil
Pe_t	Turbulent Peclet number
Pr	Prandtl number
Pr_t	Turbulent Prandtl number
P_g	Vapor pressure
P_{atm}	Atmospheric pressure
PV	Present value dollars
q	Heat flux
R	Thermal resistance of a layer or, Inner radius of pipe
Re	Reynolds number
R_f	Roughness factor multiplier
t	Time
T	Temperature
$T(r)$	Temperature at distance r from the center of the pipe
T_{db}	Indoor dry bulb temperature
T_{wb}	Indoor wet bulb temperature

T_m	Mean fluid temperature
T_{bulk}	Bulk fluid temperature
T_{wall}	Temperature of the pipe wall surface
$u(r)$	Velocity at distance r from the center of the pipe
u_*	Friction velocity
U^+	Dimensionless axial velocity
U_m	Maximum centerline velocity
$\dot{v}$	Volume flow of the fluid
$\dot{V}$	Volume flow of the air
V_z	Local wind speed calculated at the height of the surface centroid
V_{ave}	Average fluid velocity
y^+	$= \frac{yu_*}{\nu}$, dimensionless normal distance from the wall
y	Distance from the pipe wall
α	Solar absorptance of a surface
ε	Solar emissivity of a surface
ϵ_r	Relative eddy momentum diffusivity
ϵ_m	Eddy momentum diffusivity
λ	Friction factor
ν	Kinematic viscosity of the fluid= μ/ρ
ρ	Solar reflectivity of a surface or, Density of the fluid
τ	Solar tranmissivity of a surface
ω	Humidity ratio

ACKNOWLEDGMENTS

I am greatly appreciative to my advisor, Dr. James Menart. Your knowledge and expertise have been invaluable throughout this project and your guidance a major factor in the achievement of this work. The inspiration I received from you in undergraduate classes was the deciding factor in my decision to continue my education, and for that I am eternally grateful.

I would also like to thank my colleague Kyle Hughes for his support and friendship during my time spent in graduate school. I could not have had a better co-worker throughout this project.

A special thanks to the Department of Energy, this work could not have been completed without their financial support.

Finally, I would like to thank my friends and family who have been supportive of me throughout my college career. Thank You.

CHAPTER 1

INTRODUCTION

The word geothermal literally means ‘heat from the earth’, and can be used in several types of engineering applications. In areas where hot springs are prevalent, deep wells can be drilled to extract the high temperature steam to drive a turbine for electricity generation. This type of geothermal system is known as high temperature geothermal. Low temperature geothermal uses the constant temperature of the earth just a few feet below the surface for heating and cooling residential and commercial spaces. Heat is extracted or rejected to the earth using a loop made of a material like polyethylene, buried in the earth through which liquid is run. A low temperature system is the type of geothermal energy system discussed throughout this thesis.

Vertical and horizontal loops are used in a variety of geothermal applications and configurations, while basically consisting of one of two types of loops, open and closed. The open loop system pumps water from ground aquifers into the heat pump, after which the used water is dumped. This type of system does not rely on the soil for heat transfer but rather the constant temperature of the ground water. A consistent supply of flowing ground water is not prevalent everywhere and so the open loop is not as versatile or common as the closed loop. The closed loop systems pump a heat transfer liquid such as ethylene glycol through the heat pump and back out to the ground heat exchanger loop. The objective in either case is the same, but due to costs and other individual needs the design of the overall geothermal system can vary.

1.1 Ground loop geothermal system

As discussed, a ground loop geothermal system is designed to use the constant temperature of the earth as a source and sink for the heat pump to operate. This type of system is known as a heat transfer system since it literally is transferring the heat to or from the ground and to or from the building. It can also be used to provide domestic hot water and pool heating at lower operating costs than electric resistance systems. A conventional furnace, combusting natural gas or propane, can deliver thermal efficiencies as high as 95%, which makes these systems popular and in some cases economical. A ground loop geothermal system is capable of moving the earth's heat into the space using a water to air heat pump. This heat pump can move 4 units of heat while only using 1 unit of electricity, resulting in an equivalent efficiency of 400% (GeoExchange n.d.). These completely reversible systems are extremely quiet, reliable, and comfortable but do have the added cost of the loop pipe and trenching or drilling.

1.2 Objectives

The accuracy of the geothermal analysis programs currently available, leave some designers with the need to oversize the system. An oversized system will not only have higher initial costs, but will also have lower efficiencies due to more frequent and shortened run times (GeoExchange n.d.). This results in longer payback periods and a less attractive option for some home owners and businesses. To achieve a faster payback period on a replacement system or new system, the geothermal design needs to be optimized. The heat transfer analysis must be as accurate as possible to ensure that the system delivers high efficiencies for the least amount of operational cost. With technological advances in the industry, the geothermal customer can rest assured that the system will operate as designed.

The geothermal program introduced here solves the heat equation for an unsteady solution. The higher processing speeds of today's personal computers allow us to perform

millions of calculations in seconds. This gives us the ability to solve the temperature matrix on an hourly time step with incredible accuracy. The program is set up so that a turbulent model can be introduced using empirical data and accepted equations for momentum and heat diffusion. This, in combination with a highly accurate heat pump model, will achieve higher accuracies and provide a tool for optimization.

The emphasis on minimizing computation time allows the designer to iterate through several changes in the design quickly. These design iterations can be compared to conventional replacement systems using the hourly load data specific to the project. This economical comparison combines the time value of money, with fuel costs and actual calculated efficiencies from the analysis to display payback periods.

1.3 Other commercial programs

Other geothermal design programs currently in use such as GS2000, RETSCREEN, and Ground Loop Design lack the detail for a more dynamic model and shorter time steps (Ground Loop Design 2007). GS2000 was coupled to the building simulator ESP-r/HOT3000 to give the program more versatility (Purdy and Morrison 2003). This program allows the user to get daily averages and peak loads for GS2000 to use in the ground analysis. The GS2000 heat pump model uses the steady state COP with a quadratic fit of the entering water temperature to calculate the part load capacities. This model does not take into consideration the change in volume flow nor does it use any correction factors for air flow, indoor temperature, or antifreeze concentration. An accurate depiction of the operational costs would be hard to determine with this type of model. The ground loop heat exchanger is modeled using the cylinder and line source method developed in 1947 by Carslaw and Jaeger (Carslaw H.S. 1959). This method uses a one-term approximation with an effective thermal resistance that varies as a function of time.

The RETSCREEN program uses a 'bin method' to calculate the building loads. This method has been used widely in the past for building load estimations,

recommended by the ASHRAE Handbook of Fundamentals in the 1980's. The building dimensions can be entered by the user and the energy usage can be calculated, or average building energy usage can be entered manually. The load calculation is based on the outdoor air temperature and a constant indoor set point of 23°C. The heat pump model is very similar to GS2000 in that it calculates the COP and capacity as a function of the entering water temperature, but lacks any changing volume flow or correction factors. The length of the heat exchanger is calculated using a correlated equation based on heating and cooling peak requirements.

Ground Loop Design in combination with LEAD Plus calculates the building loads using a similar bin method calculation discussed in RETSCREEN (Ground Loop Design 2007). The heat pump model is a data fit model using entering water temperatures for different volume flows to calculate the capacity and power. A more accurate model is possible using load temperature and air flow correction factors. However the model does seem to lack the correction for antifreeze concentration. The ground heat transfer calculation is the same line cylinder model used in the GS2000.

1.4 Industry Trends

The market for ground source heat pumps has grown substantially in the United States in recent years. An increase in installed units of 40% was seen between 2007 and 2008 alone (GeoEnergy 2008). While the geothermal market did show a 5% decrease in the 2009 data, the market is expected to grow in 2010. The data for 2010 is expected to be released in November of this year. A graph of the annual geothermal shipments over time can be seen in Figure 1.

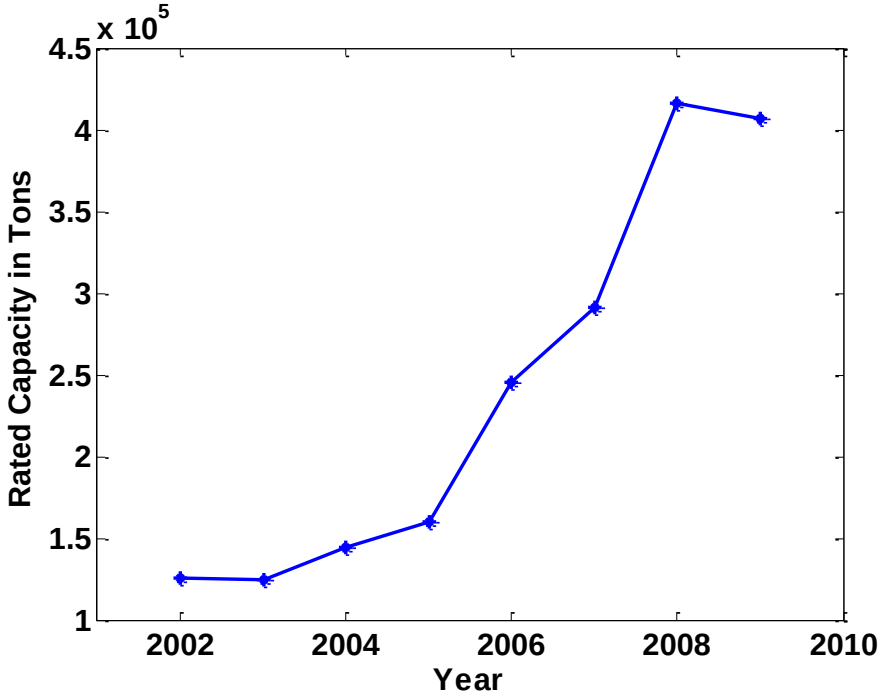

Figure 1: Geothermal heat pump shipments, 1998 – 2009 (D.O.E. 2010).

The newness of ground source heat exchangers for residential and commercial HVAC (heating, ventilation, and air conditioning) has led to some misconceptions that need to be overcome. One misconception is that geothermal only works where heating and cooling are equal. Another is that it requires a lot of land and so it could never have an application in suburban and urban areas. Recognizing the main road blocks facing geothermal can help to clear up these misconceptions and continue to grow the industry. The following are a list of key market and industry barriers as identified by the geothermal roadmap team (Roadmap n.d.).

- High initial investment cost
- Lack of knowledge, trust, and confidence among end users
- Undeveloped institutional and financial support
- Lack of research and development to support design, installation, and performance evaluation

A growing number of technological advances have gradually reduced the initial investment cost for a geothermal system. Feasibility studies assess the potential for geothermal from physical parameters on a regional scale. The geological makeup of a particular region could be less attractive to the layout than other areas. These studies can help to truly understand what the actual costs of drilling or trenching will be before the project is started (Gemelli 2011). The demand for geothermal HVAC systems has been mostly regional rather than a wide spread distribution of qualified installers throughout the country. This region has mostly been grouped together in the Midwest states and only represents 0.6% of the total HVAC market. The possibilities to expand the market throughout the mid-section of the United States, as well as areas with access to ground water, look promising. A map of the 2008 geothermal installations in Figure 2 shows how the regional installations have concentrated.

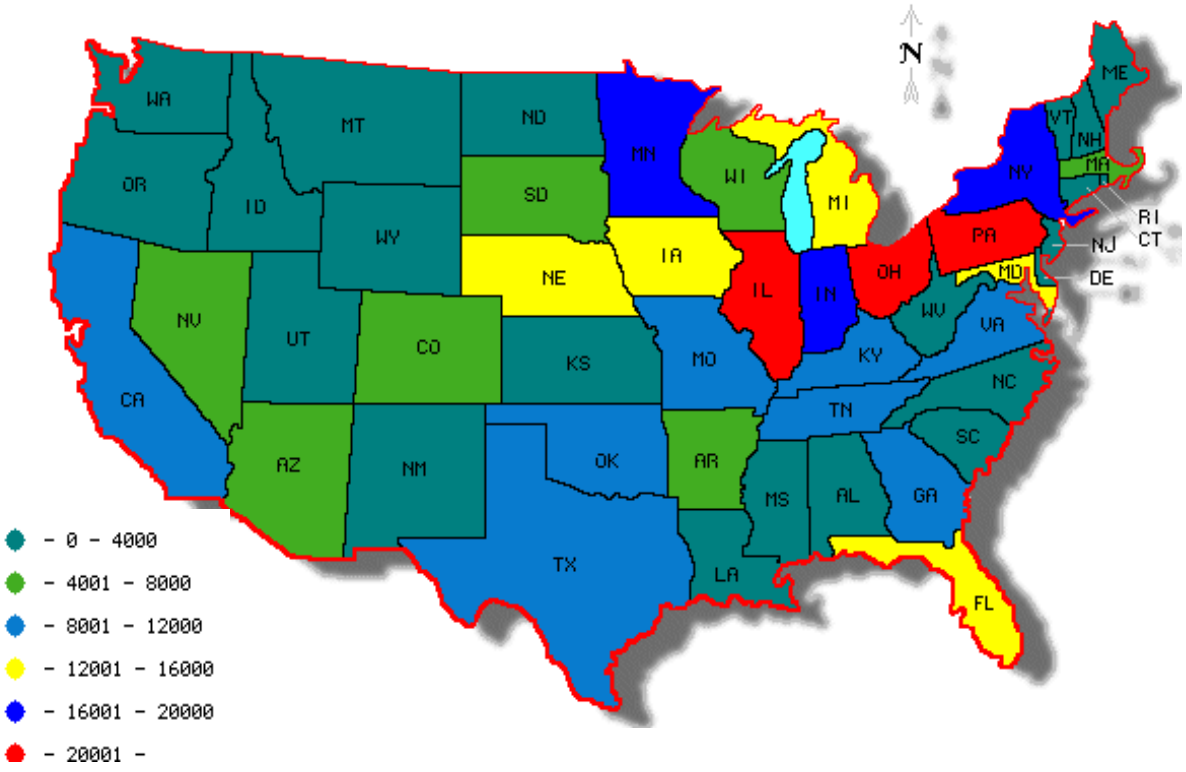

Figure 2: Number of geothermal installations by state in 2008 (D.O.E. 2010).

The overall attitude from existing owners about geothermal systems after installation is overwhelmingly positive. A survey of ground source heat pump owner

satisfaction revealed a high level of satisfaction with 'installation cost' and 'dealer service issues' receiving the lowest ratings at no lower than 84% satisfied. (Ubeg 1998)

Table 1: Ground source heat pump user/owner satisfaction levels. (Ubeg 1998)

Survey Item	Residential	Commercial
Installation Cost	86%	89%
Operating Cost	91%	92%
Maintenance/Reliability	86%	87%
Cleanliness	96%	97%
Noise Levels	95%	93%
Comfort	99%	95%
Safety	96%	95%
Dealer Service	88%	84%
Envir. Friendliness	97%	97%
Size and Appearance	96%	93%

Technological advances in new heat transfer fluids offer freeze protection to -14 C, guaranteeing ‘peace of mind’ and higher thermal conductivities at low temperatures (GEO-FLO n.d.). The ground source heat pump unit itself has increased efficiencies over time, posting an increase in cooling efficiency of 4.6% from 2008 to 2009. Also heating efficiencies for the ground source models increased 2.5 % in that same time period (D.O.E. 2010). The number of qualified installers has increased in the recent years to add to growing consumer confidence. The employment in the industry as a whole grew 50% in just the past two years.

These types of innovations along with a new reliable and accurate ground source geothermal design tool will help to grow the industry further. The geothermal analysis program will need to provide the ability to model the building as accurately as possible in order to avoid any under or over sizing issues. The heat gain/loss calculation is the single most important step in choosing a geothermal heat pump system (geothermalgenius 2011). The ability to then model a heat pump as close to its physical performance as possible will help guide the designer to an optimum conclusion. This approach has the advantage over models that only include the ground loop; this allows the model to behave in a more physically realistic way (Rees 2005). Using a combination of data fit equations

with an energy balance ensures accurate unit efficiency. The modeling of the thermal response of the ground using detailed numerical heat transfer calculations can reduce error found in line cylinder and numerical g-function methods.

The line source method was applied to the study of the thermal conductivity of the ground (Mogensen 1983), but was first developed by Carslaw and Jaeger (Monzo 2011). This model was commonly used due to its fast results and simple nature. The line source method could calculate the temperature field around a line source with constant heat flux. The thermal resistance between the fluid and the borehole wall would then have to be accounted for in an additional calculation. The g-function is then derived for a given time and borehole geometry. The principle of superposition, as seen in Figure 3, is then implemented to model time varying heat loads and to predict the thermal response of the ground. The first part of Figure 3 shows the actual heat rate and the then how they couple together over time, for example; $Q_2' = Q_2 - Q_1$ and so $Q_4' = Q_4 - Q_3$.

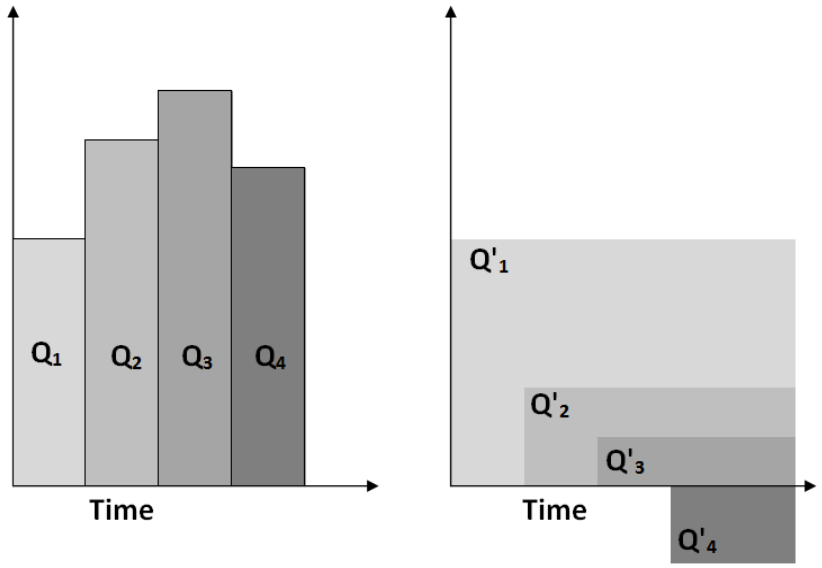

Figure 3: Principle of superposition for thermal response calculation.

This method couples the previous heat loads together into a solution for average fluid temperature using

$$\bar{T}_{f,n} = \bar{T}_g - \sum_{i=1}^{n} \frac{Q_i - Q_{i-1}}{2\pi k_g} g\left(\frac{t_n - t_{i-1}}{t_s}, \frac{r_b}{H}\right) - Q_n R_{eff}. \quad (1)$$

Where k_g is the thermal conductivity of the ground, t_s is the time scale and R_{eff} is the thermal resistance of the fluid. The equation was useful for researchers to develop the relevant line source approximations for geothermal design. This method, used by Eskilson (Monzo 2011) in the 1970's is now used in most geothermal design software on the market today. The quick calculation time and relatively accurate answers make it a useful technique.

CHAPTER 2

BUILDING LOAD CALCULATIONS

Possibly one of the most important aspects of a complete geothermal analysis program is an accurate hourly building load. Due to the complex nature of a building load calculation and the accuracy desired, EnergyPlus (EnergyPlus 2010) is interfaced with the newly developed geothermal program. The latest EnergyPlus program gives the geothermal analysis program the ability to create a quick residential type novice calculator as well as provide the expert designer the access to all of EnergyPlus through the editor. The numerous .epw weather files supplied by EnergyPlus allow the geothermal analysis program more versatility to all regions of the country.

2.1 EnergyPlus

Developed as a result of the BLAST(Building Loads Analysis and System Thermodynamics) and DOE-2 programs, EnergyPlus was designed as an energy and load simulation tool (EnergyPlus 2010). The intended use was for architects and HVAC designers to perform cost analysis and optimize energy performance. Although EnergyPlus was designed to simulate different HVAC systems, the integration of the 'HVAC template' allows for an ideal system simulation. Using this template, the building can be modeled at user defined thermostat set points to ultimately calculate hourly load data. Based on the physical description of the building, entered by the user through CAD software, the heating and cooling loads are calculated to meet the

thermostat set points. EnergyPlus is integrated directly into the GUI design as a first step in the geothermal design. The text based input files made it possible to design a 'novice' load calculator so that a user with no EnergyPlus knowledge can use the program. While the expert user has full access to the EnergyPlus editor to change material properties, constructions, internal loads and all other modeling inputs in the editor. This option does require some knowledge of EnergyPlus, even though the necessary inputs to ensure a successful simulation are prewritten.

2.2 Conduction

Using the 'HVAC:Template' to simulate an ideal load on the building, the conduction transfer function module is used. This function uses a state space technique using the environmental temperatures to solve for the heat flux. The set of matrix equations becomes

$$\begin{bmatrix} \frac{dT_1}{dt} \\ \frac{dT_2}{dt} \end{bmatrix} = \begin{bmatrix} -\frac{1}{RC} - \frac{hA}{C} & \frac{1}{RC} \\ \frac{1}{RC} & -\frac{1}{RC} - \frac{hA}{C} \end{bmatrix} \begin{bmatrix} T_1 \\ T_2 \end{bmatrix} + \begin{bmatrix} \frac{hA}{C} & 0 \\ 0 & \frac{hA}{C} \end{bmatrix} \begin{bmatrix} T_o \\ T_i \end{bmatrix} \tag{2}$$

$$\begin{bmatrix} q_o'' \\ q_i'' \end{bmatrix} = \begin{bmatrix} 0 & -h \\ h & 0 \end{bmatrix} \begin{bmatrix} T_1 \\ T_2 \end{bmatrix} + \begin{bmatrix} 0 & h \\ -h & 0 \end{bmatrix} \begin{bmatrix} T_o \\ T_i \end{bmatrix}$$

where $R = \frac{l}{kA}$ is the thermal resistance of the layer and $C = \frac{\rho C_p l A}{2}$ is the thermal capacitance. The inner and outer surface convection heat transfer coefficients are found in the following section 2.3. This technique is preferred to the previously used Laplace transform method which required solving for roots in the Laplace domain. The accuracy of the conduction transfer function was found to be within 1% of the analytical solution when an adequate number of nodes were used. The method has caused the entire simulation to diverge when used with sub-hourly time steps and with materials that are considered thermally massive due to a large number of terms in the transfer function. The inside and outside surface temperatures and heat fluxes are solved for and used in the convective calculations.

2.3 Convection

The convection algorithm uses a correlation between the convective heat transfer coefficient, surface orientation and the temperature difference. The algorithm was taken directly from Walton (1983) where a curve fit is added as a function of the cosine of the tilt angle to give values between vertical and horizontal. The curve fits were compared to ASHRAE Handbook of Fundamentals values and were found to fit well. This is determined differently depending on the difference in temperature between the surface and the indoor air along with the orientation. The equations for the convective heat transfer coefficient become

For ($\Delta T<0$ and upward facing surface) or ($\Delta T>0$ and downward facing surface) the following equation is used, (Walton 1983)

$$h_n = \frac{9.482|\Delta T|^{\frac{1}{3}}}{7.283-|cos\theta|} \text{ (W/m}^2\text{ K)}. \quad (3)$$

For ($\Delta T>0$ and upward facing surface) or ($\Delta T<0$ and downward facing surface) the following equation is used, (Walton 1983)

$$h_n = \frac{1.810|\Delta T|^{\frac{1}{3}}}{1.382+|cos\theta|} \text{ (W/m}^2\text{ K)}. \quad (4)$$

where θ is the surface tilt angle. This algorithm is the default indoor convection algorithm for EnergyPlus (EnergyPlus 2010).

The algorithm used for outside convection is in part comprised of the natural convection equations from the inside convection algorithm. The convective heat transfer coefficient is broken into the natural convection and forced convection terms. The coefficient for smooth glass is calculated using the root mean square of the natural convection term and a correlated forced term,

$$h_{glass} = \sqrt{h_n^2 + [aV_z^b]^2} \text{ (W/m}^2\text{ K)} \quad (5)$$

where V_z is the local wind speed calculated at the height of the surface centroid, and terms 'a' and 'b' are correlated coefficients given in Table 2.

Table 2: Coefficients for outside convection algorithm. (Yazdanian and Klems 1994)

Wind Direction	a	b
Windward	2.38	0.89
Leeward	2.86	0.617

The natural convective heat transfer coefficient is subtracted from the coefficient for smooth glass and then multiplied by a roughness factor. h_{glass} is then used to calculate the forced term in the following surface convection heat transfer coefficient equation,

$$h_c = h_n + R_f\left(h_{glass} - h_n\right) \text{ (W/m}^2\text{ K)} \quad (6)$$

where R_f is given in

Table 3.

Table 3: Roughness factor multiplier (EnergyPlus 2010).

Roughness Index	R_f	Example Material
1 (Very Rough)	2.17	Stucco
2 (Rough)	1.67	Brick
3 (Medium Rough)	1.52	Concrete
4 (Medium Smooth)	1.13	Clear Pine
5 (Smooth)	1.11	Smooth Plaster
6 (Very Smooth)	1.00	Glass

Summing the natural term with the forced term gives the overall surface convection heat transfer coefficient.

2.4 Solar Gains

The default solar irradiance model used in the EnergyPlus calculations is the ASHRAE Clear Sky model. The calculation starts with the direct normal irradiation on the earth's surface on a clear day. This does not yield the maximum direct normal irradiation but rather values that are representative of conditions on cloudless days. The total available irradiation is calculated using

$$I_{\circ} = \frac{A}{e^{\left(B/\sin\beta\right)}} \tag{7}$$

where A is the apparent solar irradiation with air mass of zero, B is the atmospheric extinction coefficient and β is the declination angle in degrees. The value for solar irradiance must then be multiplied by clearness numbers from ASHRAE. The values calculated for extraterrestrial solar irradiance tend to overestimate the amount of solar radiation available to the building. The total solar gain on any surface in the model is then calculated by including a combination of the direct and diffuse radiation using

$$Q_{solar} = \alpha\left(I_b cos\theta \frac{S_S}{S} + I_s F_{ss} + I_g F_{sg}\right) \tag{8}$$

where

α = solar absorptance of the surface

θ = angle of incidence of the sun's rays

S = area of the surface

S_S = sunlit area

S = area of the surface

I_b = intensity of direct beam radiation

I_s = intensity of sky diffuse radiation

I_g = intensity of ground reflected diffuse radiation

F_{ss} = angle factor between the surface and the sky

F_{sg} = angle factor between the surface and the ground

For external long wave radiation calculations, the heat exchange between surfaces is a function of material property, surface temperature, and spatial properties. The general agreement is that for building load calculations, some assumptions are reasonable such as: (Chapman n.d.)

- each surface emits or reflects diffusely and is gray and opaque ($\alpha = \varepsilon, \tau = 0, \rho = 1 - \varepsilon$),
- each surface is at uniform temperature,
- energy flux leaving a surface is evenly distributed across the surface, and
- the medium within the enclosure is non-participating.

Using these assumptions the long wave radiation heat flux is calculated as the sum of the components due to ground, sky, and air. These constituents are further broken down into the fundamental radiation heat transfer equation

$$q''_{lwr} = \varepsilon\sigma F_{gnd}\left(T_{surf}^4 - T_{gnd}^4\right) + \varepsilon\sigma F_{sky}\left(T_{surf}^4 - T_{sky}^4\right) + \varepsilon\sigma F_{air}\left(T_{surf}^4 - T_{air}^4\right). \quad (9)$$

This equation is then linearized to produce heat transfer coefficients. These coefficients are combined with another term β used to split the sky and air view factors based on the tilt angle of the surface

$$\beta = \sqrt{0.5(1 + cos\varphi)}. \quad (10)$$

The final equations for the long wave radiation heat transfer coefficients become

$$h_{r,gnd} = \frac{\varepsilon\sigma F_{gnd}\left(T_{surf}^4 - T_{air}^4\right)}{\left(T_{surf} - T_{air}\right)} (\mathrm{W/m^2\ K}), \quad (11)$$

$$h_{r,sky} = \frac{\varepsilon\sigma F_{sky}\beta\left(T_{surf}^4 - T_{sky}^4\right)}{\left(T_{surf} - T_{sky}\right)} (\mathrm{W/m^2\ K}) \quad (12)$$

and

$$h_{r,air} = \frac{\varepsilon\sigma F_{sky}(1-\beta)\left(T_{surf}^4 - T_{air}^4\right)}{\left(T_{surf} - T_{air}\right)} (\mathrm{W/m^2\ K}). \quad (13)$$

The ground temperature is assumed to be the same as the air temperature and the long wave emittance is defined by the user in the material properties.

2.5 Weather Data

Simple weather files available consist of observations of temperature, humidity, wind speed and direction, atmospheric pressure, and solar radiation made on an hourly basis. The data for simulation software are derived from this hourly set from a specific location. The 'typical' data such as TMY2 and WYEC2 contain more solar radiation and illumination data and have been found to be more accurate over longer lengths of time than averaging (Crawley, 1998). The epw file used in EnergyPlus was developed based on the TMY2 format, but with the ability to interpolate sub hourly. Another difference is the infrared sky field used to calculate effective sky temperatures for re-radiation at night (EnergyPlus 2010).

The EnergyPlus input files converted from a CAD drawing, or written by the novice load calculator, use the option to run simulation for 'weather file run periods'. This uses the weather file for an hourly simulation rather than a peak load or design load. The 'typical' weather supplied by the weather files are loaded into the model upon the selection of the location by the user.

2.6 Outputs

For the purposes of modeling a geothermal heat pump system, the hourly load data for all of the modeled zones is necessary. Other necessary building simulation data include the inside dry bulb temperature and humidity ratios for all of the simulated zones. The outside dry bulb temperature and wind speeds are also output automatically whether in expert or novice modes. This is a critical and necessary step in interfacing EnergyPlus with the geothermal program since it supplies the user with crucial data for a complete design. The indoor dry bulb and humidity ratios are used in the heat pump model

discussed in Chapter 4. The outdoor dry bulb temperature is used to suggest a soil temperature specific to a location. This is done by averaging the outdoor temperature and using it as default in the GUI discussed in more detail in Chapter 6.

CHAPTER 3

FLUID FLOW

One of the more unique parts of the geothermal analysis program is the fluid mechanics model. The control volumes that are set up in the fluid region have a velocity profile across the diameter based on the Reynolds number. Due to the transient nature of the geothermal heat transfer analysis; the convective heat transfer coefficient off of the pipe wall is always changing. The flow parameters for each control volume are modeled using empirically correlated equations for frictional velocities, eddy momentum, and turbulent thermal conductivity.

3.1 Laminar Flow

Geothermal heat transfer mainly uses turbulent flow, with Reynolds numbers greater than 20,000 (Trane November 2010). Although, to model the flow for as many cases as possible, a laminar equation is used. The equation used calculates the velocity at a given radius from the center of the pipe to the wall as:

$$u(r) = 2V_{avg}\left(1 - \frac{r^2}{R^2}\right) \tag{14}$$

where the user will input the average velocity V_{avg} and inner pipe radius *R*. The velocity $u(r)$ is then calculated for each control volume assuming fully developed flow. This model is only used when the Reynolds number is less than 2300. With viscous shear the

only stress, the effective thermal conductivity of the fluid remains simply the thermal conductivity of the fluid.

3.2 Turbulent Flow

The equation used in the case of Reynolds numbers between 2300 and 100,000 for the velocity profile is the empirically derived Power Law (Fox, McDonald and Pritchard 2006)

$$\frac{u}{U_m} = \left(\frac{y}{R}\right)^{1/n}, \tag{15}$$

where u is the velocity profile, y is the distance from the wall, n is an empirically derived exponent and U_m is the maximum centerline velocity. The value for the exponent n is calculated using the log relationship with the Reynolds number written as (Fox, McDonald and Pritchard 2006)

$$n = -1.7 + 1.8\, log_{10}(Re). \tag{16}$$

Using the calculated exponent n and the average velocity supplied by the user, the maximum centerline velocity can be calculated using (Fox, McDonald and Pritchard 2006)

$$\frac{V_{avg}}{U_m} = \frac{2n^2}{(n+1)(2n+1)}. \tag{17}$$

To further broaden the applicability of the geothermal analysis program, the velocity profile for Reynolds numbers greater than 100,000 is also modeled. This high of a Reynolds number would normally never be seen in a geothermal application, but the widest range of conditions was included in the model. For this reason the velocity profile equation (Swearingen 2009)

$$\frac{u}{V_{avg}} = 1 + 1.44\sqrt{\lambda} + 2.15\sqrt{\lambda} log_{10}\left(1 - \frac{r}{R}\right) \tag{18}$$

is used in the program as well.

With the velocity profile modeled, the friction factor for a smooth pipe is calculated using the equation (Fox, McDonald and Pritchard 2006)

$$\sqrt{\frac{8}{\lambda}} = 2.44ln\left(\sqrt{\frac{\lambda}{32}}\, Re_d\right) + 2.0 \tag{19}$$

in a trial and error convergence loop. The value for λ is compared to the Moody diagram and found to follow the curve closely as the Reynolds number is increased. To save as much computation time as possible a direct-solve equation for the friction factor is investigated. The Petukhov equation (BS. 1970) is implemented and takes the form

$$\lambda = (0.79ln(Re) - 1.64)^{-2}. \tag{20}$$

This is a one step calculation rather than a trial and error iterative process. A comparison of these factors is plotted in Figure 4 where the converged value for λ was calculated with a tolerance of 10^{-5}. The error associated with the heat transfer coefficient at steady state conditions and fully developed flow is found to be minimal in the range of Reynolds numbers typically used in geothermal systems, typically 15,000 to 30,000 Reynolds number (Trane 2009).

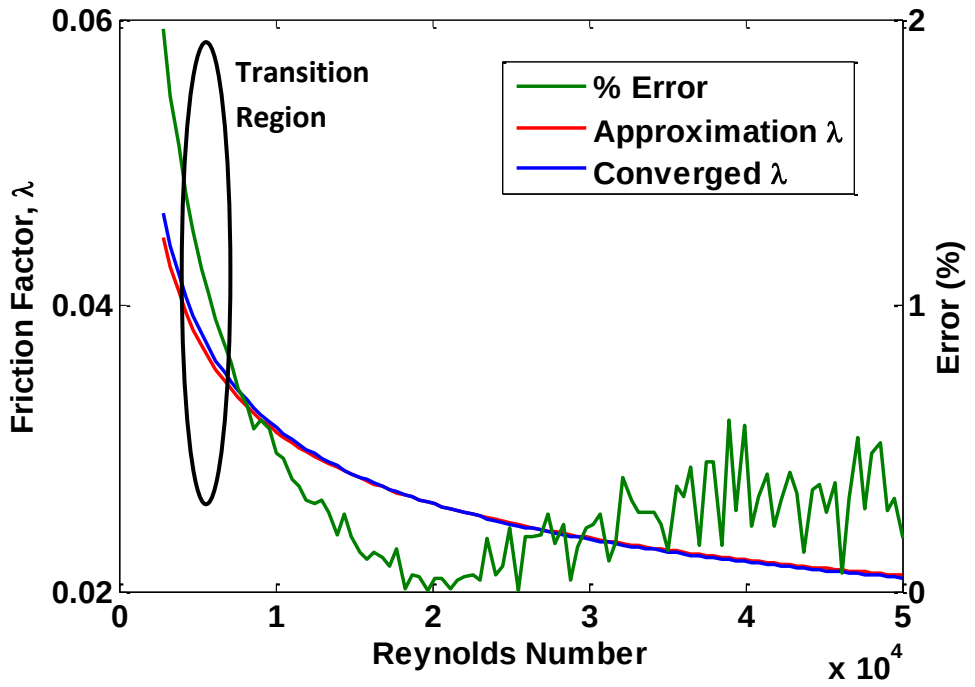

Figure 4: Calculated friction factor compared to Moody diagram.

The friction factor for smooth pipes is then used to calculate the friction velocity as (Datta 1993)

$$u_* = V_{ave}\sqrt{\frac{\lambda}{8}}. \tag{21}$$

The friction velocity is a function of the wall shear τ_w and can also be described as $\sqrt{\frac{\tau_w}{\rho}}$, where; in the region very close to the wall the viscous shear is dominant over the turbulent shear. This becomes more evident when the effective thermal conductivity is calculated. With all three of the velocity profiles complete for any Reynolds number, a plot of the nondimensional profiles can be seen in Figure 5.

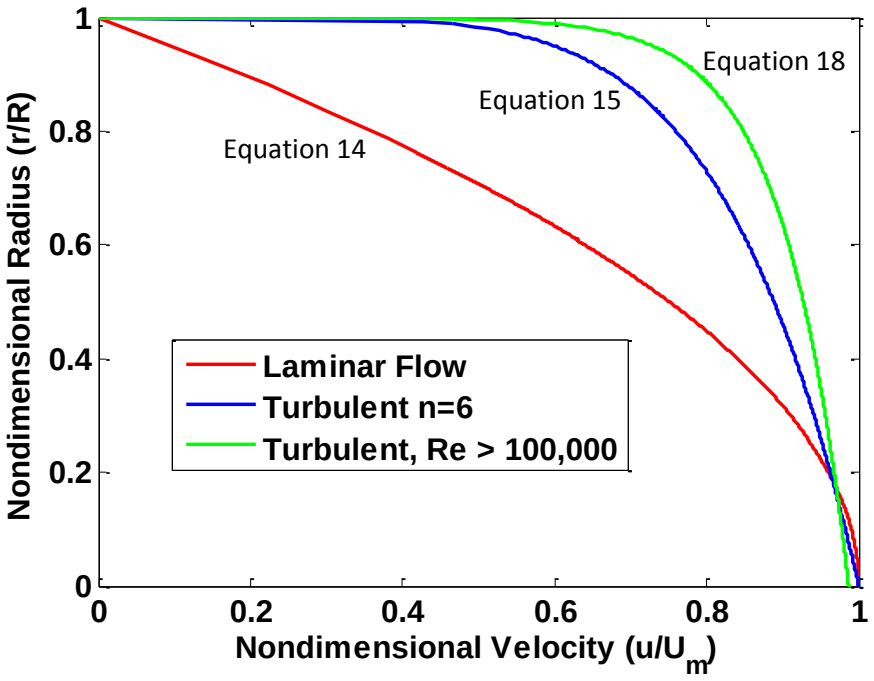

Figure 5: Velocity profiles.

The profile for the high Reynolds numbers using equation 18, does show some of its shortcomings as it does not quite reach a nondimensional velocity of one at the center of the bulk flow. The profile for turbulent flow shows the asymptotic behavior very close to the wall. This behavior becomes very important as the effective thermal conductivity of the fluid is determined. The effective thermal conductivity is calculated by dividing the fluid flow into three different regions, viscous sublayer, buffer layer, and the bulk flow. These regions are found by first calculating

$$y^+ = \frac{yu_*}{\nu} \tag{22}$$

where ν is the kinematic viscosity and y being the distance from the wall. The viscous sublayer, the region where $y^+ \leq 10.5$, is extremely close to the wall. The dimensionless axial velocity U^+can then be calculated for this region as

$$U^+ = \frac{yu_*}{\nu} = y^+. \tag{23}$$

The second layer, or buffer layer, is empirically derived for values of $10.5 < y^+ < 30$. The viscous shear and turbulent shear both play an important role in this region. The scattered data in the buffer layer is fit using a natural log relationship with the distance from the wall, the frictional velocity and the viscosity of the fluid. The dimensionless axial velocity $U^+$for the buffer layer now becomes (Fox, McDonald and Pritchard 2006)

$$U^+ = 5ln\frac{u^*y}{\nu} - 3.05. \tag{24}$$

In the bulk flow where the values of $y^+ \geq 30$, the axial velocity is dominated by the turbulent shear and the empirical correlation for U^+ becomes (Fox, McDonald and Pritchard 2006)

$$U^+ = 2.5ln\frac{u^*y}{\nu} + 5.5. \tag{25}$$

An example of the three regions and the corresponding equations for the axial velocity can be seen in Figure 6.

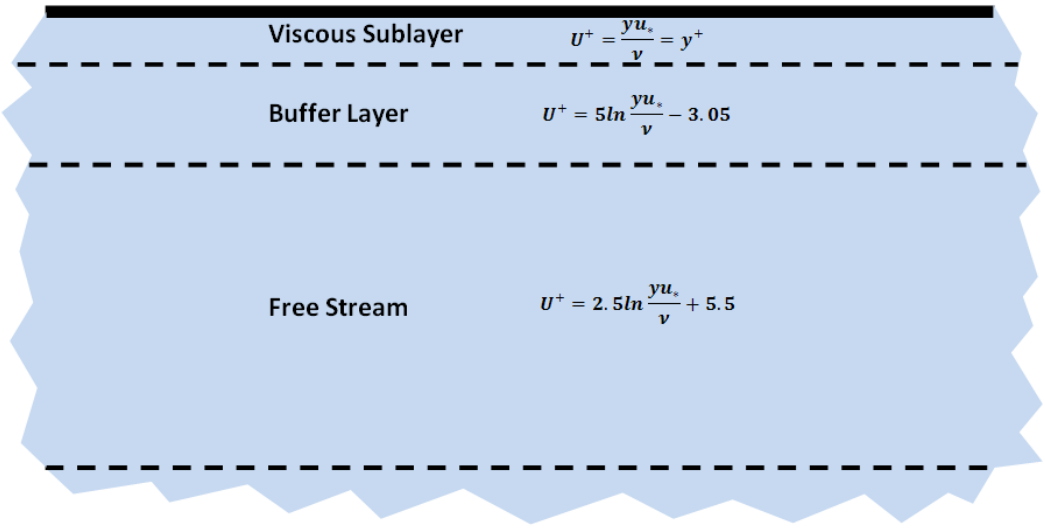

Figure 6: Three regions modeled in turbulent flow.

With the values for U^+ fully defined in the three regions, the transport of energy by means of heat diffusion and momentum are now the focus. A model for the eddy momentum diffusivity is used from dimensional analysis by Datta (Datta 1993),

$$\epsilon_r = \frac{\epsilon_m}{\nu} = sinh^4\left(\frac{U^+}{\alpha}\right)\left\{1 - \frac{sinh\left(\frac{\beta U^+}{\alpha}\right)}{sinh\left(\frac{\delta\beta U^+_{max}}{\alpha}\right)}\right\} \tag{26}$$

where it is determined that the universal constants $\alpha, \delta,$ and β are equal to 10.25, 1.008 and 4.17 respectively. This model ensures that the eddy momentum becomes $\frac{\epsilon_m}{\nu} = \sinh^4\left(\frac{U^+}{\alpha}\right)$ as y^+approaches zero. The eddy momentum is then used to describe how the bulk flow of the fluid is diffusing the heat using the Péclet number for turbulent flow. This is calculated by multiplying the ratio of the inertial and viscous forces in the Eddy momentum and kinematic viscosity by the dimensionless Prandtl number to get a turbulent Peclet number,

$$Pe_t = \epsilon_r Pr. \tag{27}$$

Pe_t is then used to calculate a turbulent Prandtl number which describes the ratio of molecular diffusion due to momentum transport to the molecular diffusion of heat, (Kays 1994)

$$Pr_t = \frac{2.0}{Pe_t} + 0.85. \tag{28}$$

With the eddy momentum already calculated from equation (26), the turbulent thermal conductivity can now be calculated using

$$k_t = \frac{C_p \epsilon_m \rho}{Pr_t} \tag{29}$$

which is simply added to the thermal conductivity of the fluid to arrive at the effective thermal conductivity for turbulent flow in the tube

$$k_{eff} = k + k_t. \tag{30}$$

Plotting the effective thermal conductivity as a function of nondimensional radius for several Reynolds numbers can be seen in Figure 7.

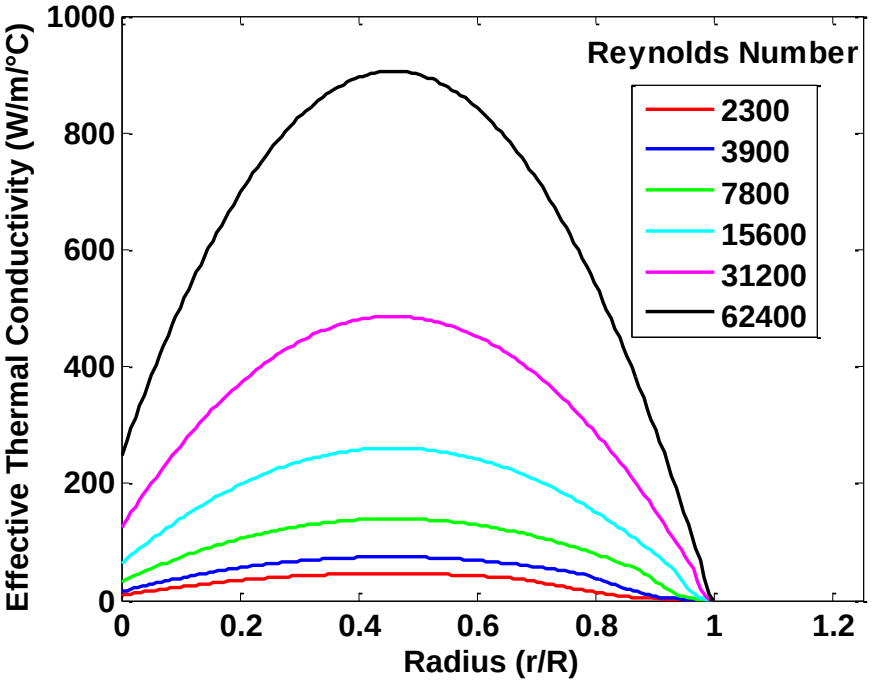

Figure 7: Effective thermal conductivity profiles.

The profile across the diameter of the pipe reveals an area in the middle of the pipe where the eddies are less prominent and result in lower thermal diffusion. Though it is difficult to see in the plot, the effective thermal conductivity receives no contribution to the turbulent equations when $\frac{r}{R} = 1$, making $k_{eff} = k$.

CHAPTER 4

HEAT PUMP MODEL

The geothermal analysis program is coupled with a heat pump model that uses an extensive coefficient of performance (COP) trend study, correction factors, and energy balance. The model is developed by using the performance data from 18 units in the Trane line of water to air heat pumps (Trane November 2010). The data analyzed provides the necessary information to define the COP as a function of the entering fluid temperature, fluid volume flow, entering air temperature, air volume flow and antifreeze concentration. The method used and the equations that result can be seen in the following sections.

4.1 COP Trend Study

A subroutine modeling a geothermal heat pump unit is executed within each time step of the ground loop simulation. The performance data is supplied with COP's for different fluid volume flows and entering water temperatures. A crude model could be developed using this data although this would neglect the indoor temperature, air flow, and antifreeze concentration factors. The most accurate model possible must include these factors and that is why the COP will be dissected into its constituents for a complete

correlation study. That is to say, equations for the capacity and power are individually studied. The hourly Energy Efficiency Ratio (EER) value can be calculated and converted to a COP value for rated conditions using the following equations for cooling and heating respectfully,

$$COP_C^u = \frac{CC^u}{CP^u} \times 0.29287 \quad (31)$$

and

$$COP_H^u = \frac{HC^u}{HP^u} \times 0.29287 \quad (32)$$

where

CC is the Gross Cooling Capacity (Mbtuh) of unit number u

CP is the compressor power (kW) of unit number u

HC is the Gross Heating Capacity (Mbtuh) of unit number u

HP is the compressor power (kW) of unit number u

The multiplying constant is a unit conversion from EER to COP.

To develop an equation for cooling capacity, the data is plotted versus the fluid volume flow in $\frac{m^3}{sec}$ for all eight entering water temperatures (EWT) provided in the performance data. A plot of each curve for a 3 ton unit can be seen in Figure 8. It is important to note that the capacity data is in English units while all other data is in metric units. This was done to easily check the gross capacity and compressor power calculations to the performance data, while also being necessary to calculate the EER properly.

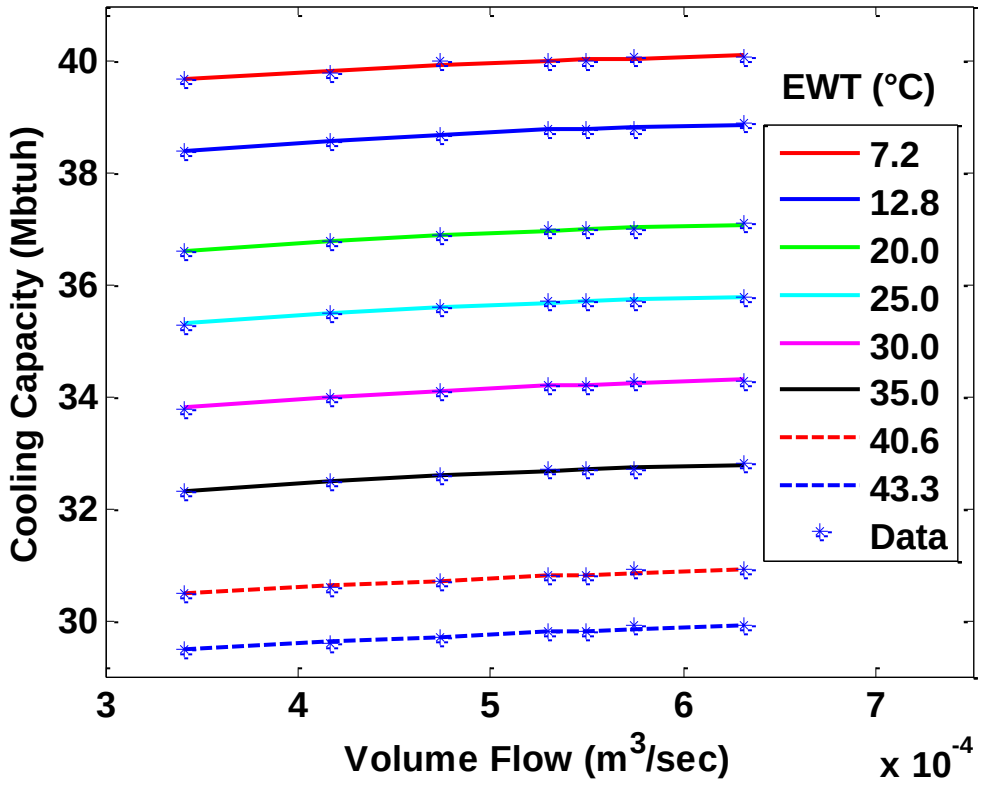

Figure 8: Cooling capacity vs. fluid flow for different entering water temperatures (Trane November 2010).

Each of the curves can now be described as a second order quadratic equation taking the form

$$CC^u = A^u_{CC}\dot{v}^2 + B^u_{CC}\,\dot{v} + C^u_{CC}. \tag{33}$$

It is recognizable that the curve and slope of each of the different sets of data appears to be somewhat constant. The coefficient A^u_{CC} from equation (33) is then plotted versus the entering water temperature for every heat pump unit size. A second order polynomial is then fit to the data and the curve describing the 3 ton unit number 8 can be seen in Figure 9.

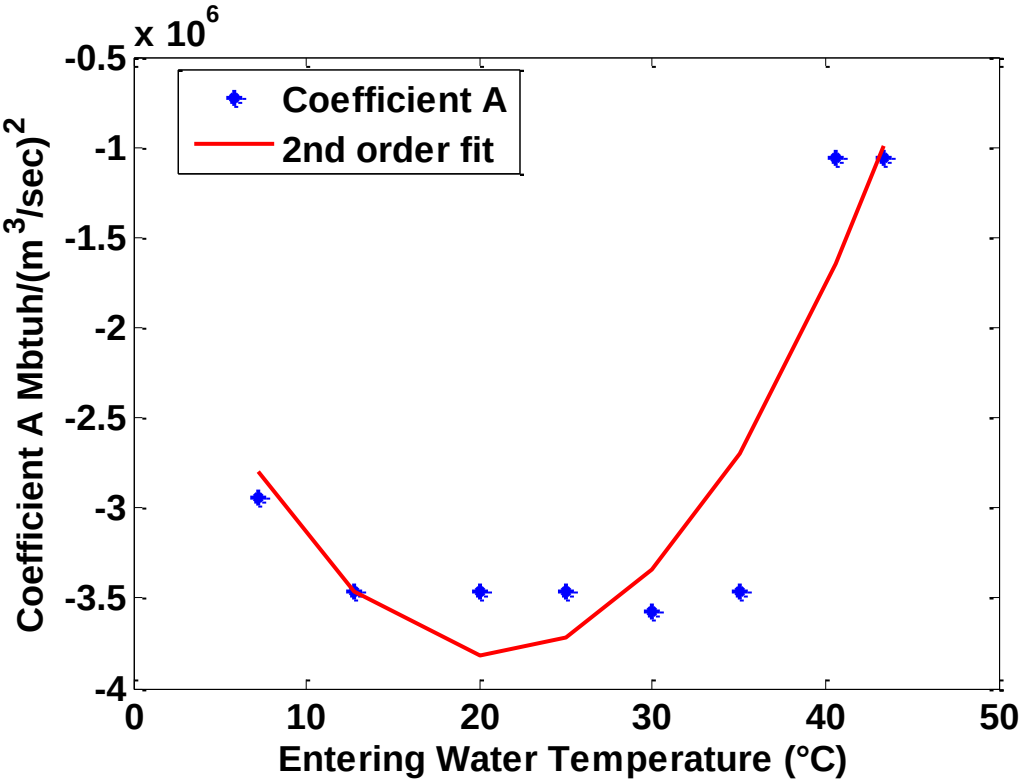

Figure 9: Coefficient A vs. entering water temperature for 3 ton unit #8.

The coefficient A_{CC}^{u} can now be written as

$$A_{CC}^{u} = a_{CC}^{u} EWT^2 + b_{CC}^{u} EWT + c_{CC}^{u} \tag{34}$$

where EWT is the entering water temperature in Celsius. The coefficients a_{CC}^{u}, b_{CC}^{u} and c_{CC}^{u} for all eighteen heat pump sizes can be found in the appendix. This coefficient describes how much the data curves in Figure 8, as the volume flow changes. At lower EWT's, the coefficient A_{CC}^{u} has larger magnitudes suggesting that the capacity is changing more with volume flow. The behavior of coefficient A_{CC}^{u} at higher EWT's suggests that the cooling capacity is dominated more by the water temperature than the volume flow.

The next coefficient to describe the cooling capacity CC^{u} in equation (31), is the linear term B_{CC}^{u}. Plotting each of the coefficients versus the respective entering water temperature, the curve and coefficient B_{CC}^{u} data points can be seen in Figure 10.

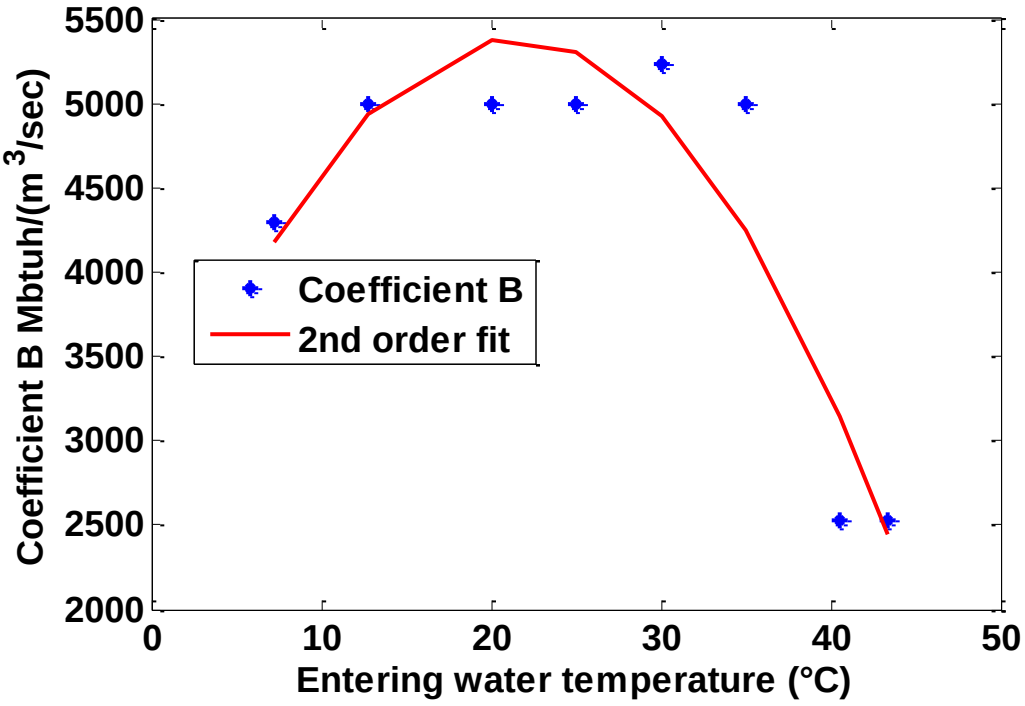

Figure 10: Coefficient B vs. entering water temperature for 3 ton unit #8.

The coefficient B_{CC}^{u} can now be written as

$$B_{CC}^{u} = d_{CC}^{u} EWT^2 + e_{CC}^{u} EWT + f_{CC}^{u} \tag{35}$$

where again, the coefficients d_{CC}^{u}, e_{CC}^{u} and f_{CC}^{u} for all eighteen heat pump sizes can be found in the appendix. The behavior of coefficients A_{CC}^{u} and B_{CC}^{u} appear to be mirror images of each other and somewhat sporadic. The behavior of coefficient B_{CC}^{u} is describing the slope of the curve from Figure 8. The slope at higher temperatures has decreased, suggesting that the cooling capacity becomes more dependent of the EWT than the volume flow at higher temperatures.

The final coefficient describing the cooling capacity is the constant term, C_{CC}^{u}. This term is what truly dominates the equation and after performing a second order regression, Figure 11 shows the correlation between coefficient C_{CC}^{u} and EWT.

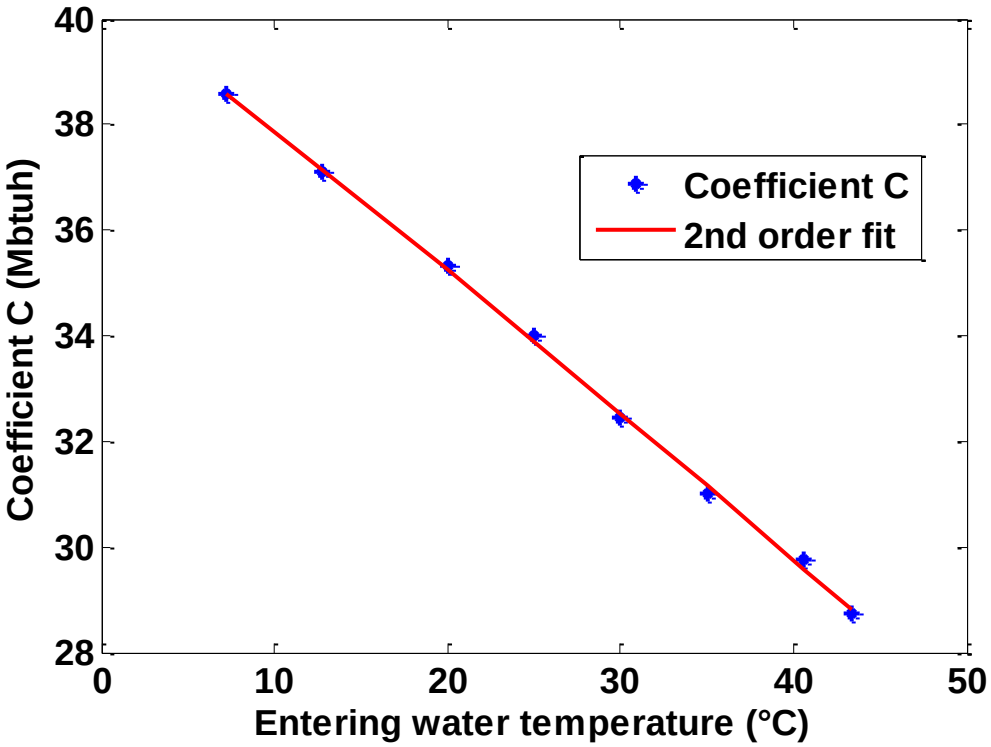

Figure 11: Coefficient C vs. entering water temperature for 3 ton unit #8.

The coefficient C_{CC}^{u} can now be written as

$$C_{CC}^{u} = g_{CC}^{u} EWT^2 + h_{CC}^{u} EWT + i_{CC}^{u} \tag{36}$$

and plugging into the original polynomial produces one equation for the cooling capacity

$$CC^{u} = (a_{CC}^{u} EWT^2 + b_{CC}^{u} EWT + c_{CC}^{u})\dot{v}^2 + (d_{CC}^{u} EWT^2 + e_{CC}^{u} EWT + f_{CC}^{u})\,\dot{v} + (g_{CC}^{u} EWT^2 + h_{CC}^{u} EWT + i_{CC}^{u}). \tag{37}$$

When plugging in the values for the coefficients a_{CC}^{u}, b_{CC}^{u}, c_{CC}^{u}, d_{CC}^{u}, e_{CC}^{u}, f_{CC}^{u}, g_{CC}^{u}, h_{CC}^{u} and i_{CC}^{u} for unit #8, and using the rated volume flow of 8.4 $\frac{gal}{min}$ =0.0005299 $\frac{m^3}{sec}$, and an entering water temperature of 25 °C, the cooling capacity is calculated to be

35.66 Mbtuh. The supplied performance data shows the cooling capacity of unit number 8 at 25°C (77°F) to be 35.7 Mbtuh at the rated volume flow. Acceptable volume flows for use with these curves are available in the appendix.

Like the cooling capacity first described in equation (33), the heating capacity, cooling compressor power, and heating compressor power are described as follows for all 18 units studied,

$$HC^u = A^u_{HC}\dot{v}^2 + B^u_{HC}\,\dot{v} + C^u_{HC}, \tag{38}$$

$$CP^u = A^u_{CP}\dot{v}^2 + B^u_{CP}\,\dot{v} + C^u_{CP}, \tag{39}$$

and

$$HP^u = A^u_{HP}\dot{v}^2 + B^u_{HP}\,\dot{v} + C^u_{HP}. \tag{40}$$

After trend studies of the coefficients were completed in the same manner as the cooling capacity trend studies above, the correlated equations for CP^u, HC^u and HP^u are developed as follows for any unit 1 through 18

$$CP^u = (a^u_{CP}EWT^2 + b^u_{CP}EWT + c^u_{CP})\dot{v}^2 + (d^u_{CP}EWT^2 + e^u_{CP}EWT + f^u_{CP})\,\dot{v} + (g^u_{CP}EWT^2 + h^u_{CP}EWT + i^u_{CP}) \tag{41}$$

$$HC^u = (a^u_{HC}EWT^2 + b^u_{HC}EWT + c^u_{HC})\dot{v}^2 + (d^u_{HC}EWT^2 + e^u_{HC}EWT + f^u_{HC})\,\dot{v} + (g^u_{HC}EWT^2 + h^u_{HC}EWT + i^u_{HC}) \tag{42}$$

$$HP^u = (a^u_{HP}EWT^2 + b^u_{HP}EWT + c^u_{HP})\dot{v}^2 + (d^u_{HP}EWT^2 + e^u_{HP}EWT + f^u_{HP})\,\dot{v} + (g^u_{HP}EWT^2 + h^u_{HP}EWT + i^u_{HP}). \tag{43}$$

Using the rated value for the volume flow, and coefficients for unit 8, CP^8 is calculated to be 2.579 kW. Using the values calculated for CC^8 and CP^8 and plugging into equation (31) gives,

$$COP_c^8 = \frac{35.666}{2.579} \times 0.29287 = 4.050 \tag{44}$$

The COP for unit 8 at the rated volume flow and an entering fluid temperature of 25 °C published in the performance data is 4.053. The COP_H^u is calculated in the same way using equation (32) with equation (42) and equation (43). The COP for heating and cooling are plotted in Figure 12 using entering water temperatures from the performance data with the unit rated volume flow. The performance data used was not extrapolated past the published EWT's.

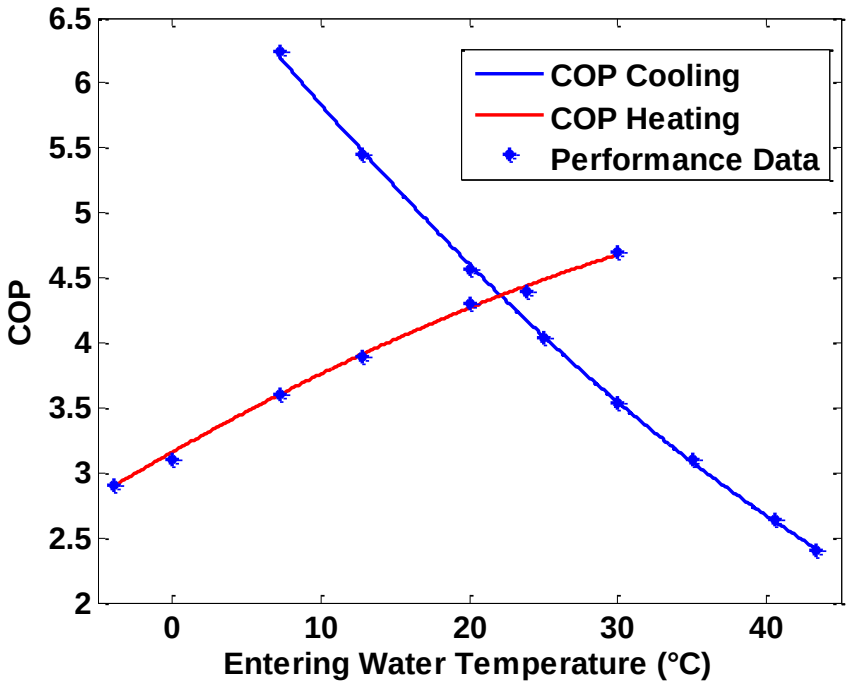

Figure 12: COP for 3 ton unit number 8 at rated volume flow (Trane November 2010).

Using second order polynomials for each coefficient describes the capacities and compressor power well enough to avoid error propagation through to the COP calculation. Evaluating all 18 units in the same manner revealed the largest error to be no

more than 0.7% for any of the capacity or compressor power calculations. Performing the correlation study on the capacity and compressor power, and not just the COP or EER, provides more room for accuracy by using correction factors for the remaining variables.

4.2 Correction Factors

The COP for any heat pump is also a function of the air flow, entering air temperature (EAT) over the heat exchanger, and the percent concentration of antifreeze in the working fluid. The previous calculations were all performed at the manufacturers rated air volume flow, air temperatures, and using water as the working fluid. The correction factors for capacities and compressor power as a function of the EAT are plotted in Figure 13. The rated EAT can be seen where the correction factor is equal to one. It is important to note that the EAT for cooling is the wet bulb temperature while for heating it is the dry bulb temperature. Calculation of the wet bulb temperature is discussed in section 4.4.

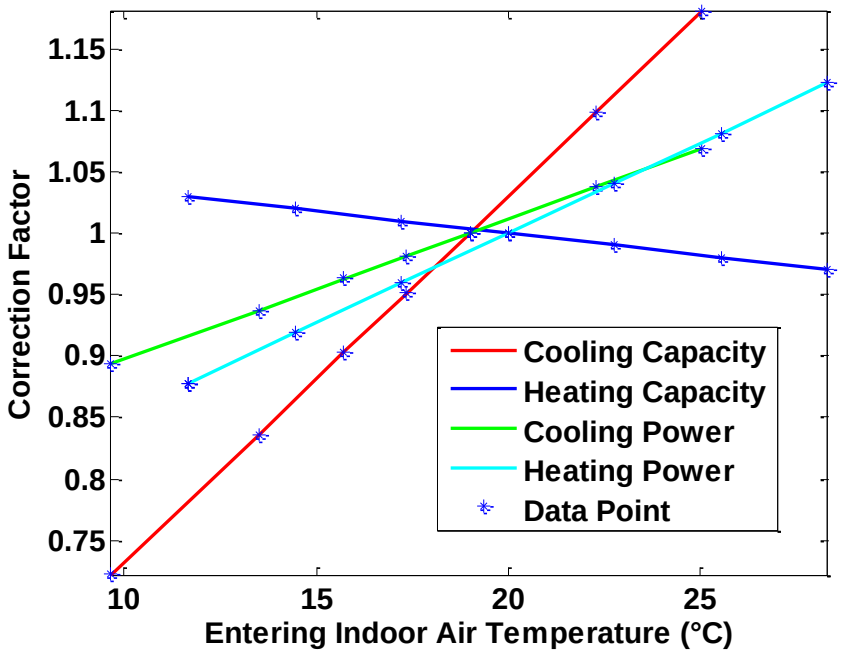

Figure 13: Correction factors for entering air temperature (Trane November 2010).

The need to fit the EAT correction factors with second order polynomial is more evident in the larger units, while the squared term for smaller units can be set to zero. The entering air temperature correction factor coefficients for all 18 units can be found in the appendix. Writing out the equations for the EAT correction factors are as follows

$$CF^{u}_{T_{db}} = A^{u}_{CF} {T_{db}}^{2} + B^{u}_{CF}\, T_{db} + C^{u}_{CF} \tag{45}$$

and

$$CF^{u}_{T_{wb}} = A^{u}_{CF} {T_{wb}}^{2} + B^{u}_{CF}\, T_{wb} + C^{u}_{CF}, \tag{46}$$

where T_{db} and T_{wb} are the indoor dry bulb temperature and indoor wet bulb temperature respectively.

The second set of correction factors is a function of the air volume flowing over the heat exchanger, plotted in Figure 14. Again the rated air volume flow for this heat pump can be seen where the correction factor is equal to one.

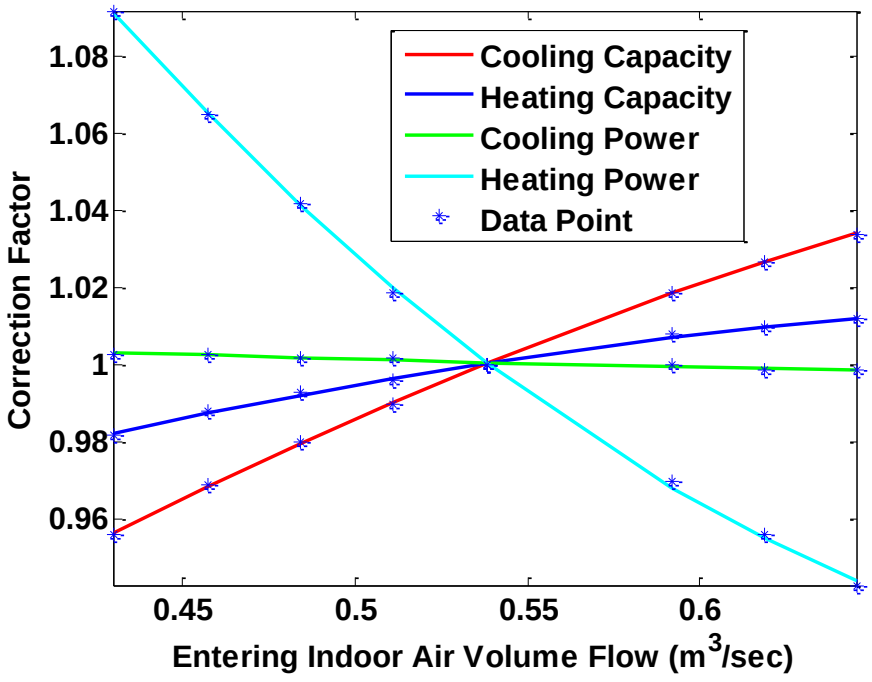

Figure 14: Correction factor for indoor air volume flow (Trane November 2010).

These curves can now be expressed as

$$CF_{\dot{V}}^{u} = A_{CF}^{u}\dot{V}_{air}^{2} + B_{CF}^{u}\dot{V}_{air} + C_{CF}^{u} \tag{47}$$

where $\dot{V}_{air}$ is the indoor air volume flow in $\frac{m^3}{sec}$. Equation (47) can be used for both heating and cooling as well as for capacity and compressor power. Each coefficient can be found in the appendix for all units in the study. The final set of correction factors is found for concentrations of methanol, ethylene glycol and propylene glycol from zero to fifty percent. The correction factor as a function of percent concentration of ethylene glycol can be seen in Figure 15.

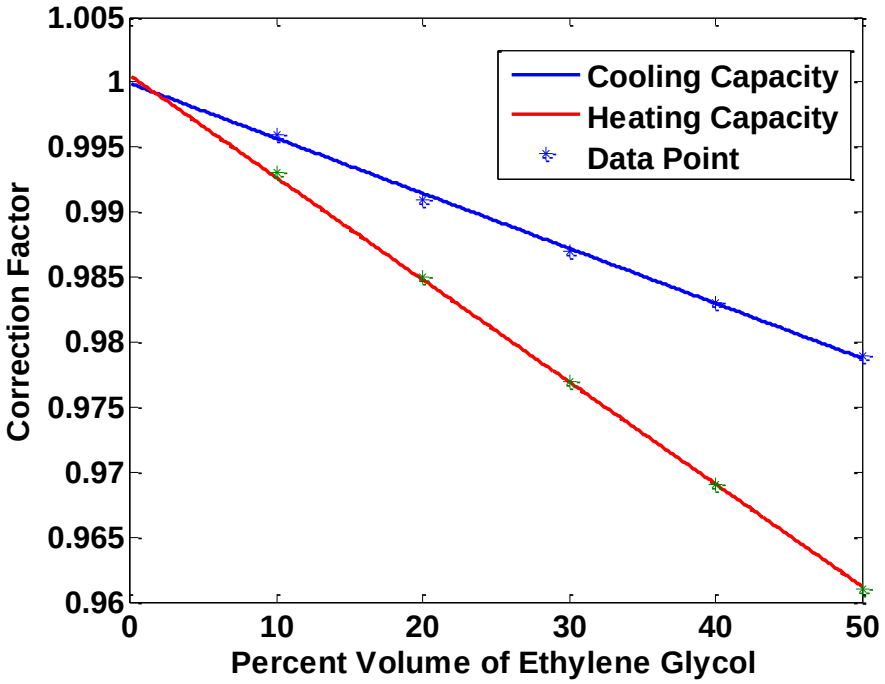

Figure 15: Correction factor for capacity as a function of concentration of antifreeze (Trane November 2010).

The linear regression analysis allows the equation for capacity correction factor to be written as

$$CF_{\%af}^{u} = A_{CF}^{u}(\%af) + B_{CF}^{u} \tag{48}$$

where $\%af$ is the percent concentration of antifreeze. Coefficients for all three types of antifreeze can be seen in the appendix. Finally, with the correction factors $CF^u_{T_{db}}$, $CF^u_{T_{wb}}$, $CF^u_{\dot{V}}$ and $CF^u_{\%af}$, the equations for COP become

$$COP^u_C = \frac{CF^u_{\%af} CF^u_{\dot{V}} CF^u_{T_{wb}} CC^u}{CF^u_{\dot{V}} CF^u_{T_{wb}} CP^u} \times 0.29287 \tag{49}$$

and

$$COP^u_H = \frac{CF^u_{\%af} CF^u_{\dot{V}} CF^u_{T_{db}} HC^u}{CF^u_{\dot{V}} CF^u_{T_{db}} HP^u} \times 0.29287. \tag{50}$$

The variables necessary to calculate the COP for cooling and heating are now

$COP^u_C(\dot{v}, EWT, T_{wb}, \dot{V}_{air}, \%af)$

and

$COP^u_H(\dot{v}, EWT, T_{db}, \dot{V}_{air}, \%af)$ respectively.

The variables $\dot{v}$, $\dot{V}_{air}$ and $\%af$ are user defined and will remain constant throughout the calculation. The variable, T_{db}, is determined in the load calculations through EnergyPlus and changes every time step. This leaves EWT and T_{wb} to complete the heat pump model.

4.3 Entering Water Temperature

Upon convergence of the temperature field in each time step, the temperature of the fluid exiting the loop becomes the entering fluid temperature to the heat pump. The bulk fluid temperature is then determined for the working fluid exiting the pipe. Using the velocity profile $u(r)$ discussed in Chapter 3 and the temperature profile $T(r)$, calculated at every iteration, the energy in the fluid is integrated and divided by the mass flow and specific heat. The bulk fluid temperature is then determined as

$$T_m = \frac{\int_0^R C_p T(r) \rho u(r) 2\pi r dr}{\rho V_{ave}(\pi R^2) C_p} = EWT. \quad (51)$$

The idealized result can be seen in Figure 16 where the rate at which the energy is transported with the fluid is the same in either case (Cengel 2007).

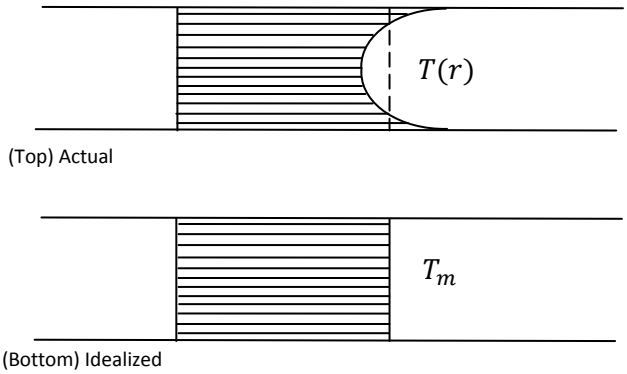

Figure 16: Temperature profiles for flow in a tube

The numerator in Equation (51) is the sum of the energy being delivered to the heat pump from the loop. The change in energy across the heat pump is then calculated using the first law of thermodynamics. The thermodynamic heat pump and refrigeration cycle equation is used

$$Q_L + W_{in} = Q_H \quad (52)$$

where, for heating:

Q_L is the change in energy transported by the fluid, Q_H is the simulated hourly building load and W_{in} is the building load divided by the COP_H, or work done on the system.

and for cooling:

Q_L is the simulated hourly building load, Q_H is the change in energy transported by the fluid, and W_{in} is the building load divided by the COP_C.

The temperature of the fluid leaving the heat pump and entering back into the loop is then calculated using

$$T_{bulk} = T_m - \frac{\Delta E}{\rho V_{ave}(\pi R^2) C_p}. \quad (53)$$

It is important to note that the sign convention must remain negative for cooling and positive for heating throughout the calculation. This method assumes that the fluid fully mixes and achieves a uniform temperature profile before leaving the heat exchanger. This uniform temperature profile then becomes the entering fluid temperature to the geothermal ground loop for the next iteration of the time loop.

4.4 Calculating Wet Bulb Temperature

The EnergyPlus building loads output file was set up to provide the inside dry bulb temperature T_{db} and the humidity ratio ω_1. The wet bulb temperature is the temperature the air would be if allowed to cool adiabatically to saturation by evaporating water into it. In a thermodynamic process the wet bulb temperature can be understood and calculated from knowing the properties of the state. A schematic of the thermodynamic process can be seen in Figure 17.

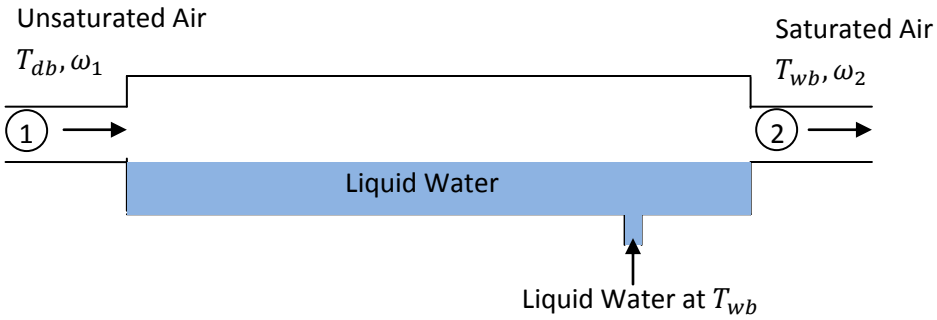

Figure 17: Adiabatic saturation process

In order to calculate the indoor wet bulb temperature, a trial and error solution must be followed using the following equation

$$T_{wb} = \frac{(\omega_1(h_{g,1} - h_{f,2}) - (\omega_2 h_{fg,2}) + T_{db} C_p)}{C_p} \tag{54}$$

where h is the enthalpy and C_p is the specific heat of air. The specific humidity at state two is then calculated using

$$\omega_2 = \frac{0.622 P_{g,2}}{P_{atm} - P_{g,2}} \tag{55}$$

The values for P_g, h_g and h_f can be found in the water tables. These values were plotted and fit with an equation as a function of the temperature. The curves used for P_g, h_g and h_f can be seen in Figure 18.

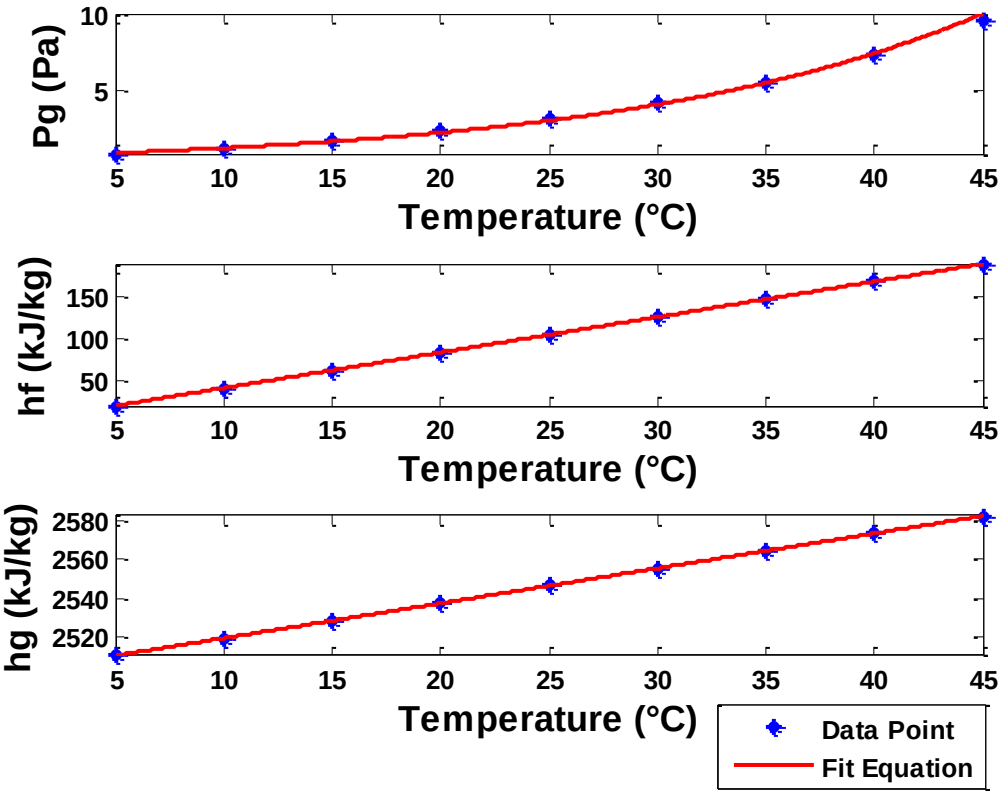

Figure 18: Vapor pressure, fluid enthalpy, and vapor enthalpy plotted and fit.

The pressure as a function of temperature is fit with an exponential function taking the form

$$P_g = 0.6834 e^{0.0599T}. \tag{56}$$

The energy in the fluid at temperature *T* is fit linearly along with the energy in the vapor. These two equations are then subtracted from one another to give h_{fg} as seen in the following equations.

$$h_f = 4.1845T + 0.1789, \tag{57}$$

$$h_g = 1.8097T + 2501.2, \tag{58}$$

and $$h_{fg} = -2.3748T + 2501.0211. \tag{59}$$

The wet bulb temperature can now be calculated and used in the correction factor for cooling capacity and cooling compressor power. This is done each time step in an iterative process when cooling is needed from the heat pump.

CHAPTER 5

ECONOMICS

A cost analysis is performed to evaluate whether geothermal heating and cooling is a more attractive option over conventional systems. The size and initial cost of the system, fuel costs, efficiencies, and interest rate all contribute to the cost over time. The hourly loads, hourly COP (in the case of the air-to-air heat pump and the vapor compression air conditioner), and weather information is used to simulate conventional systems for comparison. The time value of money with a user defined interest rate and initial system costs are plotted and show the time required to pay back the initial investment on the geothermal system. The user also has the option of changing the efficiencies of the conventional units for further detail.

5.1 Pricing Unit and Installation Costs

The potential of the data generated from the building load calculations and the geothermal analysis are fully realized when applied to a payback period calculation. The initial cost of the geothermal system is estimated using pricing from heat pump, trenching/drilling, installation, water pump, and material costs. The heat pump unit cost was found to be an average cost of $835.21/ton (D.O.E. 2010). The trenching costs were estimated from some local companies to be $2/foot for 5 foot depth including back filling

and $9/foot for 10 foot depth. The drilling costs were estimated at $10/foot but will vary greatly depending on the specific job. The water pump and material costs were found in a catalog from geo-hydro supply (Geo-Hydro 2011). A function for the price per foot was derived with the catalog information and used to extrapolate other pipe sizes for theoretical circumstances. The cost per linear foot as a function of the diameter can be seen in Figure 19.

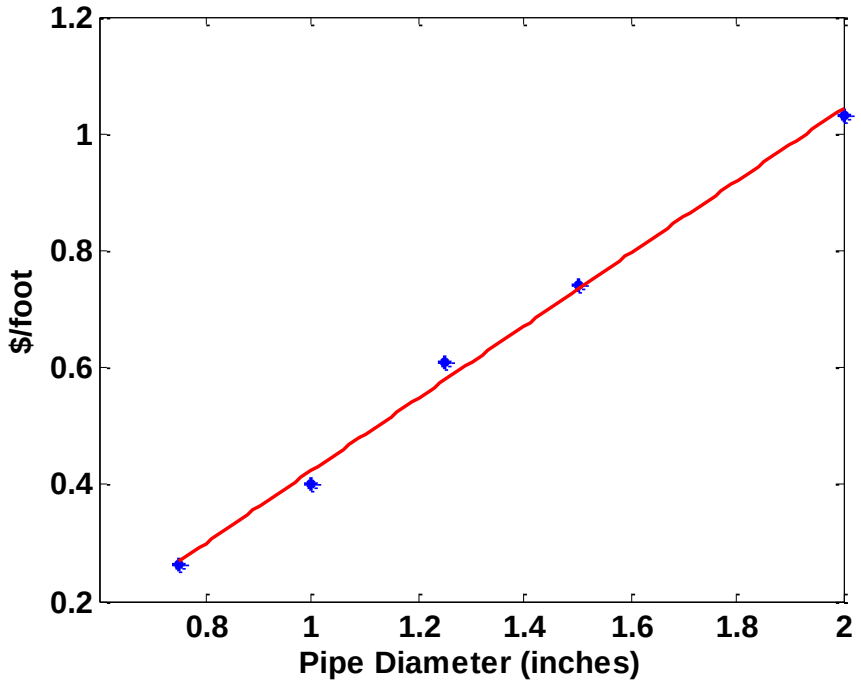

Figure 19: Price per foot of geothermal tubing.

The water pumps ranged from $300 to $2000 and were determined linearly depending on the size of the heat pump. With these initial cost estimations, the designer can determine cost savings based on accurate sizing of the system. These values are all hard coded into the program and will require updating in the future.

5.2 Operational Costs

The operating costs for five different systems are calculated using the hourly building load data. The natural gas, fuel oil, and propane systems are simulated with a vapor compression air conditioner for the cooling needs. Every conventional unit has the user option to change its efficiency with the exception of the geothermal system, since its COP has already been determined in the geothermal analysis. The price for the fuel to run each unit has a default value, but can be changed depending on where the user is located and the particular price of the fuel. It is known that the price of some fossil fuels change from day to day and the cost of electricity can change from region to region. The geothermal systems hourly operational cost is calculated using

$$Hourly\ Geothermal\ Cost = \frac{Q_{Load}(Wh)}{COP_{geo,hourly}} \cdot \frac{1kWh}{1000Wh} \cdot \frac{\$}{kWh_{elect.}} + \frac{W_{pump}}{eff_{pump}} \cdot \frac{\$}{kWh_{elect.}}. \quad (60)$$

If the user chooses a run-time step larger than hourly for the geothermal analysis, then the hourly COP is approximated. The air-to-air heat pump operational cost is modeled similarly to the geothermal cost calculation, with a few differences. The first difference is that a COP function was developed for cooling and heating as a function of outdoor air temperature. This was done for five different seasonal energy efficiency ratings (SEER). The cooling data is a function of the air volume flow and wet bulb temperature as well; however, the curves are plotted using the rated values.

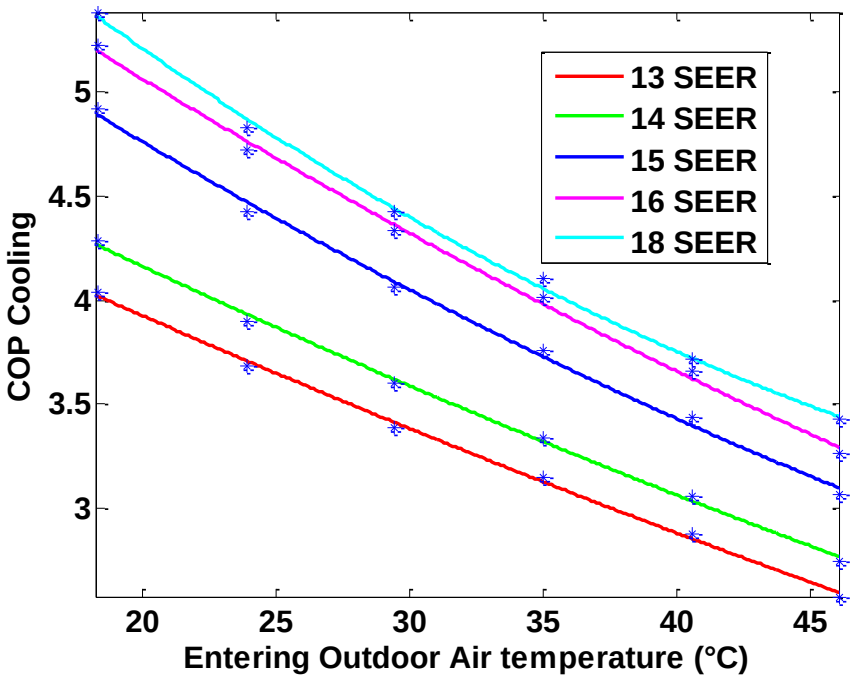

Figure 20: COP for air-to-air heat pump in cooling mode.

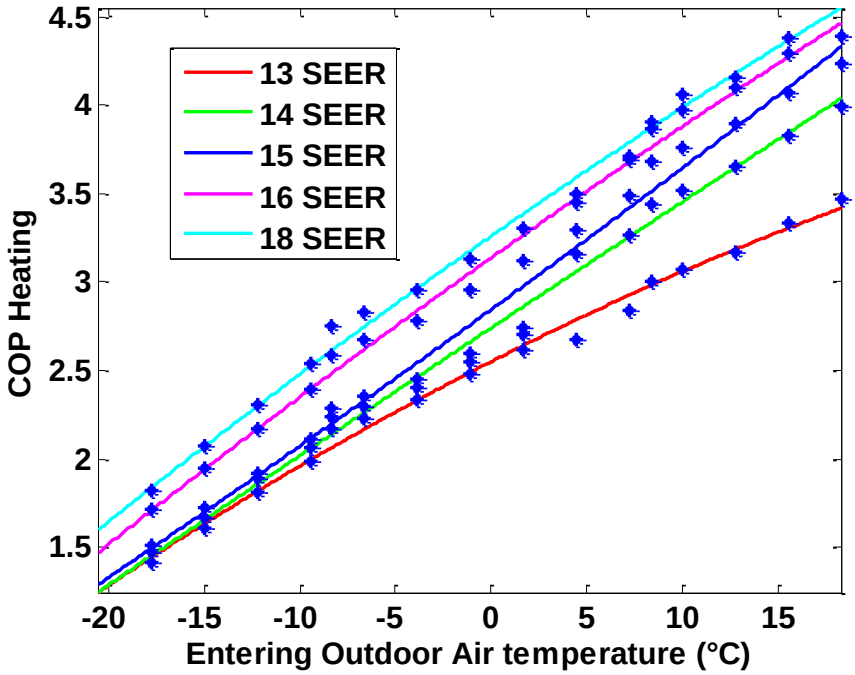

Figure 21: COP for air-to-air heat pump in heating mode.

The equation developed for each is used in the hourly calculations for hourly air-to-air cost, except when the outdoor temperature is less than -5 degrees Celsius. Then the COP is set equal to one to simulate a backup electric resistance heating system. The air-to-air system's hourly operational cost is calculated using

$$Hourly\ Air-to-Air\ Cost = \frac{Q_{Load}(Wh)}{COP_{airhp,hourly}} \cdot \frac{1kWh}{1000Wh} \cdot \frac{\$}{kWh_{elect.}}. \quad (61)$$

To model the natural gas furnace operational costs, the hourly heating load is divided by the furnace efficiency. A value for the energy available for combustion per cubic foot of natural gas was found to be approximately $292\ \frac{Wh}{ft^3}$ (Cengel and Boles 2008). This makes the hourly cost equation for natural gas heating,

$$Hourly\ Natural\ Gas\ Heating\ Cost = \frac{Q_{Load}(Wh)}{eff_{ng}} \cdot \frac{1ft^3}{292Wh} \cdot \frac{\$}{ft^3}. \quad (62)$$

The hourly loads that are negative, referring to cooling needs, is modeled using the COP cooling study from Figure 20. The user-defined SEER value are used to simulate any efficiency of an air conditioner. This will allow the user to model several different combinations of cooling and heating systems including ultra-high efficient systems.

The propane and fuel oil systems are modeled the same way as the natural gas using $40{,}883\ \frac{Wh}{gal}$ for fuel oil and $26{,}945\ \frac{Wh}{gal}$ for propane energy content (Cengel and Boles 2008). The cooling needs of these systems are also modeled using the vapor compression model as discussed above. The equations for fuel oil and propane hourly operational heating are

$$Hourly\ Fuel\ Oil\ Heating\ Cost = \frac{Q_{Load}(Wh)}{eff_{oil}} \cdot \frac{1gal}{40{,}883Wh} \cdot \frac{\$}{gal} \quad (63)$$

and

$$Hourly\ Propane\ Heating\ Cost = \frac{Q_{Load}(Wh)}{eff_{pr}} \cdot \frac{1gal}{26{,}945Wh} \cdot \frac{\$}{gal}. \quad (64)$$

The hourly operational costs over an entire year for each system now make it possible to more accurately calculate the operational costs and couple them with the initial system costs for payback periods.

5.3 Payback Period

To more accurately calculate the payback period of the geothermal system compared to conventional systems, including the time value of money is necessary. The initial value of the different systems is entered by the user to represent the total installation and equipment costs of the system. In the case of geothermal this would be the cost of the trenching or drilling, pipe materials, water pumps, installation, and heat pump. With the yearly operational cost for each system calculated as described in the previous section, a multiyear scenario will show which system costs the user the least over time. To do this, the user will enter the desired number of years to calculate along with the interest rate to be used. The present day dollar value of the system at year n is calculated by adding the present day value of the operational cost at the end of year n to the previous year's present value using

$$PV = \sum_{t=0}^{n} \frac{FV_t}{(1+i)^t} \tag{65}$$

where the present value of the operational cost is calculated for n years at interest rate i. The present value of each system is then plotted and the iteration repeats, giving a curve of present day cost over time. The point, at which the geothermal curve crosses the conventional system's curve, is the year at which the geothermal system has paid for itself. A screen shot of the economics page can be seen in Figure 22 as an example of what the user will see.

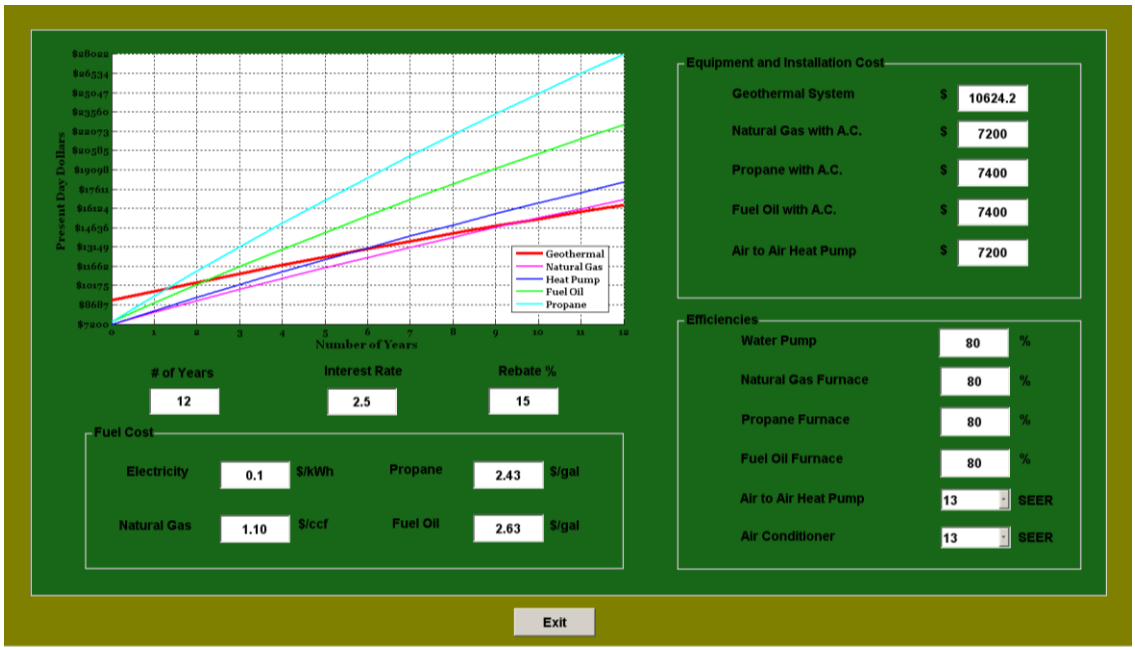

Figure 22: Screen Shot of the Economics Page.

Using this tool, the designer can see how changing certain parameters of the geothermal design will ultimately affect the final cost. By using the hourly load data with the heat pump model, a designer can see what economic impact a system will have by reducing the length or size of pipe, types of fluid, or even the geothermal configuration itself.

CHAPTER 6

GUI DESIGN

The user interface was written in MATLAB and was designed to allow the user to easily input the many design parameters needed for a geothermal system design. The home screen was written so the user will be guided through the program, enabling screens and buttons when the necessary information has been entered. Upon selection of a new project, the user designates a folder in the 'project files' directory where the raw data is stored. A file in the 'project files' directory with the name supplied is stored and is to be selected whenever the user returns to the project in the future. Once the user names a new project, the units and location are selected and will be locked in throughout the program. Upon selection of the location, the weather file associated with that location is copied to 'in.epw' for use in the EnergyPlus simulator.

6.1 Building Specifics

The next step in the program is for the user to design the building or home. The user can do this on their own or use an already drawn .idf input file to convert for use with the geothermal program. As seen in Figure 23 the user is asked to choose either 'novice' or 'expert' for use with EnergyPlus.

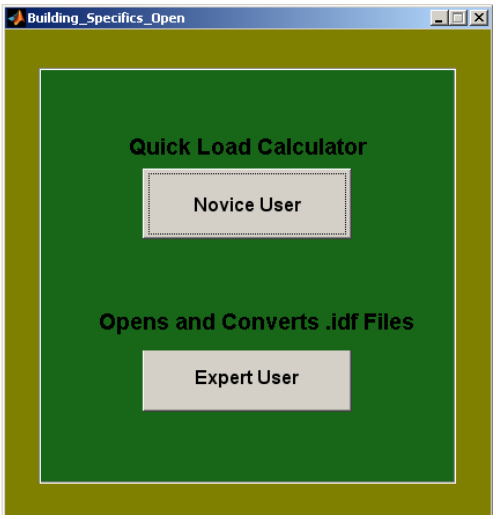

Figure 23: Building specifics options GUI.

The flow through the 'Building Specifics' can best be described in a flow chart where both choices lead to hourly loads and other data needed for the geothermal analysis.

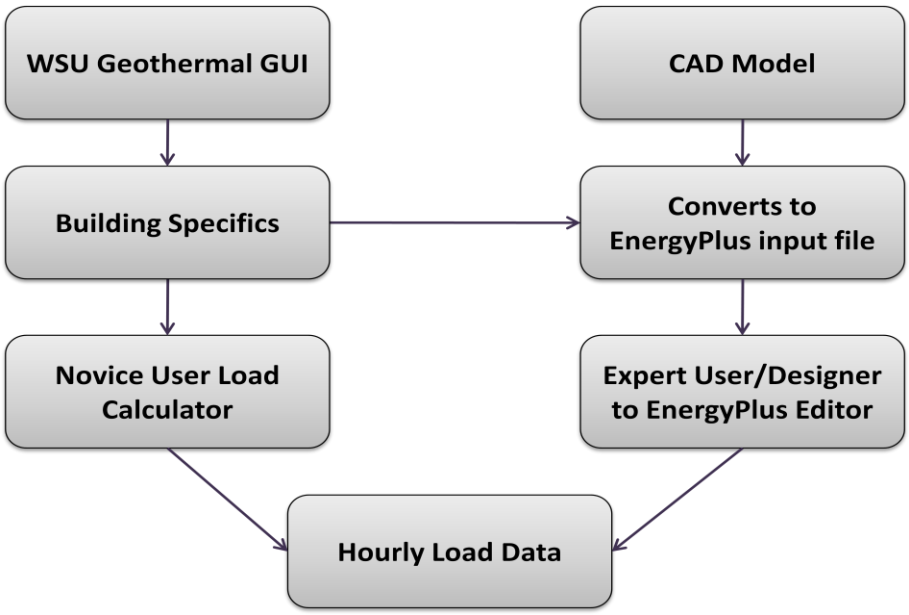

Figure 24: Flow chart of the building specifics GUI.

6.1.1 Novice User

The 'novice' choice does not require the user to know anything about EnergyPlus or how it exports data. The user is displayed a screen which consists of different shaped floor plans to choose. When the user selects one, boxes are enabled for the dimensions of the areas. The '.idf' input file is written specifically to these shapes and any complex geometry or overhangs should be done in the expert section. An example of the building specifics GUI can be seen in Figure 25.

Once the user has selected the floor plan and dimensions of the space, a second story option and ground conditions are chosen. The second floor option allows the user to input dimensions up to the same size as the first floor. The ground condition was modeled as the four most common types; unconditioned basement, conditioned basement, crawl space, and slab. These conditions are all modeled differently in EnergyPlus, but are easily chosen and analyzed in the GUI.

The unconditioned basement is modeled as a separate zone with concrete walls, slab floor, eight foot ceilings and no insulation. The concrete walls are modeled using the 'C-Factor' method of construction in EnergyPlus. The value for the C-factor was chosen from the ACM Joint Appendix on page 4-37, in a table of C-factors for masonry walls (ASHRAE n.d.). The chosen C-factor is for empty medium density concrete masonry units. The concrete floor is modeled using the F-factor method and the value for the F-factor was modeled as having no insulation. The conditioned basement model was done in the same manner, with the exception of having been modeled with wood framed insulated walls and floors, and equipped with a thermostat that is set to maintain the desired temperature. The concrete slab option was modeled using the F-factor method for on-grade with 36 inches of insulation around the perimeter of the slab. The crawl space was modeled using an option in EnergyPlus called 'OtherSideCoefficients', where the floor is given a convective heat transfer coefficient of $0.51\frac{W}{m^{2}\text{°C}}$ to simulate a vented space.

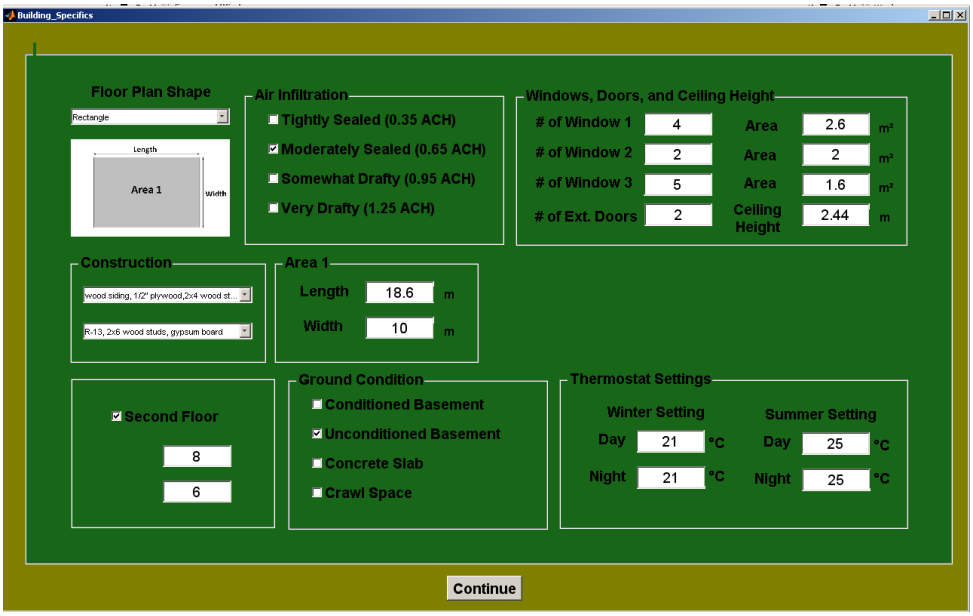

Figure 25: Novice load calculator.

The user must now select the air infiltration desired to be modeled. Equally spaced values, from a tightly sealed construction to a loosely constructed home is available to choose. The values are given in air changes per hour ACH, which indicates how many times all of the air in the zone is exchanged with outdoor air in a one hour time period. This is also how this heat exchange process is entered into EnergyPlus. Anything below 0.35 ACH is not recommended due to a lack of fresh air in the zone causing health problems (ASHRAE n.d.). Any value above 1.25 ACH is considered to be extremely drafty; any other infiltration conditions should be modeled in the expert option.

The novice user is given the option to enter three different sized windows but does not have to specify their location; the model treats it as a square area of window and divides it equally among the wall area. The exterior door is modeled as a multiplier and is set to a standard size of 3 feet wide by 7 feet tall. The material is modeled with layers of metal with insulation board between. Any complex door conditions should be modeled in the expert option.

The user must now select the construction of the exterior walls and ceiling using the dropdown menu. These constructions were supplied in the EnergyPlus's

'compositewallconstruction.idf' file and could be added to for more options in the future. The ceiling height is then entered and the user can now enter the desired thermostat temperature for the heating and cooling season for both day and night settings. With these values selected, the user clicks on the 'continue' button; the input file is written, the thermostat template is expanded, EnergyPlus is executed and the load simulation begins.

6.1.2 Expert User

If the user were to select the 'expert' button, a page will pop up giving the option of converting an already existing input file, from a CAD drawing, or simply opening without converting. The 'convert' button, seen in Figure 26, should only be used to input a file drawn in CAD using OpenStudio and not for already started projects. This button collects all of the geometry needed to virtually draw the building in the simulation and adds it to some scheduling, materials, constructions, and outputs so that the tedious process of adding these things can be avoided.

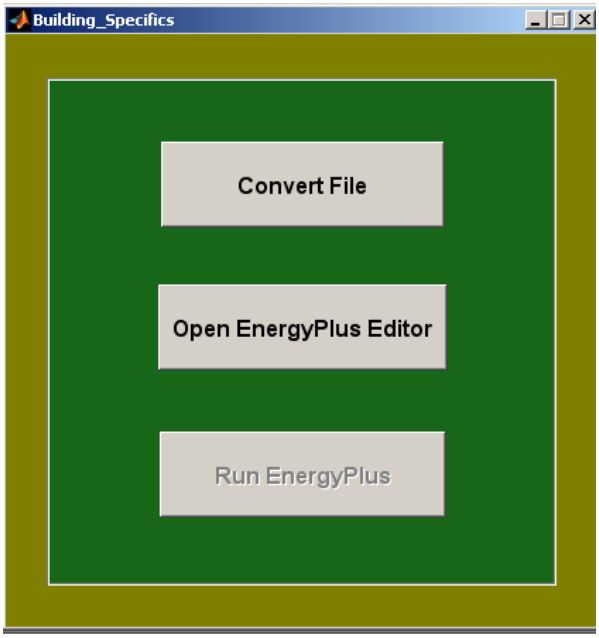

Figure 26: Expert options for load calculations.

Once a file has been converted, the user is asked to select the zones that are to be analyzed for a single heat pump, and the EnergyPlus editor is launched for the designer to make any changes. The designer now has full access to the entire EnergyPlus program. It is important to preselect some things to insure the geothermal program has the proper data to continue, otherwise an error will occcur. The designer can then save any changes such as internal loads, schedules, material properties, shading, etc. The designer clicks on the 'continue' button; the input file is written, the thermostat template is expanded, EnergyPlus is executed and the load simulation begins.

If the user selects the 'open EnergyPlus' button, they are asked to select their .idf file and it is then opened for editing. This should only be used for already converted files so that when all of the editing is complete, the file will run with the GUI.

6.1.3 Heat Pump Selection

The data collected is all on an hourly time step and includes the temperatures, humidity ratios, individual zone loads, outside air temperatures and wind speeds. The next step is to read this information based on the zones selected by the user. The maximum cooling and heating loads are then determined and the 'heat pump select' window is launched. The maximum loads are displayed for the user in kilowatt-hours along with the recommended heat pump selected from the heat pump performance study in Chapter 4. The user can simply click continue to use the recommendation or can choose any machine in the program via the drop down menu. If the building energy analysis comes back with a peak load that is larger than the rated capacity of the heat pump line, then a 'warning' message is displayed. An example of a heat pump selection figure can be seen in Figure 27.

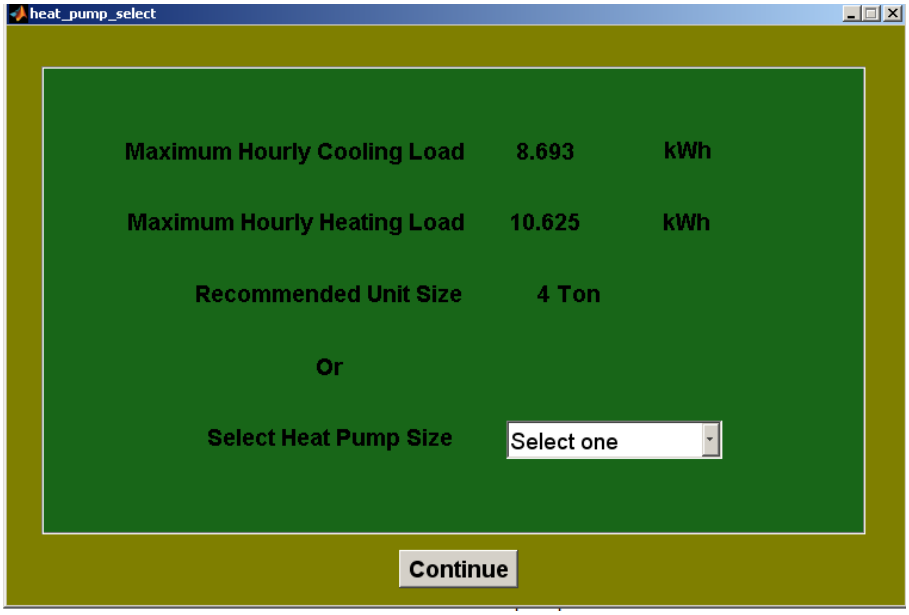

Figure 27: Heat pump selection GUI.

The rated volume flow for the heat pump selected is used along with the manufacturer's recommended pipe diameter to calculate a recommended fluid velocity. It is important to note that all of these values can be changed by the designer and are only displayed as a guide. The value for the air flow across the heat exchanger is set to the manufacturers rated volume for the selected heat pump. This value is used in the correction factor equation only and could be adjusted based on ductwork design and configuration.

6.2 Geothermal Inputs

With the building simulated and the heat pump selected, the user will now begin to design the thermal system. The first step is to define the type of fluid to be used in the analysis. The user will first notice that any antifreeze concentration can be selected with the thermal properties automatically calculated as they are selected. Also a value for the initial fluid temperature to start the simulation is calculated as the average ground temperature. The fluid velocity will also have a calculated default value based on the

rated volume flow and pipe size of the heat pump selected in the previous step. The values for these inputs are only recommended values and can be changed by the user. An example of the fluid selection GUI can be seen in Figure 28.

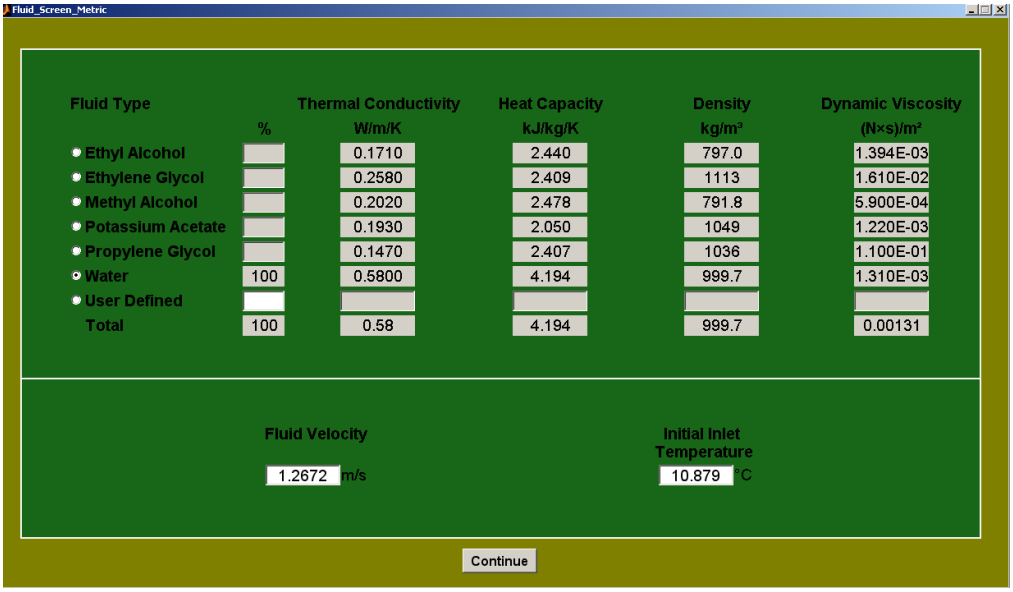

Figure 28: Fluid properties selection GUI.

Upon completion of the fluid section, the user might notice the values showing up on the home screen for inspection. The next step takes the user to the pipe selection, where the recommended pipe based on the heat pump selected, is displayed. The user can define their own properties or select from the three supplied materials and their corresponding pipe size. Copper was used to give the designer options with other heat transfer design work. An example of the pipe selection page can be seen in Figure 29.

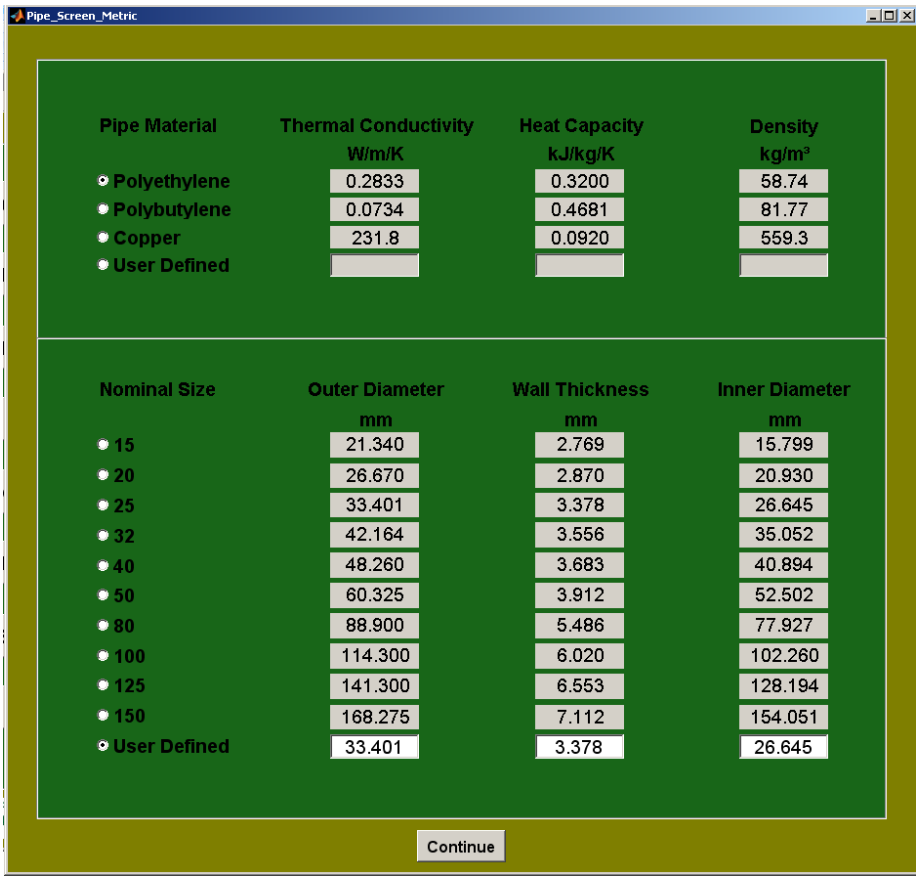

Figure 29: Pipe material selection GUI.

The only thermal properties left to enter are for the soil. The user can select from nine different types of soil or enter their own properties. A future grout selection option, currently being developed, will allow for an added layer of material used mainly in vertical loops. An example of the soil properties page can be seen in Figure 30.

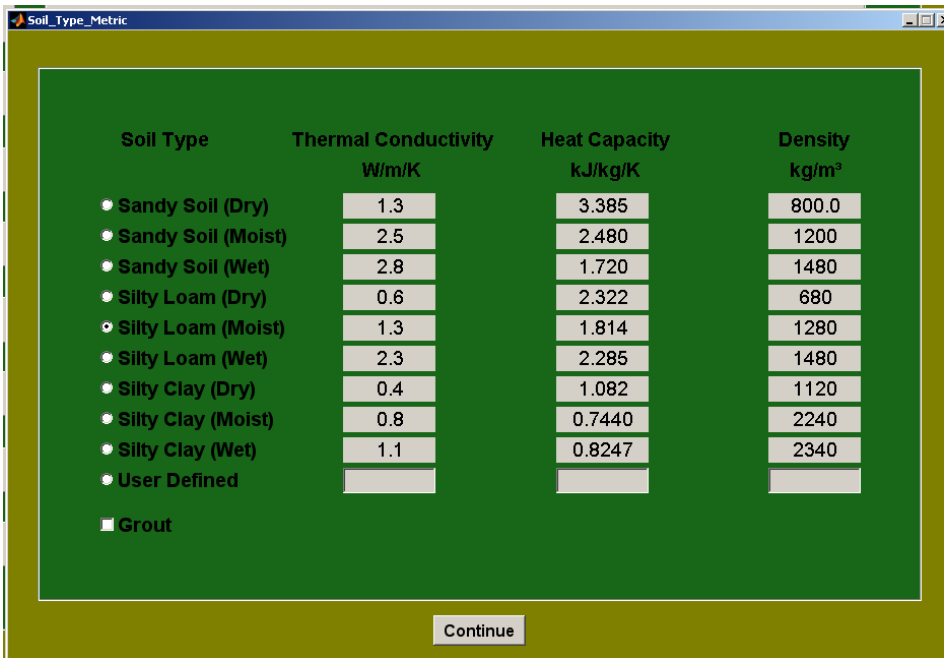

Figure 30: Soil properties selection GUI.

The loop configuration button will open a figure that allows the user to choose between the four main types of geothermal systems; horizontal closed loop, vertical closed loop, vertical open loop, and a pond loop. The recommended pipe length is calculated as a starting point for the geothermal design and is based on a rule of thumb of 100 meters per ton. Other essential information about the loop is given here such as depth of trench, number of boreholes, etc. An example of the loop configuration screen can be seen in Figure 31.

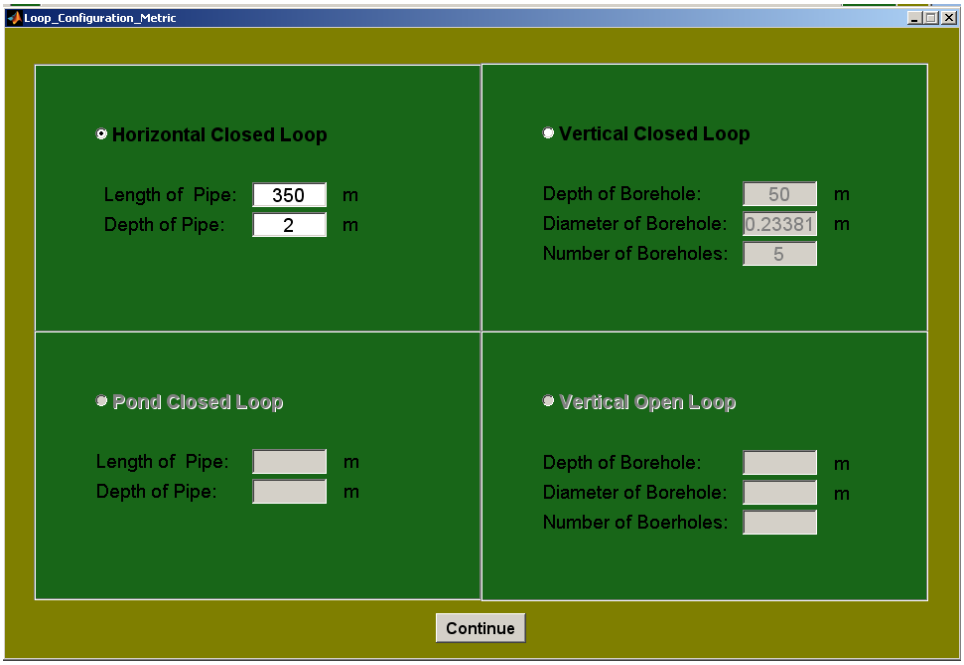

Figure 31: Loop configuration selection GUI.

Moving on to the 'Calculate GSHE' button, the suggested ground temperature is displayed. This value is calculated by simply averaging the outside dry bulb temperatures supplied by the EnergyPlus output files. The suggested values for the fluid grid points are calculated based on the study performed in Chapter 7. Once the number of time steps and time step size is selected, the soil radius and corresponding suggested number of grid points is displayed. These values are also based on the grid study performed in Chapter 7. Once all other values have been selected and the 'Continue' button is pushed, the variables for the geothermal analysis are all checked to make sure they have been defined. The input file for the geothermal program is then written and the FORTRAN executable is called. An example of the page used to collect the final simulation parameters can be seen in Figure 32.

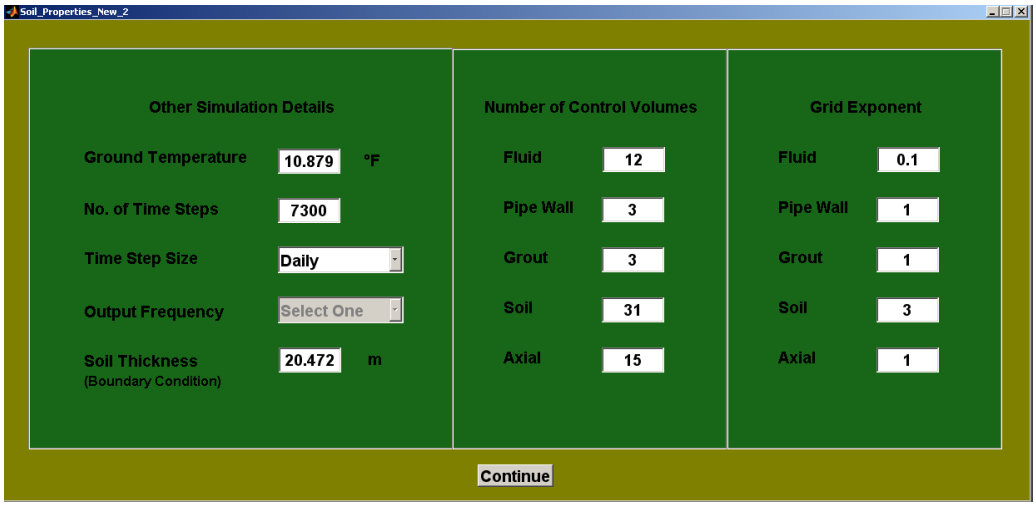

Figure 32: Other simulation details selection.

Upon completion of the calculations, the 'Economics' and 'Outputs' buttons are enabled. Careful attention was taken to ensure the user would have as much access to the data as possible. This is ensured by allowing the user full use of the plotting tools in the MATLAB figures.

CHAPTER 7

GRID STUDY

The computation time needed to run multi-year analysis with the geothermal heat exchanger program was a concern from the beginning of the project. In order to minimize the time and therefore make the program useful for optimizing a design, the number of control volumes used to model the loop must be minimized. A grid study is performed to reduce the number of calculations, while not compromising the accuracy of the converged solution.

A broad range of conditions were evaluated in the grid study to ensure that the program maintain its versatility. By looking at the extreme cases that would not be found in any real world geothermal application, the program is thoroughly documented. The ranges pertaining to the geothermal simulation will be discussed here while all other data is available upon request.

7.1 Fluid grid study

The number of grid points necessary in the fluid region is particularly important since this is where the energy to and from the ground is transferred. With the use of the effective thermal conductivity discussed in Chapter 3, the heat transfer to the fluid is calculated. Knowing the temperature of the first grid point in the fluid as well as the first grid point in the wall, the temperature on the pipe wall is calculated using Fourier's law.

In Figure 33, an example of the grid layout can be seen where each control volume lies a distance from the pipe surface and has a corresponding thermal conductivity and temperature.

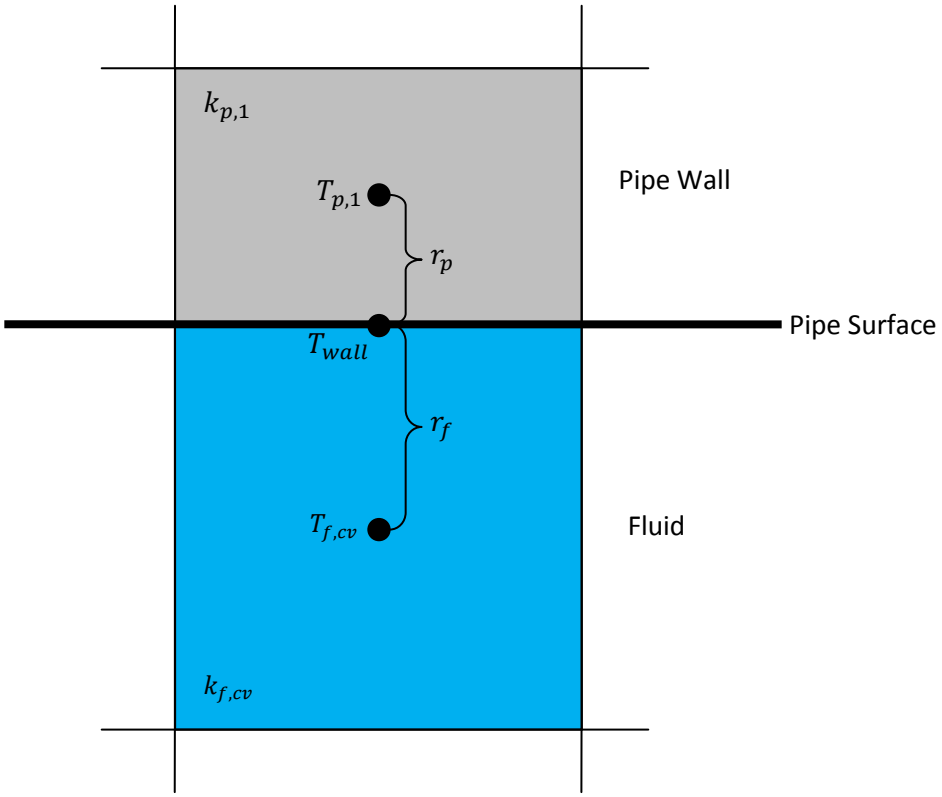

Figure 33: An example of the control volume layout.

The heat flux on the pipe surface from either side can now be set equal to each other and solved for T_{wall} using

$$k_{p,1}\left(\frac{T_{p,1}-T_{wall}}{r_p}\right) = k_{f,cv}\left(\frac{T_{wall}-T_{f,cv}}{r_f}\right) = q_{flux}. \tag{66}$$

Rearranging, the equation for the temperature of the surface of the wall at any time step and any location along the pipe axially becomes

$$T_{wall} = \frac{(T_p k_{p,1} r_f)+(T_{f,cv} k_{f,cv} r_p)}{(k_{p,1} r_f + k_{f,cv} r_p)} \tag{67}$$

where cv represents the last control volume in the fluid region. To determine when the number of grid points used is enough, the calculated heat transfer coefficient on the tube inside wall is used. To calculate the convective heat transfer coefficient at any point along the length of the pipe, the bulk temperature T_{bulk} must first be determined. This is done using the same integration technique discussed in Chapter 4. The convective heat transfer coefficient can now be calculated and used for analysis

$$h = \frac{q_{flux}}{(T_{wall} - T_{bulk})}. \tag{68}$$

It is important to note, the value for h, in a steady state condition, is used to determine what the converged solution is in the grid study. This value is not used in the unsteady energy equation solution nor was any empirically derived equations used. They are not needed.

The hydrodynamic entry length for fully developed flow for turbulent velocities is small compared to laminar flow. Therefore a length of pipe was used to make sure it supports a fully developed flow for all Reynolds numbers. The grid study was performed over a range of Reynolds numbers from 2,300 to 1,000,000. It was also studied at different diameters and dynamic viscosities. For the purposes of this study, the data ranging on the high and low end of typical conditions in geothermal systems are displayed using a diameter of 2 centimeters.

The convective heat transfer coefficient is now plotted versus the total number of grid points in the fluid. The grid spacing exponent was set to 1 and 0.1 to further the understanding of this behavior. With 15 grid points in the viscous sub layer region, the number of grid points in the bulk flow was increased and plotted. The converged value for the case of grid exponent set to 0.1 was determined quickly. It can be seen in Figure 34 that the grid exponent of 1 slowly reaches the same point, but requires an order of magnitude more grid points. As the number of grid points is increased, numerical instability can be seen in the grid exponent of 0.1.

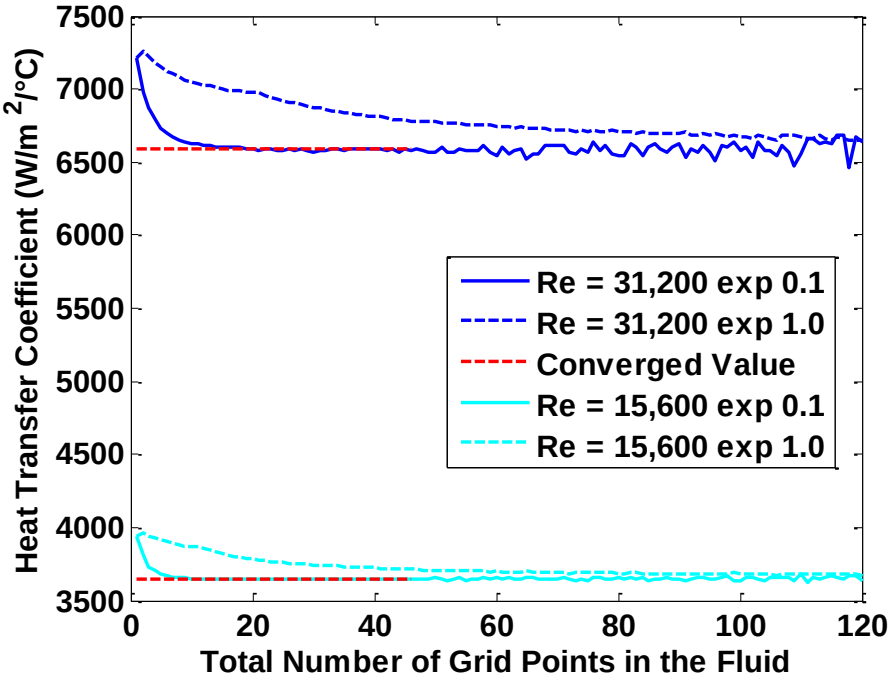

Figure 34: Heat transfer coefficient as fluid grid points increase.

With a converged value determined by inspection, the number of grid points in the viscous sub-layer region needs to be minimized. The viscous sub layer region plays a very important role in the calculation of the convective heat transfer coefficient due to the viscous shear and its role in the effective thermal conductivity discussed in Chapter 3. With the number of grid points in the bulk flow set to 60, the number of grids in the viscous sub-layer region is analyzed. The behavior can be seen in Figure 35 , where the grid exponents of 0.1 and 1 are again displayed for the same Reynolds numbers as in Figure 34. The study comprised of pipe radii ranging from one millimeter to half a meter for all of the Reynolds numbers mentioned. The number of grid points necessary in the viscous sub layer region was determined to be five. Five grid points in this region was enough to cover all of the different cases in the study. Numerical instability was recognized when the grid points in this region were increased above 20.

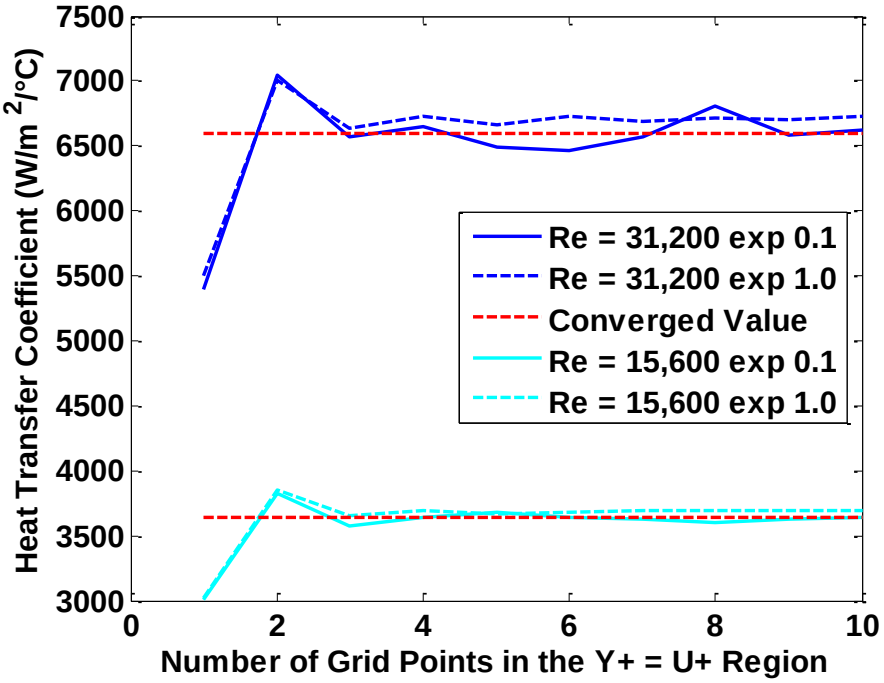

Figure 35: Minimizing grid points in the Y+ = U+ region.

The next step in the study was to minimize the number of points necessary in the bulk flow. With the viscous sub-layer region already determined and set, the number of grid points in the bulk flow is compared to the chosen converged value. It is found that with a grid exponent of 0.1, the number of points necessary for Reynolds numbers of 15,600 and 31,200 are 5 and 6 respectively. This was chosen as the minimum number of points needed to be within 1% error from the converged value as seen in Figure 36.

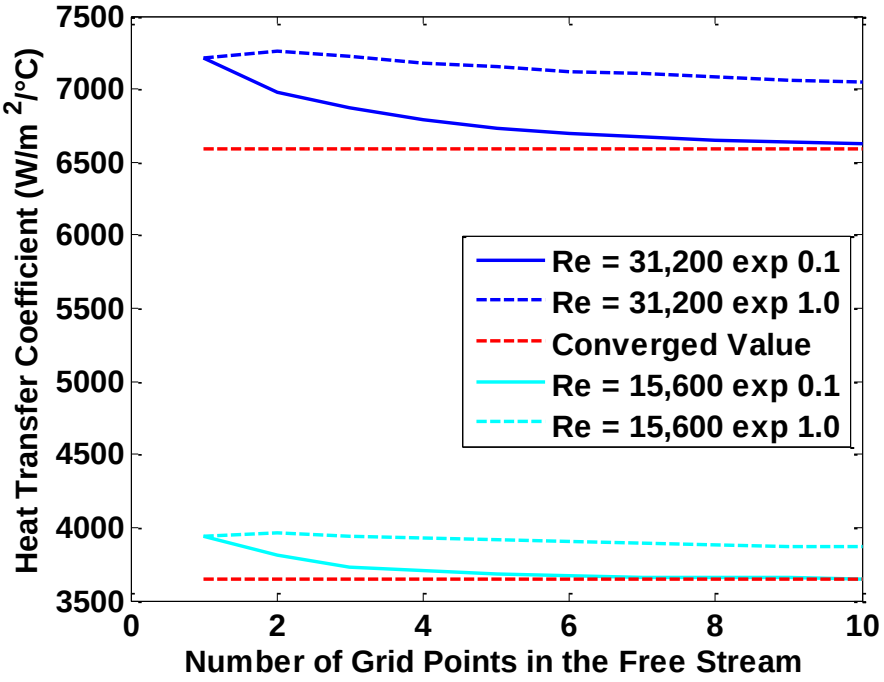

Figure 36: Minimizing grid points in the free steam.

The same procedure was used for the range of Reynolds numbers and diameters to determine an equation. The results of the study for the grid exponent of 0.1 was determined to be

$$Grid_{free\ stream} = ceil(1.4612 * ln(Re) - 9.1534) \tag{69}$$

This equation can now be used to suggest to the user the minimum number of grid points that can be used to ensure an error of less than 1% from the converged value. The equation plotted with the data points and before and after the ceiling function can be seen in Figure 37.

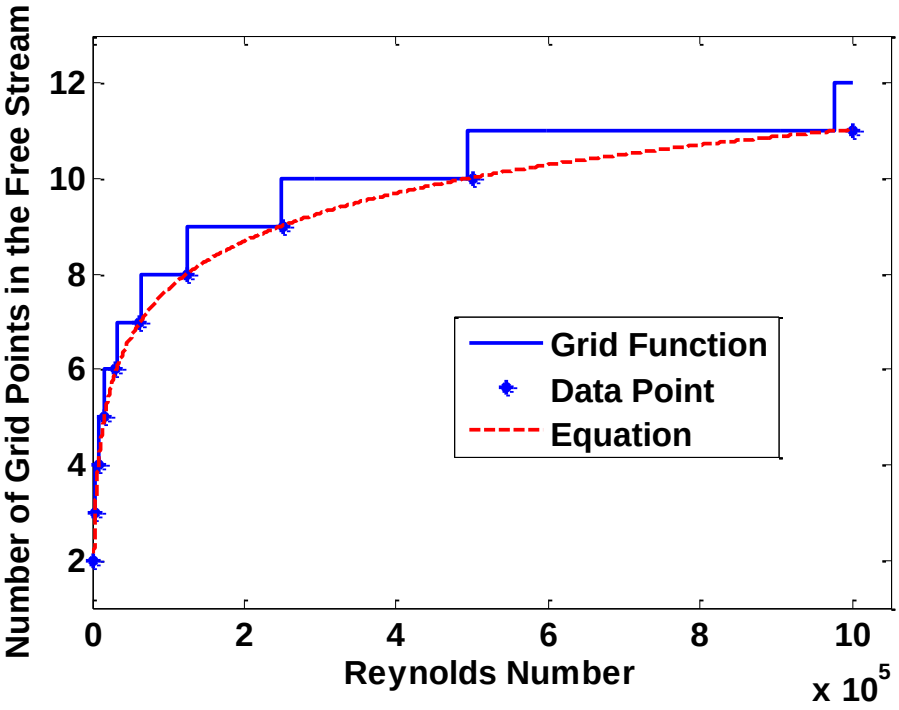

Figure 37: Equation for number of grid points in the bulk flow.

7.2 Soil boundary radius

The number of grid points necessary in the soil is a function of the radius and therefore the soil boundary radius needs to be minimized first. The boundary condition to solve the heat equation in an infinite medium is setup so that the temperature is always the ground temperature. This condition is adiabatic and therefore the radius must be far enough to not interfere with the heat flow, yet minimized to reduce the computation time. It is determined that the boundary condition for the soil is a function of the thermal conductivity of the soil, length of pipe, heating ratio, and time.

Extreme scenarios were simulated using a 3 ½ ton heat pump and hourly loads that were of its capacity. A range of heating ratios is used from 0% to 100% and each ratio was studied with a range of thermal conductivities and analysis time up to forty years. The length of pipe is itself a function of these variables and its value was decided

through an extensive trial and error process. The length was determined by not letting the exiting fluid temperature drop below -5 °C or get above 43°C so as to simulate a worst case scenario without exceeding the performance data of the heat pump discussed in Chapter 4. With the length of pipe iteratively determined, it is decided that interpolation between heating ratios will help to reduce the complexity of the study, therefore an equation for each of six heating ratios is reduced to functions of thermal conductivity and time.

The procedure used for each heating ratio is the same, but for purposes of this paper the 60% case is explained here. The first step after finding the extreme length necessary to stay within the heat pump curves, is to find a converged value for the amount of energy moving in and out of the pipe at the end of each run. The converged solution is found by setting the soil radius to 100 meters and doubling the number of grid points in the soil until the converged solution resulted. Simulation times of 1, 3, 10, 20 and 40 years were correlated in this study with soil thermal conductivities of 0.5, 1, 2, and 4 $\frac{W}{m^{2}℃}$. It is important to note that a grid exponent of three was used for the entire study and is recommended to the user as well.

The minimum radius was then determined by increasing the radius 1 meter at a time comparing the final time step's energy value to the converged value. An error of just 0.1% was set as the tolerance and the final radius is determined by linearly interpolating between the integer values. As a result, four different curves as a function of time can be plotted for each thermal conductivity. Exponential regression analysis reveals an equation for each curve and these can be seen in Figure 38.

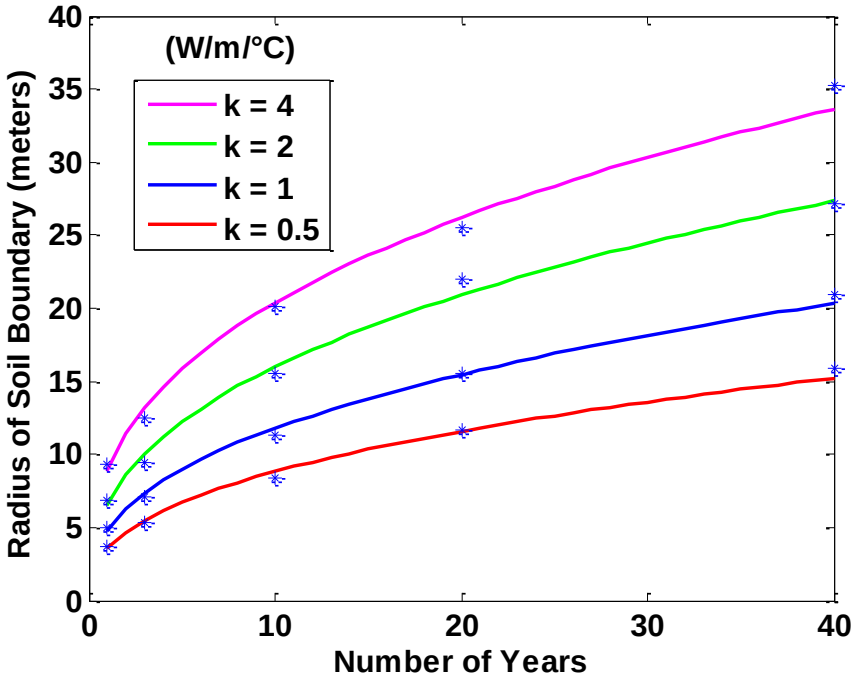

Figure 38: Soil radius as a function of years.

The equation for radius with 60% heating ratio as a function of time in years becomes

$$soil\ radius = A(years)^B \tag{70}$$

where the coefficients A and B are both functions of the thermal conductivity of the soil. Plotting the coefficient A and determining its behavior as a function of the soil thermal conductivity can be seen in Figure 39. A second order polynomial equation was derived to fit the data points tightly which is important since the behavior is dominated by this coefficient.

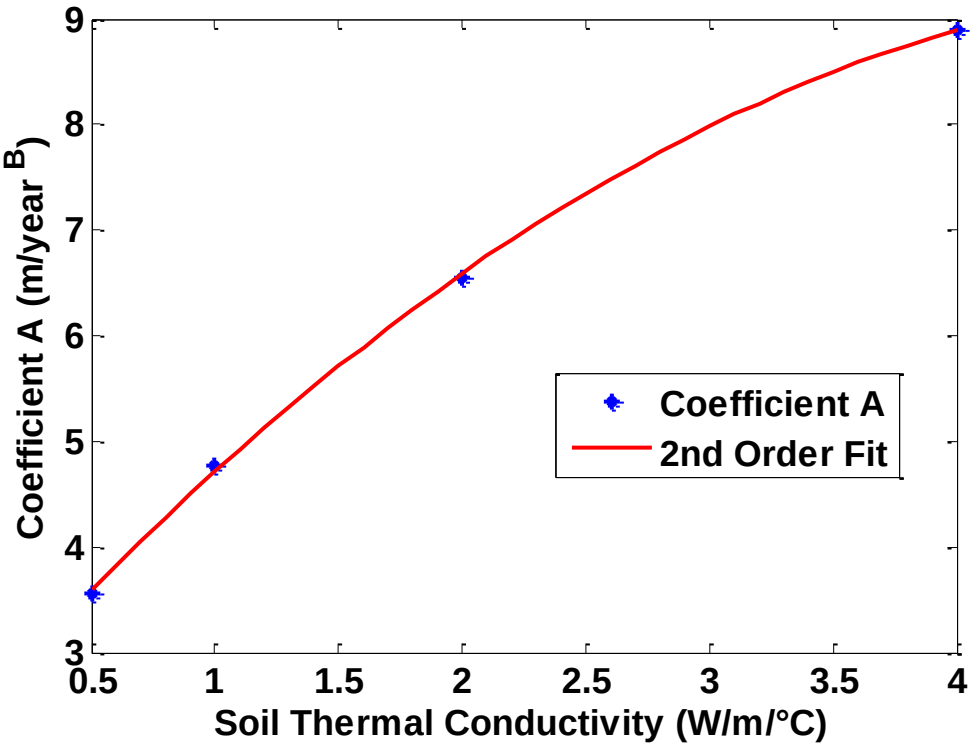

Figure 39: Coefficient A for 60% heating ratio.

The quadratic fit for coefficient A now takes the form

$$A = ak_{soil}^2 + bk_{soil} + c \qquad 71$$

where the coefficients a, b, and c can be found for six different heating ratios upon request. The coefficient B from equation (70) is now plotted as a function of the soil thermal conductivity. The behavior of the data points appears to be linear and does not change in magnitude much. A linear regression was performed for this coefficient, though an average value would work fine in this case. A plot of this curve can be seen in Figure 40.

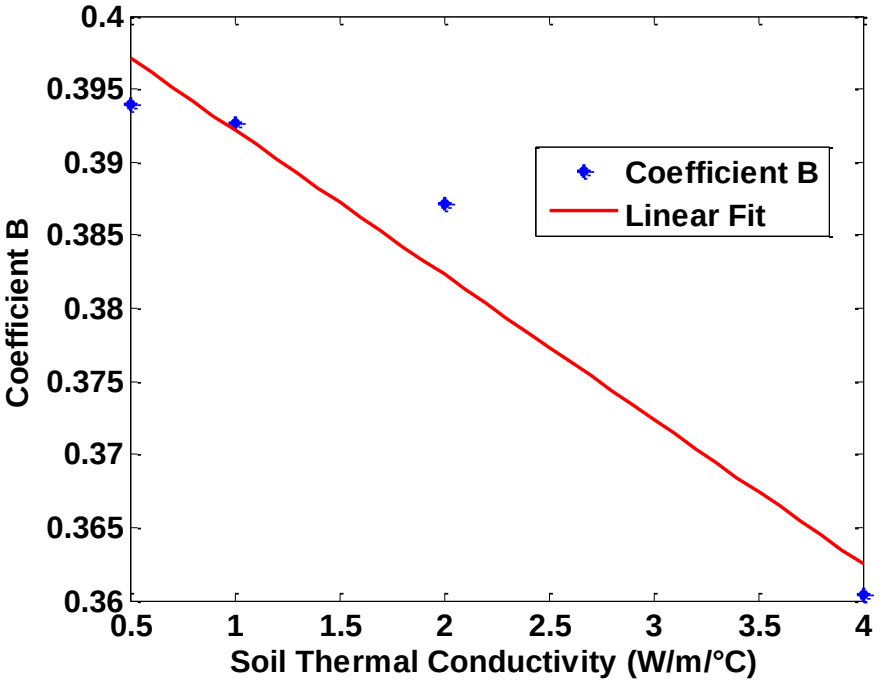

Figure 40: Coefficient B for 60% heating ratio.

The equation for coefficient B now takes the form

$$B = dk_{soil} + e \tag{72}$$

and combining equations and with equation (71) gives one equation for the radial soil boundary condition as

$$Boundary\ Radius = (ak_{soil}^2 + bk_{soil} + c)years^{dk_{soil}+e}. \tag{73}$$

Plugging in the values for soil thermal conductivity and years used in the correlation study, reveals errors no greater than 7%. The larger errors are seen in the shorter runs, which can most likely be contributed to the initial conditions fading away in time. As discussed in Chapter 6, the earth radius boundary condition is a default number, calculated using equation (73) for the user, and can be changed in the GUI.

7.3 Earth grid study

With the radius of the soil boundary condition determined, the value interpolated between the heating ratios can be used to determine the number of control volumes in the soil. First a minimal number of grid points must be determined while maintaining accuracy. The grid study will be conducted for an exponent of 1, 2, 3, and 4 and interpolated in the GUI for other values. The total energy moving to and from the pipe is once again used to show convergence for different earth grid point numbers. The number of control volumes was doubled for the boundary condition radius, ranging from 2 meters to 128 meters. The converged value was decided by inspection and used to compare to, for purposes of minimizing the number of points required to achieve a 1% error.

The number of grid points required to meet the tolerance is determined and plotted as a function of radius. An exponential regression analysis is completed and a ceiling function is applied to ensure an integer value for the number of grids. A plot of the grid exponents 2, 3, and 4 can be seen in Figure 41.

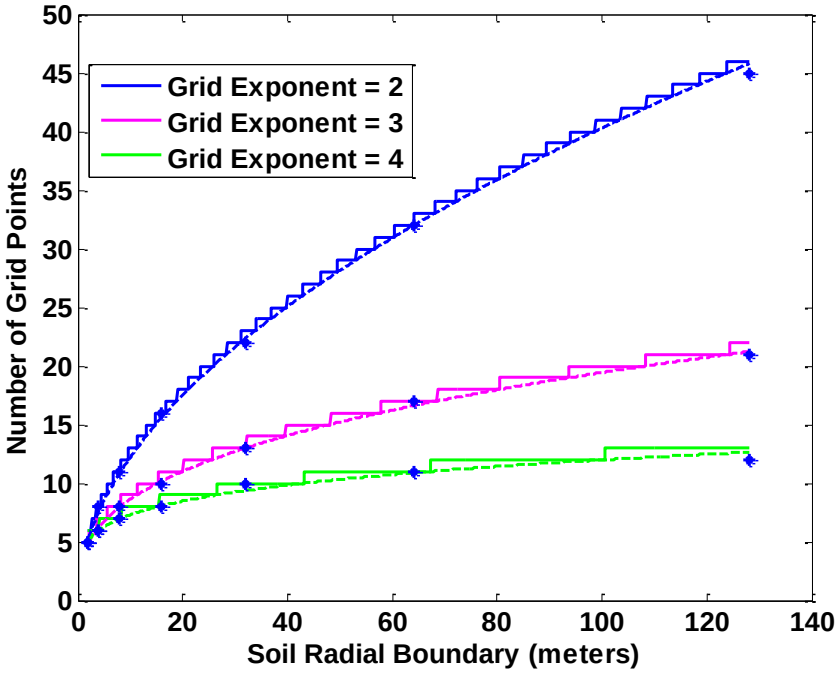

Figure 41: Soil grid study for different exponents.

The equations for the number of grid points needed in the earth for a corresponding exponent and radius become

$$Grid_{soil} = ceil(A \cdot radius^{B}). \tag{73}$$

The current configuration recommends using the grid exponent of three in all cases. The reason for this is so that the model avoids numerical instability that can occur when the grid exponent is set too high and the number of grid points is increased. The amount of grid points necessary for an exponent of one leads to a long computational time and some higher errors. The errors associated with a daily time step and simulated building loads can be seen in Figure 42. The difference in temperatures never exceeded more than 0.2 °C at for any grid exponent number.

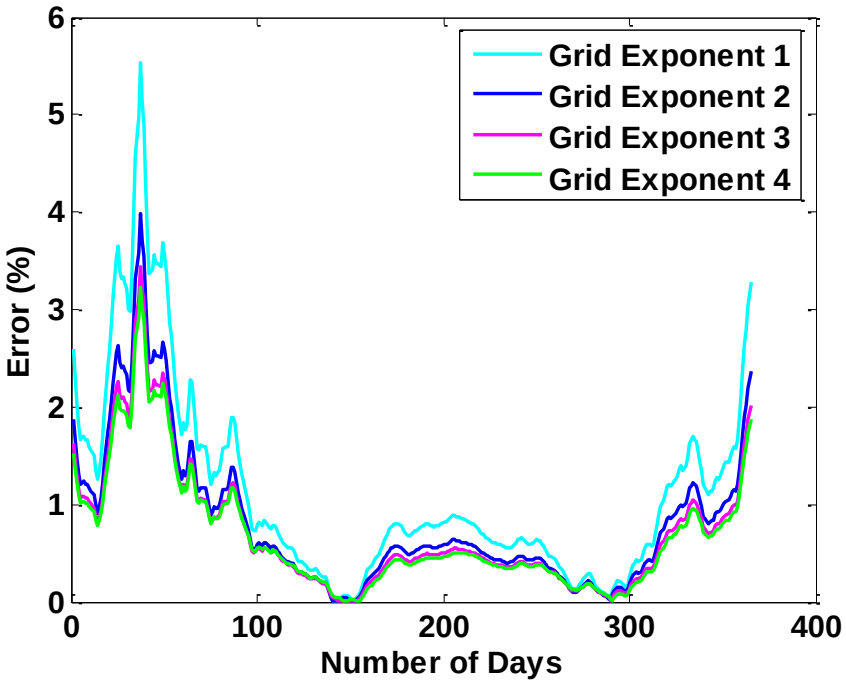

Figure 42: Error in entering water temperature

Using the unique feature of the grid exponent can greatly reduce the computation time by reducing the necessary number of control volumes in the earth. The number of iterations can also be reduced significantly by using the daily time step over the hourly

time step. A typical residential case was run to compare the computation time saved using a larger grid exponent and using hourly and daily time steps. The results can be seen in Table 4.

Table 4: Computation time required for changing exponent and time step.

Time step	Years	Earth Grid Exponent	Earth Control Volumes	Computation Time (sec.)
Hourly	10	2	44	214
		3	28	168
Daily	10	2	44	14.1
		3	28	13.4
5 Day	10	2	44	3
		3	28	2.7
Monthly	10	2	44	1
		3	28	.75

A plot of the EWT for four different time steps and a grid exponent of three can be seen in Figure 43.

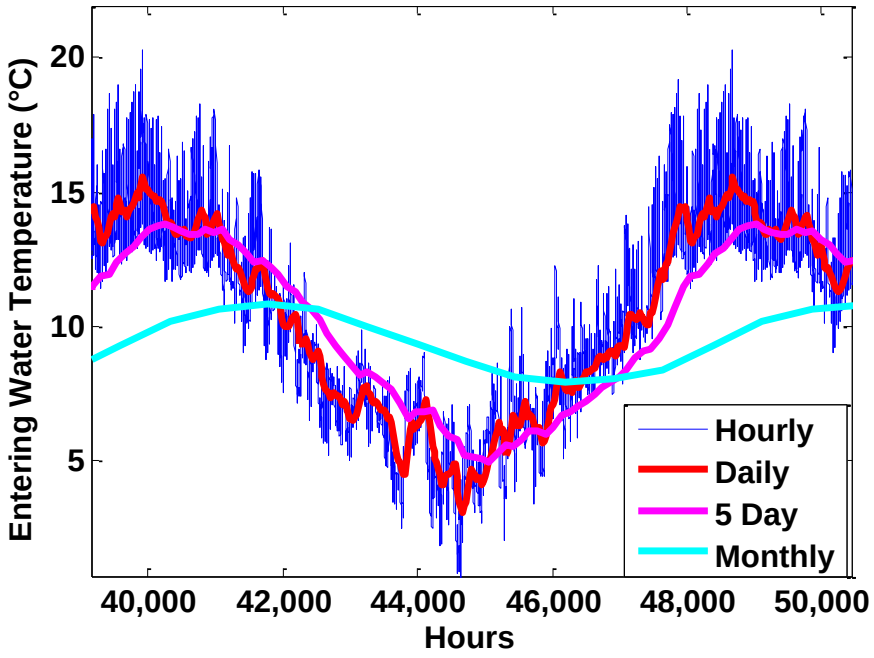

Figure 43: Accuracy with changing time step.

CHAPTER 8

PROGRAM OUTPUTS

As the program came together, many case studies were performed to test the completeness of the entire program. One such case study is a hypothetical 2500 square foot house in Dayton, Ohio. This house was virtually constructed using the 'novice' load calculator as a typical two story home with an unconditioned basement. A horizontal closed loop system was designed using the recommended 4 ton heat pump. The recommended pipe size, fluid velocity, ground temperature, and grid parameters were used. The working fluid was chosen to be 100% water and the soil type 'silty loam (moist)'. The length of tubing used in the design was chosen to be 350 meters and the simulation was run on daily time steps for a twenty year analysis. A screen shot of the home screen including the selected design parameters can be seen in Figure 44.

Figure 44: Home screen for case study.

The first output is a daily COP, as seen in Figure 45 for twenty years; this gives the designer a good sense of how the efficiencies change with the different seasons.

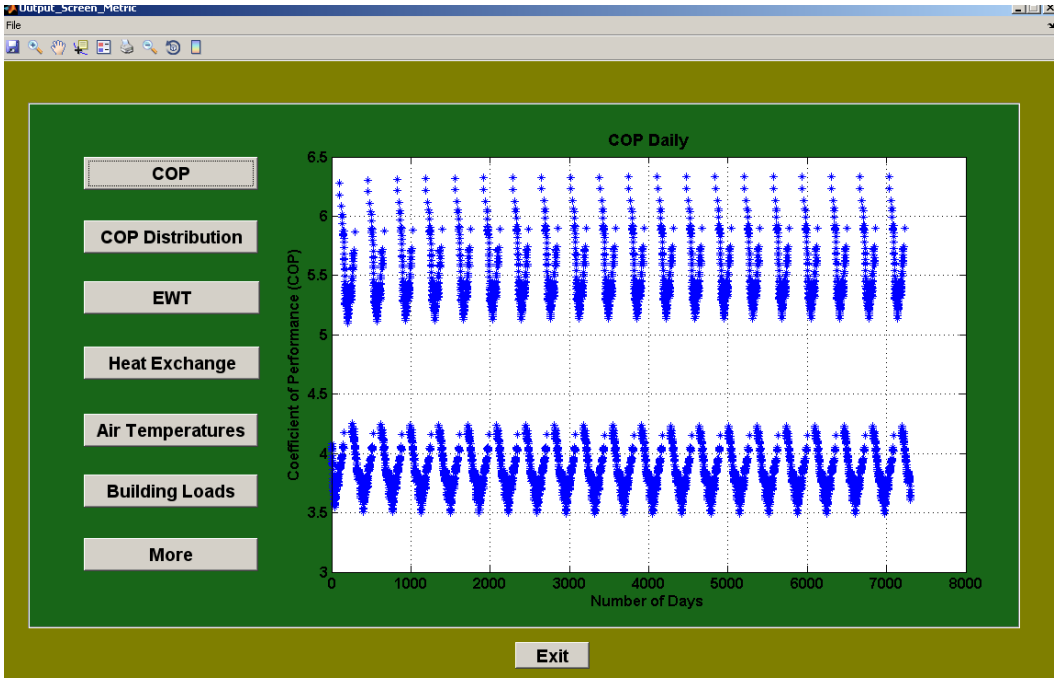

Figure 45: Case study daily COP.

The outputs available to the designer are intended to allow the user to iterate the design to achieve optimum results. Maximizing the amount of time the COP is a higher value can lead to a more efficient, cost effective design. A histogram of COP's allows the designer to see the frequency at which a range of efficiencies occur. An example of a COP histogram can be seen in Figure 46.

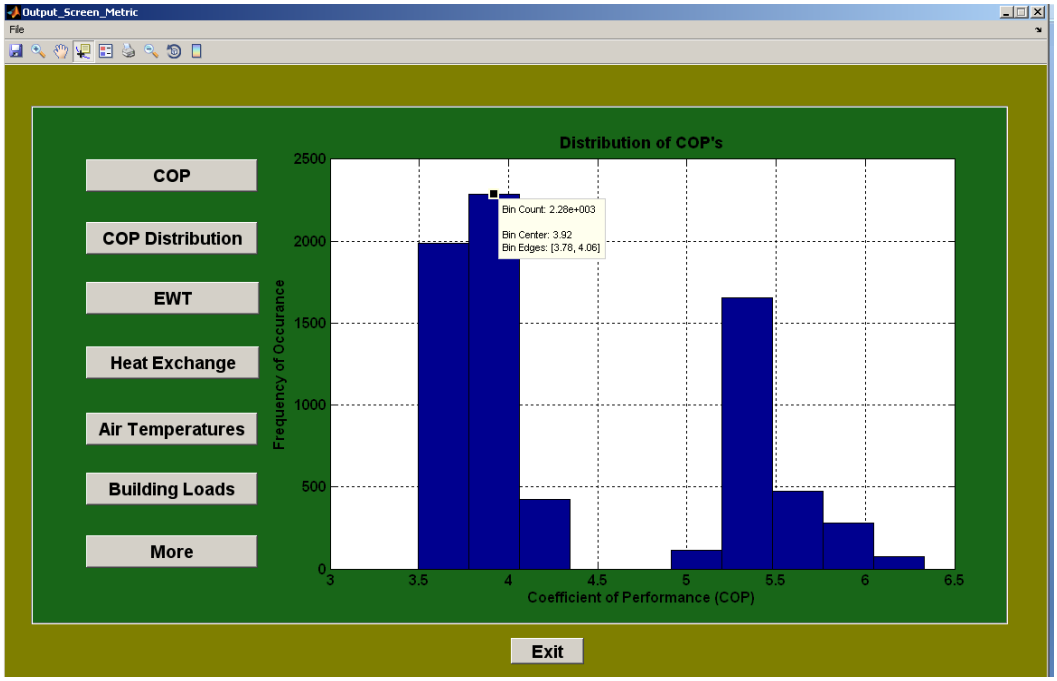

Figure 46: Histogram of COP's.

A cost effective heating dominated design can sometimes require longer length of tube or antifreeze as the working fluid. The result in Figure 47 allows the designer to reduce unnecessary cost in material by watching how close the fluid gets to the desired temperature. Some geothermal systems will use a higher concentration of antifreeze and allow the entering water temperature to drop below the freezing point of water during extreme winter conditions.

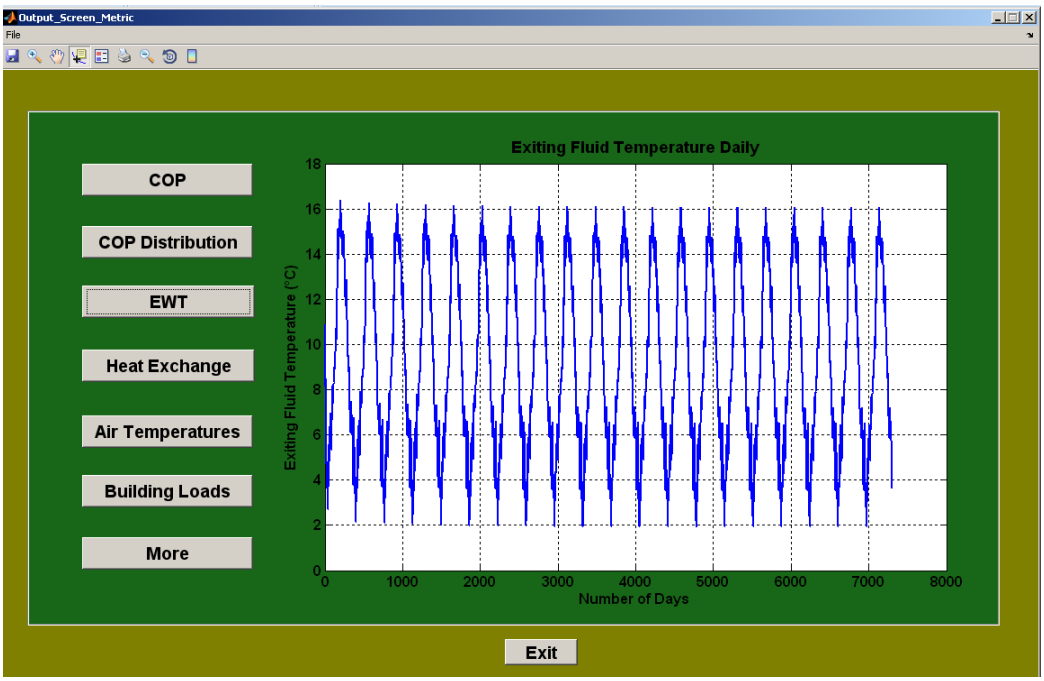

Figure 47: Entering water temperature to the heat pump.

The total amount of heat being exchanged to and from the pipe is displayed to give the designer better understanding of the thermal response of the system.

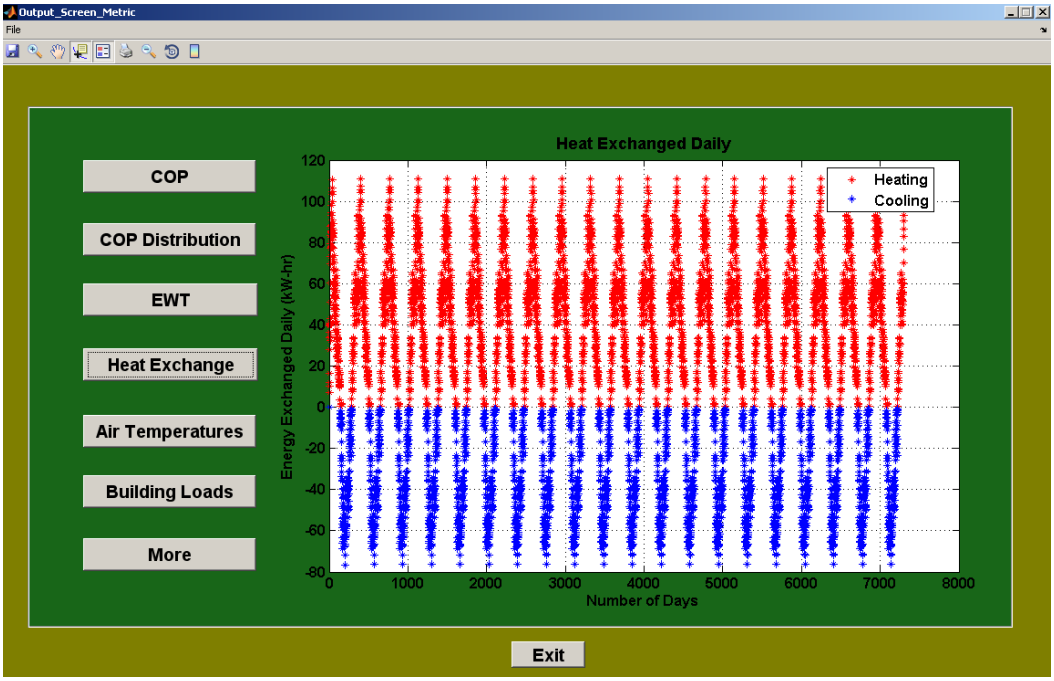

Figure 48: Heat exchanged with the working fluid.

Some EnergyPlus data is displayed such as the indoor and outdoor dry bulb temperatures as seen in Figure 49 and the hourly building loads in Figure 50.

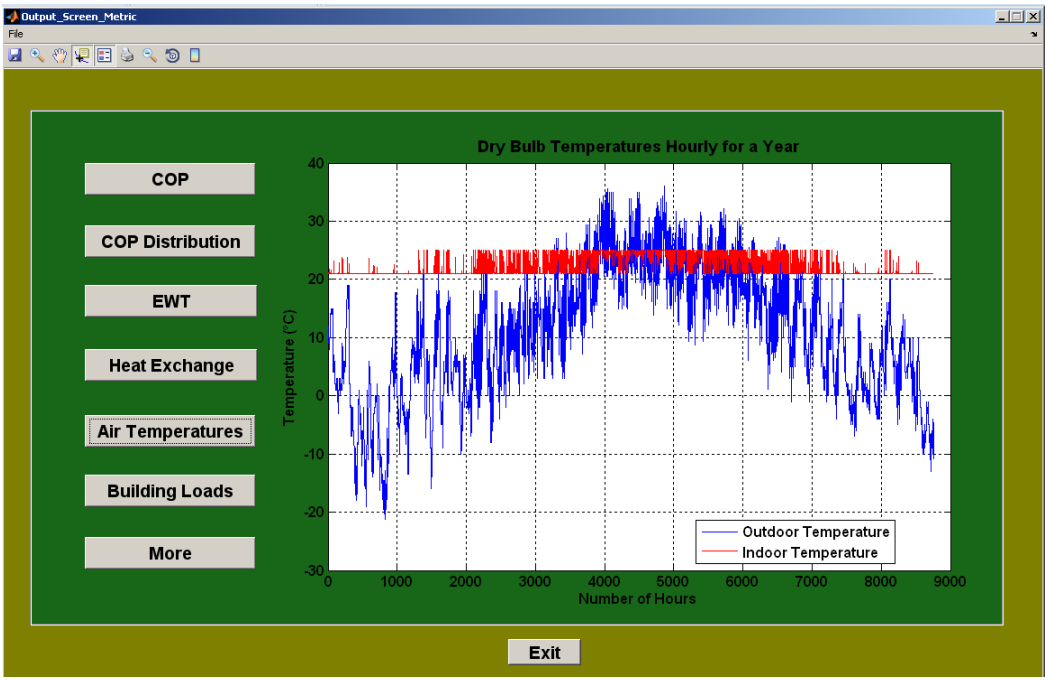

Figure 49: Indoor and outdoor dry-bulb temperatures.

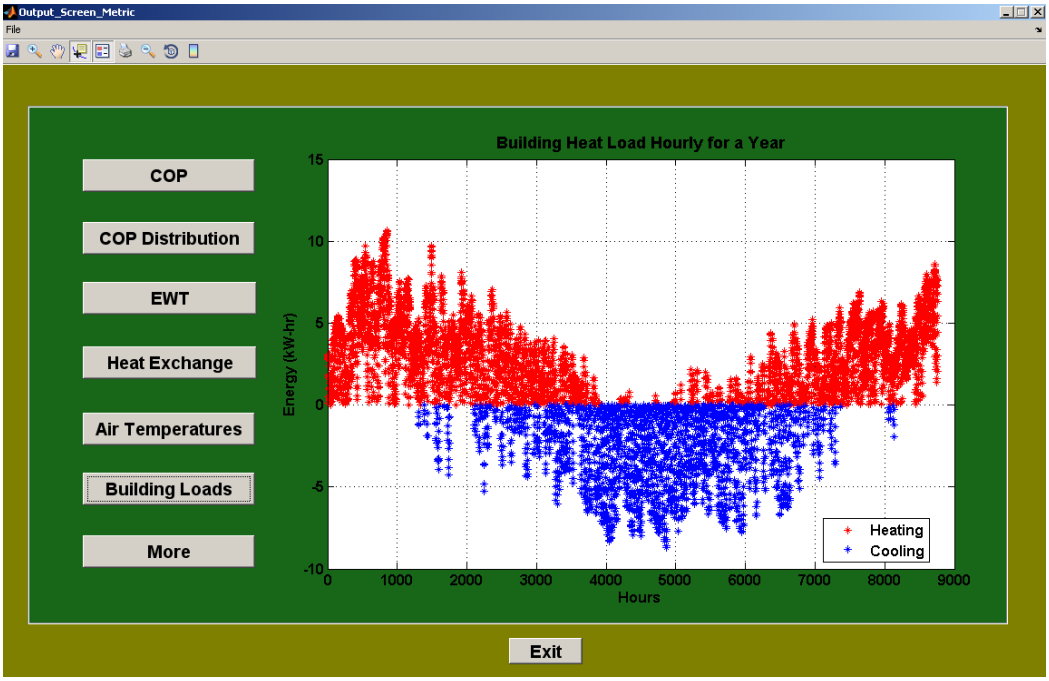

Figure 50: Hourly heat loads from EnergyPlus.

The temperature field is displayed to the user at any output frequency desired. This allows the designer to analyze the thermal response of the ground and alter the spacing of the tubes based on the heat pulse over time. The temperature field during the heating season after twenty years can be seen in Figure 51.

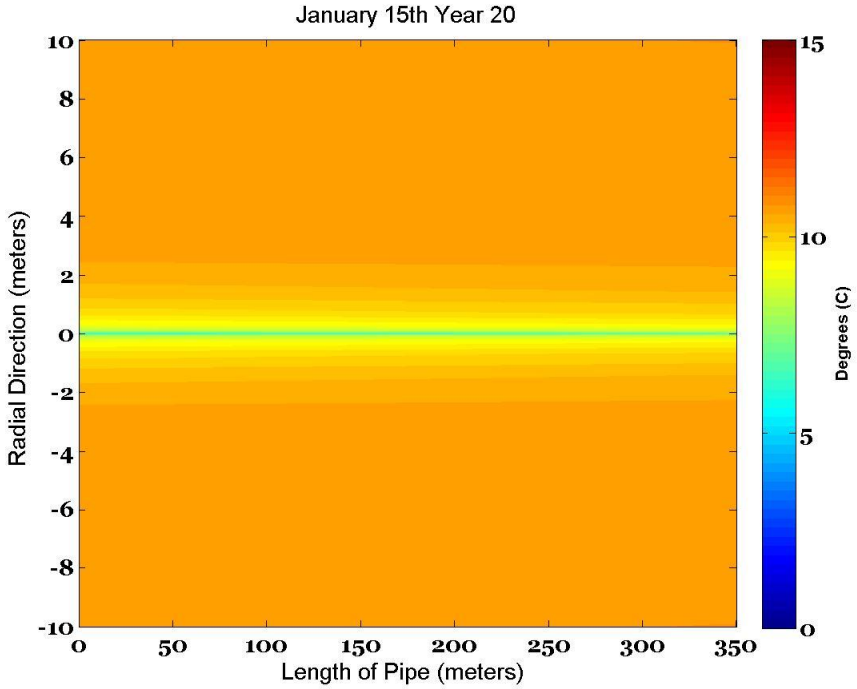

Figure 51: Example of a temperature field during heating season.

These outputs supplied to the designer in conjunction with the emphasis on accuracy and computation time will help push the geothermal industry forward. A better program and more confidence in the results will ultimately begin to reduce the overall cost of the system making geothermal an even more attractive option for consumers.

CHAPTER 9

SUMMARY AND CONCLUSION

The geothermal industry has proven its place in the HVAC market even with some of the barriers and misconceptions it faces. With technological advances in the industry and more accurate modeling tools, the geothermal designers can begin to optimize a design and reduce the payback periods. The first step in this process begins with the iterative process of solving a finite volume model of the loop configuration. This ensures the most accurate solution of the thermal response of the ground and eliminates line-cylinder and g-function approximations. The sizing of the system is critical to the overall efficiency which is why the most reliable load calculator, EnergyPlus, was interfaced. This provides the designer with all of the necessary building inputs to ensure an accurate building load on an hourly basis using trusted Typical Meteorlogical Year version 2 (TMY2) format weather files.

The fluid mechanics model introduced simulates a wide range of Reynolds numbers using empirically correlated equations. An effective thermal conductivity for turbulent flow is used to model the convective heat transfer and energy transport. A complete heat pump performance study was done to accurately calculate COP on an hourly basis while implementing correction factors for indoor dry bulb temperature, air flow, humidity, and antifreeze concentration. The leaving water temperature is calculated

using the first law of thermodynamics and a uniform temperature profile to start the next iteration is assumed.

A complete Graphical User Interface was employed to ease the designer through the process of selecting the geothermal design parameters. The data collected from the building simulation is used to help suggest values for heat pump size, pipe size, fluid velocity, and soil temperature. The user is left with full control over all of the inputs including the number of control volumes, time steps, and even the exponent used for grid spacing. A grid study was performed to suggest values for an accurate but fast calculation.

Finally, after running multiyear analysis, the user is equipped with multiple graphical outputs including EWT versus time, heat flow in the pipe, temperature fields, and even a histogram of COP's. The actual COP's calculated in the geothermal analysis are used in the operational cost calculation to help optimize the design. The payback period calculator calculates the time value of money with the operational costs to compare geothermal systems to conventional systems.

REFERENCES

ASHRAE. "U-factor, C-factor, and Thermal Mass Data." *2008 Joint Appendices – June 2007 Workshop Draft.* Page 4-1.

BS., Petukhov. *Advances.* Vols. 6:503–564. 1970.

Carslaw H.S., J.J.C. *Conduction of Heat in Solids.* 2d ed Great Britain: Oxford Science Publications., 1959.

Cengel, Yunus A. 3rd. Vol. Heat and mass transfer a practical approach. New York: Mcgraw-Hill, 2007.

Cengel, Yunus A., and Michael A. Boles. sixth. Vol. Thermodynamics. New York: McGraw-Hill, 2008.

Chapman, A.J. "Heat Transfer." (Macmillan Publishing Company) 4th Edition.

Cheng, Nian-Sheng. "Formulas for friction factor in transitional regimes." (Journal of Hydraulic Engineering, ASCE) 134, no. 9 (2008): 1357-1362.

Crawley, Drury B. "Which Weather Data Should You Use for Energy Simulations of Commercial Buildings." Washington DC, 1998, 104 Part 2.

D.O.E. "Geothermal Heat Pump Manufacturing Activities." (U.S. Energy Information Administration), no. http://www.eia.gov/fuelrenewable.html (2010).

Datta, Ravindra. *Eddy Viscosity and Velocity Distribution in Turbulent Pipe Flow Revisited.* Vol. 39. Iowa City, IA: AIChE Journal, 1993.

EnergyPlus. "Engineering Reference." *The reference to EnergyPlus calculations*, 2010: 1-1075.

Fox, Robert W., Alan T. McDonald, and Phillip J. Pritchard. *Introduction to Fluid Mechanics.* sixth. Danvers, MA: John Wiley & Sons, 2006.

Gemelli, Alberto. "GIS-based energy-economic model of low temperature geothermal resources:." (Elsevier Ltd. All rights reserved.) Renewable Energy 36 (2011) 2474e2483 (2011).

GeoEnergy. "Energy Information Administration/Geothermal Heat Pump Manufacturing Activities." (http://www.eia.doe.gov/cneaf/solar.renewables/page/ghpsurvey/geothermalrpt.pdf) 2008.

GeoExchange. *GeoExchange.* http://www.geoexchange.org/ (accessed 2011).

GEO-FLO. *GEO-FLO TM ALL.* www.recochem.com. Montréal • Toronto • Edmonton • Vancouver.

Geo-Hydro. "MAY 2011 Price & Product Catalog." (www.geohydrosupply.com) 2011.

geothermalgenius. "sizing up a geothermal system." (http://www.geothermalgenius.org/thinking-of-buying/industry-issues/sizing.html) 2011.

Gilat, Amos. *MATLAB an introduction with applications.* second. Danvers, MA: John Wiley & Sons, 2005.

Ground Loop Design. "Geothermal Design Studio." *Ground Loop Design™ Premier Version 5.0 for Windows ®.* Celsia, 2007.

Hamada, Yasuhiro, Makoto Nakamura, Kiyoshi Ochifuji, Shintaro Yokoyama, and Katsunori Nagano. "Development of a database of low energyhomes around the world and analyses of their trends." (www.elsevier.com) Renewable Energy 28 (2002): 321–328.

Kays. *Turbulent Prandtl Number-Where are we?* Vol. 116. J.Heat Transfer, 1994.

M.Conde Engineering. "Thermophysical properties of brines." Zurich, 2002.

Marchand, Patrick, and O.Thomas Holland. *Graphics and GUIs with MATLAB.* third. Boca Raton: Chapman & Hall/CRC, 2003.

Mogensen, P. "Fluid to Duct Wall Heat Transfer in Duct System Heat Storages." (The international Conference on Subsurface Heat Storage in Theory and Practice) 1983.

Monzo, Patricia M. "Comparison of different Line Source Model approaches for analysis of Thermal Response Test in a U-pipe Borehole Heat Exchanger." Stockholm, Sweden, 2011.

Oregon Residential Energy Code. "Residential thermal performance calcualtions." no. No. 10. Oregon, april 2008.

Purdy, Julia, and Andrew Morrison. "GROUND-SOURCE HEAT PUMP SIMULATION WITHIN A WHOLE-BUILDING ANALYSIS." (Eighth International IBPSA Conference) 2003.

Rafferty, Kevin. "Scaling in Geothermal Heat Pump Systems." Department of Energy, Klamath Falls, OR, 1999.

Rees, Daniel E. Fisher and Simon J. "MODELING GROUND SOURCE HEAT PUMP SYSTEMS IN A BUILDING." (Ninth International IBPSA Conference), no. pp 311 (2005).

Roadmap. "Ground-source Heat Pump Roadmap - Version 2.2." (http://ghpsrus.com/documents/GHP%20Roadmap_Version%202.2.pdf).

Swearingen, Corte. *http://www.coleparmer.com/techinfo/techinfo.asp?htmlfile=V_PDeviations.htm&ID=815*. Cole-Parmer Technical Library. September 25, 2009.

Trane. "Axiom Horizontal/Vertical Water-Source Heat Pump." *GEHE/GEVE - R - 410A 1/2 to 5 tons - 60 hz.* no. WSHP-PRC017-EN. Trane, 2009.

—. "Water Source Heat Pump." *Axiom™ Horizontal/Vertical — GEH/GEV.* no. WSHP-PRC016-EN. Trane, November 2010.

Ubeg. "Geothermal Heat Pumps." (Zum Boden), no. ubeg@ubeg.de (1998).

Vanek, Francis M., and Louis D. Albright. *Energy Systems Engineering evaluation and implemention.* McGraw-Hill, 2008.

Walton, G. N. *Thermal Analysis Research Program Reference Manual.* National Bureau of Standards, 1983.

Yazdanian, M, and J H Klems. *Measurement of the Exterior Convective Film Coefficient for Windows in Low-Rise Buildings.* Vols. 100, Part 1, p.1087. ASHRAE Transactions, 1994.

APPENDIX

Table 5: Acceptable Volume Flows for Modeled heat Pumps.

Unit Size and #	Minimum Volume Flow (gpm / m^3/sec)	Maximum Volume Flow (gpm / m^3/sec)	Rated Volume Flow (gpm / m^3/sec)
1/2 Ton Unit #1	1.1 / 6.9399E-05	2 / 1.2618E-04	1.8 / 1.1356E-04
3/4 Ton Unit #2	1.4 / 8.8326E-05	2.5 / 1.5773E-04	2.1 / 1.3249E-04
1 Ton Unit #3	1.8 / 1.1356E-04	3.4 / 2.1451E-04	2.8 / 1.7665E-04
1 1/4 Ton Unit #4	2.2 / 1.3880E-04	4.2 / 2.6498E-04	3.5 / 2.2082E-04
1 1/2 Ton Unit #5	2.7 / 1.7034E-04	5 / 3.1545E-04	4.2 / 2.6498E-04
2 Ton Unit #6	3.6 / 2.2712E-04	6.6 / 4.1640E-04	5.6 / 3.5331E-04
2 1/2 Ton Unit #7	4.5 / 2.8391E-04	8.3 / 5.2365E-04	7 / 4.4163E-04
3 Ton Unit #8	5.4 / 3.4069E-04	10 / 6.3090E-04	8.4 / 5.2996E-04
3 1/2 Ton Unit #9	6.3 / 3.9747E-04	11.6 / 7.3185E-04	9.8 / 6.1828E-04
4 Ton Unit #10	7.2 / 4.5425E-04	13.2 / 8.3279E-04	11.2 / 7.0661E-04
5 Ton Unit #11	9.4 / 5.9305E-04	17.4 / 1.0978E-03	14 / 8.8326E-04
6 Ton Unit #12	9 / 5.6781E-04	21 / 1.3249E-03	18 / 1.1356E-03
7 1/2 Ton Unit #13	11.3 / 7.1292E-04	26.3 / 1.6593E-03	22.5 / 1.4195E-03
10 Ton Unit #14	15 / 9.4635E-04	35 / 2.2082E-03	30 / 1.8927E-03
12 1/2 Ton Unit #15	18.8 / 1.1861E-03	43.8 / 2.7634E-03	37.5 / 2.3659E-03
15 Ton Unit #16	22.5 / 1.4195E-03	52.5 / 3.3122E-03	45 / 2.8391E-03
20 Ton Unit #17	30 / 1.8927E-03	70 / 4.4163E-03	60 / 3.7854E-03
25 Ton Unit #18	37.5 / 2.3659E-03	87.5 / 5.5204E-03	75 / 4.7318E-03

Table 6: Cooling Capacity Coefficients for Modeled Heat Pumps.

Cooling Capacity = (Aa*EWT^2+Ab*EWT+Ac)*vol^2+(Ba*EWT^2+Bb*EWT+Bc)*vol+(Ca*EWT^2+Cb*EWT+Cc)								
	a	b	c			a	b	c
Coefficient	1/2 Ton Unit #1				Coefficient	4 Ton Unit #10		
A	1.0250E+05	-6.2448E+06	6.5557E+07		A	7.3564E+03	-3.6198E+05	-6.6578E+05
B	-1.3874E+01	8.1579E+02	-4.6697E+03		B	-9.9364E+00	4.7684E+02	3.8926E+03
C	3.1118E-04	-6.3528E-02	8.6484E+00		C	-2.3876E-05	-3.8262E-01	5.5142E+01
	3/4 Ton Unit #2					5 Ton Unit #11		
A	2.0327E+04	-3.4096E+05	-2.2074E+07		A	-4.0215E+02	-7.0073E+02	-1.6626E+06
B	-1.3397E+00	-2.6142E+02	1.3438E+04		B	6.9096E-01	-9.4914E+00	4.9991E+03
C	4.0868E-04	-5.4936E-02	9.7341E+00		C	-4.1563E-03	-2.9592E-01	6.8917E+01
	1 Ton Unit #3					6 Ton Unit #12		
A	-6.4291E+04	3.1644E+06	-3.5128E+07		A	-1.2865E+03	8.9371E+04	-5.0145E+06
B	2.3471E+01	-1.1875E+03	1.4580E+04		B	3.8862E+00	-3.0117E+02	1.5424E+04
C	-2.6784E-03	7.0506E-02	1.1608E+01		C	-4.0397E-03	-3.4095E-01	8.5100E+01
	1 1/4 Ton Unit #4					7 1/2 Ton Unit #13		
A	1.7654E+04	-5.5514E+05	-5.6715E+06		A	-8.3704E+02	5.6828E+04	-2.3069E+06
B	-8.1142E+00	2.1948E+02	4.1346E+03		B	2.9976E+00	-2.1328E+02	8.4519E+03
C	1.9178E-04	-6.3796E-02	1.5382E+01		C	-6.4523E-03	-3.5065E-01	1.0713E+02
	1 1/2 Ton Unit #5					10 Ton Unit #14		

A	5.2452E+04	-2.7999E+06	2.5280E+07		A	-8.3760E+01	5.8570E+03	-1.7731E+06
B	-2.8219E+01	1.5156E+03	-1.3144E+04		B	6.8517E-01	-5.0399E+01	8.5574E+03
C	1.5258E-03	-1.7262E-01	2.0400E+01		C	-6.6560E-03	-6.3576E-01	1.4308E+02
	2 Ton Unit #6					12 1/2 Ton Unit #15		
A	6.5291E+03	-1.2308E+05	-8.2274E+06		A	4.2192E+02	-3.4062E+04	-6.0161E+05
B	-3.0572E+00	-1.0313E+01	8.8395E+03		B	-2.5635E-01	4.6272E+01	5.8797E+03
C	-1.2099E-03	-8.6739E-02	2.4689E+01		C	-8.9406E-03	-8.0930E-01	1.8304E+02
	2 1/2 Ton Unit #7					15 Ton Unit #16		
A	-5.9872E+03	4.2799E+05	-1.2425E+07		A	4.0492E+02	-2.9353E+04	-5.0611E+04
B	5.6759E+00	-4.2456E+02	1.3975E+04		B	-2.0944E+00	1.5249E+02	1.0828E+03
C	-2.7685E-03	-5.1090E-02	3.1093E+01		C	-8.3298E-03	-1.0380E+00	2.2752E+02
	3 Ton Unit #8					20 Ton Unit #17		
A	5.5444E+03	-2.3046E+05	-1.4224E+06		A	7.6346E+02	-4.6350E+04	1.5389E+05
B	-6.0822E+00	2.5953E+02	2.6186E+03		B	-3.3398E+00	1.8603E+02	2.0955E+03
C	-4.2249E-04	-2.4943E-01	4.0399E+01		C	-1.0566E-02	-1.2642E+00	3.0045E+02
	3 1/2 Ton Unit #9					25 Ton Unit #18		
A	-3.8439E+03	2.0464E+05	-5.0576E+06		A	-1.5954E+02	9.6243E+03	-7.7060E+05
B	3.7955E+00	-2.1043E+02	7.1542E+03		B	2.2705E+00	-1.4696E+02	9.4904E+03
C	-3.1525E-03	-1.7025E-01	4.6711E+01		C	-2.0209E-02	-1.3570E+00	3.6263E+02

Table 7: Heating Capacity Coefficients for Modeled Heat Pumps.

Heating Capacity = (Aa*EWT^2+Ab*EWT+Ac)*vol^2+(Ba*EWT^2+Bb*EWT+Bc)*vol+(Ca*EWT^2+Cb*EWT+Cc)								
	a	b	c			a	b	c
Coefficient	1/2 Ton Unit #1				Coefficient	4 Ton Unit #10		
A	1.7501E+05	-7.4008E+06	-4.5246E+07		A	-5.4254E+03	-1.4423E+05	-7.0597E+06
B	-3.2737E+01	1.6310E+03	1.5065E+04		B	8.8731E+00	2.9662E+02	1.4450E+04
C	1.3954E-03	8.7651E-02	5.3860E+00		C	-1.7203E-03	8.9124E-01	3.3231E+01
	3/4 Ton Unit #2					5 Ton Unit #11		
A	5.8581E+04	-2.3972E+06	-3.7696E+07		A	-9.5268E+03	-6.3270E+04	-3.9731E+06
B	-1.4501E+01	8.2084E+02	1.4915E+04		B	1.7907E+01	2.1058E+02	1.1117E+04
C	1.2936E-03	1.3574E-01	6.0853E+00		C	-3.5229E-03	1.1439E+00	4.4132E+01
	1 Ton Unit #3					6 Ton Unit #12		
A	-3.0145E+04	-4.1898E+05	-1.7418E+07		A	3.5154E+03	-3.6318E+05	-4.3284E+06
B	9.5101E+00	3.4962E+02	1.0995E+04		B	-6.3370E+00	8.4615E+02	1.3511E+04
C	-5.6630E-04	2.0962E-01	8.3613E+00		C	6.9979E-03	1.0476E+00	4.3009E+01
	1 1/4 Ton Unit #4					7 1/2 Ton Unit #13		
A	6.2398E+04	-2.5635E+06	-1.7806E+07		A	5.1937E+03	-4.3555E+05	-1.3784E+06
B	-2.5078E+01	1.2293E+03	1.2465E+04		B	-9.2332E+00	1.1131E+03	8.9542E+03
C	2.9572E-03	1.7086E-01	1.0389E+01		C	9.2000E-03	1.0510E+00	5.3703E+01

	1 1/2 Ton Unit #5					10 Ton Unit #14		
A	3.3490E+04	-1.4121E+06	-1.6052E+07		A	-1.7523E+03	-8.0050E+04	-2.8241E+06
B	-2.1904E+01	9.4180E+02	1.3528E+04		B	5.9715E+00	4.0839E+02	1.3891E+04
C	2.3619E-03	2.6831E-01	1.2114E+01		C	4.3885E-03	1.8089E+00	6.8104E+01
	2 Ton Unit #6					12 1/2 Ton Unit #15		
A	-1.1901E+04	-3.1749E+05	-1.4813E+07		A	-2.2619E+03	-9.7966E+04	-2.4295E+06
B	6.6409E+00	3.5640E+02	1.4076E+04		B	1.2077E+01	4.7514E+02	1.4456E+04
C	8.8718E-06	4.3251E-01	1.6362E+01		C	1.8695E-03	2.4430E+00	9.7847E+01
	2 1/2 Ton Unit #7					15 Ton Unit #16		
A	6.0613E+03	-6.8468E+05	-1.0254E+07		A	7.5410E+02	-1.8379E+05	-1.3676E+06
B	-3.2562E+00	6.6522E+02	1.3232E+04		B	-2.7436E+00	1.0557E+03	1.0388E+04
C	1.7915E-03	4.7235E-01	2.0524E+01		C	2.7056E-02	2.0251E+00	1.2662E+02
	3 Ton Unit #8					20 Ton Unit #17		
A	-2.4290E+03	-3.7575E+05	-8.9687E+06		A	-1.3384E+03	-4.4165E+04	-1.4125E+06
B	3.1579E+00	4.8579E+02	1.3734E+04		B	1.1736E+01	4.6897E+02	1.3913E+04
C	1.8371E-03	6.4054E-01	2.6121E+01		C	8.0309E-03	3.4513E+00	1.4182E+02
	3 1/2 Ton Unit #9					25 Ton Unit #18		
A	-5.9527E+02	-2.9397E+05	-9.7462E+06		A	-8.4890E+02	-4.0803E+04	-1.1959E+06
B	2.5761E+00	4.1799E+02	1.5713E+04		B	9.6994E+00	5.0733E+02	1.4751E+04
C	1.8604E-03	7.5497E-01	2.8908E+01		C	9.6871E-03	4.4033E+00	1.8838E+02

Table 8: Cooling Power Coefficients for Modeled Heat Pumps.

Cooling Power = (Aa*EWT^2+Ab*EWT+Ac)*vol^2+(Ba*EWT^2+Bb*EWT+Bc)*vol+(Ca*EWT^2+Cb*EWT+Cc)								
	a	b	c			a	b	c
Coefficient	1/2 Ton Unit #1				Coefficient	4 Ton Unit #10		
A	-5.1427E+03	2.9263E+05	2.1948E+06		A	-8.6495E+01	1.4898E+04	6.9783E+05
B	1.1179E+00	-7.6491E+01	-6.5933E+02		B	-5.3105E-02	-1.9226E+01	-1.4026E+03
C	1.0474E-04	6.5892E-03	4.8980E-01		C	9.3867E-04	3.2483E-02	3.0210E+00
	3/4 Ton Unit #2					5 Ton Unit #11		
A	-1.9274E+03	3.5073E+05	-1.3680E+06		A	3.1743E+02	-1.1631E+04	7.1826E+05
B	2.9911E-01	-9.7185E+01	2.0495E+02		B	-8.0568E-01	3.1448E+01	-1.8691E+03
C	3.2229E-04	2.4733E-03	5.5559E-01		C	1.0119E-03	3.8518E-02	3.8222E+00
	1 Ton Unit #3					6 Ton Unit #12		
A	5.1475E+02	8.2013E+04	1.1697E+06		A	2.8129E+02	-8.6271E+03	8.5580E+05
B	-3.1308E-01	-2.9453E+01	-7.9120E+02		B	-8.2733E-01	2.8426E+01	-2.4757E+03
C	2.6375E-04	8.3560E-03	6.5437E-01		C	1.3334E-03	5.5362E-02	3.1774E+00
	1 1/4 Ton Unit #4					7 1/2 Ton Unit #13		
A	1.1813E+03	-6.0647E+04	3.8857E+06		A	2.1913E+02	-3.6708E+03	5.7719E+05
B	-7.7326E-01	3.7299E+01	-2.3112E+03		B	-7.6950E-01	1.4725E+01	-2.0442E+03

C	2.6079E-04	1.0202E-02	8.5496E-01		C	1.9127E-03	5.1304E-02	4.1029E+00
	1 1/2 Ton Unit #5					10 Ton Unit #14		
A	-9.3371E+02	8.8741E+04	1.2799E+06		A	1.0110E+02	-4.4052E+03	4.5596E+05
B	1.5492E-01	-3.5981E+01	-1.2147E+03		B	-4.5492E-01	1.9772E+01	-2.1174E+03
C	3.1755E-04	1.6399E-02	9.9904E-01		C	1.4056E-03	9.2900E-02	5.0375E+00
	2 Ton Unit #6					12 1/2 Ton Unit #15		
A	-2.0999E+02	4.9178E+04	9.0126E+05		A	-2.9109E+02	2.0270E+04	4.6341E+04
B	-1.4953E-01	-2.0665E+01	-1.3151E+03		B	1.0666E+00	-7.9300E+01	-7.9607E+02
C	3.9509E-04	2.4180E-02	1.2514E+00		C	6.8122E-04	1.7179E-01	6.7212E+00
	2 1/2 Ton Unit #7					15 Ton Unit #16		
A	-2.1954E+02	1.6093E+04	1.0088E+06		A	-2.6119E+00	3.7767E+03	2.0424E+05
B	-5.5027E-02	-4.7708E+00	-1.4021E+03		B	-2.9527E-01	-7.5144E+00	-1.6436E+03
C	3.7691E-04	2.4220E-02	1.6526E+00		C	3.1225E-03	1.0571E-01	9.8124E+00
	3 Ton Unit #8					20 Ton Unit #17		
A	1.2349E+02	7.7430E+03	7.8386E+05		A	-4.1115E+01	5.4968E+03	9.6335E+04
B	-2.2098E-01	-8.4476E+00	-1.1975E+03		B	9.7888E-02	-3.2676E+01	-1.1284E+03
C	5.6942E-04	2.5370E-02	2.1127E+00		C	3.0999E-03	1.8744E-01	1.0598E+01
	3 1/2 Ton Unit #9					25 Ton Unit #18		
A	6.0225E+02	-1.5694E+04	9.7250E+05		A	6.5023E+00	1.4405E+03	1.1584E+05
B	-7.1180E-01	1.3238E+01	-1.5265E+03		B	2.7362E-02	-2.2312E+01	-1.2370E+03
C	7.9616E-04	2.5886E-02	2.5040E+00		C	3.4711E-03	2.1199E-01	1.4463E+01

Table 9: Heating Power Coefficients for Modeled Heat Pumps.

Heating Power = (Aa*EWT^2+Ab*EWT+Ac)*vol^2+(Ba*EWT^2+Bb*EWT+Bc)*vol+(Ca*EWT^2+Cb*EWT+Cc)								
	a	b	c			a	b	c
Coefficient	1/2 Ton Unit #1				Coefficient	4 Ton Unit #10		
A	-1.9700E+04	4.9248E+05	-1.2476E+06		A	-6.4762E+02	3.7381E+03	7.1777E+03
B	4.0273E+00	-9.1573E+01	3.0210E+02		B	9.1505E-01	-3.0757E+00	7.8314E+01
C	-1.6854E-04	6.9527E-03	5.8213E-01		C	-1.4004E-04	1.6964E-02	3.4202E+00
	3/4 Ton Unit #2					5 Ton Unit #11		
A	1.9387E+04	-5.6149E+05	5.6307E+05		A	-4.3602E+02	2.6405E+03	-4.9921E+04
B	-4.3600E+00	1.3153E+02	-4.1796E+01		B	1.0082E+00	-6.3495E+00	1.7149E+02
C	2.4406E-04	-4.2771E-03	6.5135E-01		C	-1.2815E-04	2.6095E-02	4.5035E+00
	1 Ton Unit #3					6 Ton Unit #12		
A	-4.6989E+03	8.2343E+04	2.7339E+05		A	-6.9990E+01	-1.7475E+03	-7.8533E+04
B	1.5997E+00	-2.5931E+01	-9.7547E+00		B	1.1580E-01	5.8509E+00	2.2182E+02
C	-1.2200E-04	5.8221E-03	8.8547E-01		C	1.4743E-04	1.6035E-02	3.8844E+00
	1 1/4 Ton Unit #4					7 1/2 Ton Unit #13		
A	4.1888E+03	-1.2052E+05	-6.9380E+05		A	5.7017E+01	-5.7936E+03	-9.3580E+03

B	-1.7445E+00	5.2798E+01	3.7521E+02		B	-1.5106E-01	1.7221E+01	7.1231E+01
C	1.4395E-04	1.5099E-03	1.0537E+00		C	3.1562E-04	8.0151E-03	4.6135E+00
	1 1/2 Ton Unit #5					10 Ton Unit #14		
A	-1.6783E+03	3.5314E+04	-4.8878E+05		A	-6.2575E+01	-2.2752E+03	-2.8815E+04
B	4.1203E-01	-9.4553E+00	3.5735E+02		B	2.8621E-01	9.4356E+00	1.6067E+02
C	-1.1898E-04	9.6875E-03	1.2211E+00		C	2.7280E-04	1.9047E-02	5.9025E+00
	2 Ton Unit #6					12 1/2 Ton Unit #15		
A	-7.1673E+02	-5.3709E+03	-4.4967E+05		A	-6.9662E+01	-1.5904E+03	-2.1376E+04
B	5.5913E-01	6.9879E+00	3.4301E+02		B	3.7611E-01	6.1585E+00	1.2434E+02
C	8.7920E-05	6.2236E-03	1.8595E+00		C	1.6303E-04	2.8731E-02	8.4808E+00
	2 1/2 Ton Unit #7					15 Ton Unit #16		
A	-5.9042E+02	-1.5560E+04	7.6066E+04		A	-4.3675E+01	-3.4558E+03	-2.8530E+04
B	6.8002E-01	1.2594E+01	3.4810E+01		B	3.0844E-01	2.0340E+01	2.0560E+02
C	5.5329E-06	8.7861E-03	2.1757E+00		C	7.1842E-04	4.4005E-02	9.9043E+00
	3 Ton Unit #8					20 Ton Unit #17		
A	-3.6894E+02	-4.7578E+03	-1.2207E+05		A	-6.1580E+01	-3.6143E+02	-2.2728E+04
B	4.2856E-01	6.8373E+00	1.9408E+02		B	6.3123E-01	4.2403E+00	2.3577E+02
C	1.6330E-04	1.2960E-02	2.7960E+00		C	2.9160E-04	5.7667E-02	1.1973E+01
	3 1/2 Ton Unit #9					25 Ton Unit #18		
A	-5.6522E+01	5.3260E+03	-3.3723E+05		A	-3.2504E+01	-1.5225E+03	-1.6816E+04
B	2.1195E-01	-7.7777E+00	4.7419E+02		B	5.0638E-01	1.2408E+01	2.6233E+02
C	1.1775E-04	2.0232E-02	2.9874E+00		C	3.2466E-04	9.2190E-02	1.6549E+01

Table 10: EAT Cooling Capacity Correction Factors.

EAT Cooling Capacity Correction Factor			
CCCF = A*EAT^2+B*EAT+C			
	A	B	C
1/2 Ton Unit #1	-7.4621E-07	2.9851E-02	4.3348E-01
3/4 Ton Unit #2	-7.4621E-07	2.9851E-02	4.3348E-01
1 Ton Unit #3	-7.4621E-07	2.9851E-02	4.3348E-01
1 1/4 Ton Unit #4	-7.4621E-07	2.9851E-02	4.3348E-01
1 1/2 Ton Unit #5	-7.4621E-07	2.9851E-02	4.3348E-01
2 Ton Unit #6	-7.4621E-07	2.9851E-02	4.3348E-01
2 1/2 Ton Unit #7	-7.4621E-07	2.9851E-02	4.3348E-01
3 Ton Unit #8	-7.4621E-07	2.9851E-02	4.3348E-01
3 1/2 Ton Unit #9	-7.4621E-07	2.9851E-02	4.3348E-01
4 Ton Unit #10	-7.4621E-07	2.9851E-02	4.3348E-01
5 Ton Unit #11	-7.4621E-07	2.9851E-02	4.3348E-01
6 Ton Unit #12	1.1874E-03	-2.7131E-02	1.0894E+00
7 1/2 Ton Unit #13	1.2807E-03	-2.9034E-02	1.0925E+00

10 Ton Unit #14	1.2844E-03	-2.9156E-02	1.0932E+00
12 1/2 Ton Unit #15	1.3086E-03	-2.9352E-02	1.0858E+00
15 Ton Unit #16	1.3201E-03	-2.9547E-02	1.0880E+00
20 Ton Unit #17	1.4350E-03	-3.2847E-02	1.1111E+00
25 Ton Unit #18	1.3409E-03	-3.0275E-02	1.0943E+00

Table 11: EAT Heating Capacity Correction Factors.

EAT Heating Capacity Correction Factor			
HCCF = A*EAT^2+B*EAT+C			
	A	B	C
1/2 Ton Unit #1	1.4109E-18	-3.6000E-03	1.0720E+00
3/4 Ton Unit #2	1.4109E-18	-3.6000E-03	1.0720E+00
1 Ton Unit #3	1.4109E-18	-3.6000E-03	1.0720E+00
1 1/4 Ton Unit #4	1.4109E-18	-3.6000E-03	1.0720E+00
1 1/2 Ton Unit #5	1.4109E-18	-3.6000E-03	1.0720E+00
2 Ton Unit #6	1.4109E-18	-3.6000E-03	1.0720E+00
2 1/2 Ton Unit #7	1.4109E-18	-3.6000E-03	1.0720E+00
3 Ton Unit #8	1.4109E-18	-3.6000E-03	1.0720E+00
3 1/2 Ton Unit #9	1.4109E-18	-3.6000E-03	1.0720E+00
4 Ton Unit #10	1.4109E-18	-3.6000E-03	1.0720E+00
5 Ton Unit #11	1.4109E-18	-3.6000E-03	1.0720E+00
6 Ton Unit #12	2.2371E-05	-5.0584E-03	1.0917E+00
7 1/2 Ton Unit #13	2.3143E-06	-4.9719E-03	1.0994E+00
10 Ton Unit #14	1.5429E-05	-5.8457E-03	1.1101E+00
12 1/2 Ton Unit #15	-3.3943E-05	-3.1251E-03	1.0766E+00
15 Ton Unit #16	-4.6286E-05	-2.2714E-03	1.0759E+00
20 Ton Unit #17	-7.7143E-07	-4.2141E-03	1.0848E+00
25 Ton Unit #18	1.0029E-05	-4.5647E-03	1.0870E+00

Table 12: EAT Cooling Power Correction Factor.

EAT Cooling Power Correction Factor			
CPCF = A*EAT^2+B*EAT+C			
	A	B	C
1/2 Ton Unit #1	-8.0076E-06	1.1725E-02	7.8035E-01
3/4 Ton Unit #2	-8.0076E-06	1.1725E-02	7.8035E-01
1 Ton Unit #3	-8.0076E-06	1.1725E-02	7.8035E-01
1 1/4 Ton Unit #4	-8.0076E-06	1.1725E-02	7.8035E-01

1 1/2 Ton Unit #5	-8.0076E-06	1.1725E-02	7.8035E-01
2 Ton Unit #6	-8.0076E-06	1.1725E-02	7.8035E-01
2 1/2 Ton Unit #7	-8.0076E-06	1.1725E-02	7.8035E-01
3 Ton Unit #8	-8.0076E-06	1.1725E-02	7.8035E-01
3 1/2 Ton Unit #9	-8.0076E-06	1.1725E-02	7.8035E-01
4 Ton Unit #10	-8.0076E-06	1.1725E-02	7.8035E-01
5 Ton Unit #11	-8.0076E-06	1.1725E-02	7.8035E-01
6 Ton Unit #12	2.5028E-04	-5.3176E-03	1.0087E+00
7 1/2 Ton Unit #13	3.0220E-04	-6.4977E-03	1.0128E+00
10 Ton Unit #14	7.8466E-05	-1.8594E-03	1.0069E+00
12 1/2 Ton Unit #15	1.1863E-04	-2.6608E-03	1.0075E+00
15 Ton Unit #16	9.0811E-05	-2.1203E-03	1.0061E+00
20 Ton Unit #17	2.4695E-04	-5.7052E-03	1.0206E+00
25 Ton Unit #18	1.8926E-04	-4.4354E-03	1.0162E+00

Table 13: EAT Heating Power Correction Factor.

EAT Heating Power Correction Factor			
HPCF = A*EAT^2+B*EAT+C			
	A	B	C
1/2 Ton Unit #1	3.1274E-07	1.4620E-02	7.0746E-01
3/4 Ton Unit #2	3.1274E-07	1.4620E-02	7.0746E-01
1 Ton Unit #3	3.1274E-07	1.4620E-02	7.0746E-01
1 1/4 Ton Unit #4	3.1274E-07	1.4620E-02	7.0746E-01
1 1/2 Ton Unit #5	3.1274E-07	1.4620E-02	7.0746E-01
2 Ton Unit #6	3.1274E-07	1.4620E-02	7.0746E-01
2 1/2 Ton Unit #7	3.1274E-07	1.4620E-02	7.0746E-01
3 Ton Unit #8	3.1274E-07	1.4620E-02	7.0746E-01
3 1/2 Ton Unit #9	3.1274E-07	1.4620E-02	7.0746E-01
4 Ton Unit #10	3.1274E-07	1.4620E-02	7.0746E-01
5 Ton Unit #11	3.1274E-07	1.4620E-02	7.0746E-01
6 Ton Unit #12	1.7126E-04	1.7711E-02	5.7745E-01
7 1/2 Ton Unit #13	1.4966E-04	1.6758E-02	6.0633E-01
10 Ton Unit #14	1.2111E-04	1.7203E-02	6.0747E-01
12 1/2 Ton Unit #15	1.4349E-04	1.3336E-02	6.7631E-01
15 Ton Unit #16	1.3577E-04	1.1301E-02	6.7216E-01
20 Ton Unit #17	1.5429E-04	1.2686E-02	6.8621E-01
25 Ton Unit #18	1.8206E-04	1.1378E-02	6.9934E-01

Table 14: Fan Cooling Capacity Correction Factor.

Fan Cooling Capacity Correction Factor			
CCCF = A*Air_Flow^2+B*Air_Flow+C			
	A	B	C
1/2 Ton Unit #1	-1.2895E+01	4.5760E+00	6.6791E-01
3/4 Ton Unit #2	-9.0698E+00	3.7066E+00	6.6604E-01
1 Ton Unit #3	-4.0819E+00	2.4675E+00	6.8894E-01
1 1/4 Ton Unit #4	-2.3295E+00	1.8417E+00	7.0419E-01
1 1/2 Ton Unit #5	-2.0246E+00	1.6756E+00	6.9602E-01
2 Ton Unit #6	-8.1819E-01	1.0990E+00	7.1116E-01
2 1/2 Ton Unit #7	-7.3675E-01	1.0660E+00	6.7999E-01
3 Ton Unit #8	-4.4556E-01	8.4118E-01	6.7687E-01
3 1/2 Ton Unit #9	-4.0587E-01	8.0587E-01	6.5403E-01
4 Ton Unit #10	-2.6092E-01	6.1167E-01	6.9503E-01
5 Ton Unit #11	-1.6412E-01	5.0055E-01	6.8296E-01
6 Ton Unit #12	-1.0717E-01	3.8294E-01	7.0338E-01
7 1/2 Ton Unit #13	-5.5341E-02	2.8135E-01	7.1266E-01
10 Ton Unit #14	-2.9595E-02	2.0562E-01	7.1703E-01
12 1/2 Ton Unit #15	-2.1747E-02	1.8105E-01	6.9369E-01
15 Ton Unit #16	-2.1338E-02	1.8866E-01	6.3729E-01
20 Ton Unit #17	-8.8785E-03	1.1585E-01	6.8932E-01
25 Ton Unit #18	-5.6822E-03	9.2681E-02	6.8932E-01

Table 15: Fan Heating Capacity Correction Factors.

Fan Heating Capacity Correction Factor			
HCCF = A*Air_Flow^2+B*Air_Flow+C			
	A	B	C
1/2 Ton Unit #1	-9.6521E+00	2.7769E+00	8.2104E-01
3/4 Ton Unit #2	-2.9152E+00	1.2278E+00	8.8604E-01
1 Ton Unit #3	-2.5355E+00	1.1662E+00	8.7145E-01
1 1/4 Ton Unit #4	-9.6534E-01	5.3797E-01	9.2645E-01
1 1/2 Ton Unit #5	-1.4938E+00	9.8906E-01	8.4119E-01
2 Ton Unit #6	-5.6289E-01	6.3314E-01	8.4517E-01
2 1/2 Ton Unit #7	-2.6245E-02	2.2980E-01	9.0914E-01
3 Ton Unit #8	-2.8815E-01	4.4894E-01	8.4250E-01

3 1/2 Ton Unit #9	-1.9349E-01	3.4872E-01	8.5840E-01
4 Ton Unit #10	-1.3543E-01	3.1126E-01	8.4709E-01
5 Ton Unit #11	-5.0850E-02	1.8099E-01	8.7923E-01
6 Ton Unit #12	-8.2817E-02	2.6629E-01	8.0586E-01
7 1/2 Ton Unit #13	-3.9362E-02	1.7853E-01	8.2631E-01
10 Ton Unit #14	-8.9881E-03	8.2413E-02	8.7635E-01
12 1/2 Ton Unit #15	-5.7524E-03	6.5930E-02	8.7635E-01
15 Ton Unit #16	-1.1205E-02	9.8567E-02	8.1037E-01
20 Ton Unit #17	-7.9468E-03	8.9709E-02	7.7466E-01
25 Ton Unit #18	-5.0859E-03	7.1767E-02	7.7466E-01

Table 16: Fan Cooling Power Correction Factor.

Fan Cooling Power Correction Factor			
CPCF = A*Air_Flow^2+B*Air_Flow+C			
	A	B	C
1/2 Ton Unit #1	2.0918E+00	-4.3262E-01	1.0220E+00
3/4 Ton Unit #2	-7.5279E-01	1.2224E-01	9.9824E-01
1 Ton Unit #3	6.8353E-01	-3.4693E-01	1.0403E+00
1 1/4 Ton Unit #4	3.2081E-01	-2.4377E-01	1.0385E+00
1 1/2 Ton Unit #5	4.3864E-01	-2.6211E-01	1.0390E+00
2 Ton Unit #6	5.2608E-01	-4.3536E-01	1.0880E+00
2 1/2 Ton Unit #7	-3.0203E-03	-7.6243E-03	1.0040E+00
3 Ton Unit #8	2.3304E-02	-4.5979E-02	1.0188E+00
3 1/2 Ton Unit #9	6.5685E-02	-1.0177E-01	1.0382E+00
4 Ton Unit #10	-1.8403E-02	2.6193E-03	1.0073E+00
5 Ton Unit #11	-1.4886E-02	1.8860E-02	9.9436E-01
6 Ton Unit #12	3.6537E-03	-2.7121E-02	1.0260E+00
7 1/2 Ton Unit #13	1.3251E-02	-5.3259E-02	1.0493E+00
10 Ton Unit #14	-4.3844E-03	2.0692E-02	9.7666E-01
12 1/2 Ton Unit #15	-2.8060E-03	1.6554E-02	9.7666E-01
15 Ton Unit #16	2.6307E-03	-2.0918E-02	1.0377E+00
20 Ton Unit #17	5.4805E-04	-1.4071E-04	9.9237E-01
25 Ton Unit #18	3.5075E-04	-1.1257E-04	9.9237E-01

Table 17: Fan Heating Capacity Correction Factors.

Fan Heating Capacity Correction Factor

HPCF = A*Air_Flow^2+B*Air_Flow+C			
	A	B	C
1/2 Ton Unit #1	4.2274E+01	-1.2240E+01	1.8075E+00
3/4 Ton Unit #2	2.3674E+01	-8.9465E+00	1.7742E+00
1 Ton Unit #3	1.3680E+01	-7.0576E+00	1.8238E+00
1 1/4 Ton Unit #4	8.6301E+00	-5.7016E+00	1.8430E+00
1 1/2 Ton Unit #5	5.3653E+00	-4.2786E+00	1.7611E+00
2 Ton Unit #6	3.3598E+00	-3.5542E+00	1.8420E+00
2 1/2 Ton Unit #7	2.5665E+00	-3.0239E+00	1.8231E+00
3 Ton Unit #8	1.4818E+00	-2.2776E+00	1.7971E+00
3 1/2 Ton Unit #9	9.3649E-01	-1.7116E+00	1.7055E+00
4 Ton Unit #10	7.3238E-01	-1.5063E+00	1.7047E+00
5 Ton Unit #11	4.4505E-01	-1.1423E+00	1.6663E+00
6 Ton Unit #12	3.1178E-01	-1.0277E+00	1.7778E+00
7 1/2 Ton Unit #13	2.0656E-01	-8.4625E-01	1.7837E+00
10 Ton Unit #14	1.1531E-01	-6.1890E-01	1.7573E+00
12 1/2 Ton Unit #15	7.3799E-02	-4.9512E-01	1.7573E+00
15 Ton Unit #16	4.6377E-02	-3.8199E-01	1.7097E+00
20 Ton Unit #17	2.5539E-02	-2.7099E-01	1.6587E+00
25 Ton Unit #18	1.6345E-02	-2.1679E-01	1.6587E+00